TECHNICAL REPORT STANDARD PAGE

1. Report No.	2. Government Accession No.	3. Recipient's Catalog No.
FHWA/LA.18/588		

4. Title and Subtitle	5. Report Date
Minimizing Shrinkage Cracking in Cement-Stabilized Bases through Micro-Cracking	October 2018
	6. Performing Organization Code LTRC Project Number: 12-3P SIO Number: 30000729
7. Author(s) Zhong Wu, Yilong Liu and Ferdous Intaj	**8. Performing Organization Report No.**
9. Performing Organization Name and Address Department of Civil and Environmental Engineering Louisiana State University Baton Rouge, LA 70803	**10. Work Unit No.** **11. Contract or Grant No.**
12. Sponsoring Agency Name and Address Louisiana Department of Transportation and Development P.O. Box 94245 Baton Rouge, LA 70804-9245	**13. Type of Report and Period Covered** **Final Report** **11/2012 to 10/2017** **14. Sponsoring Agency Code**

15. Supplementary Notes
Conducted in Cooperation with the U.S. Department of Transportation, Federal Highway Administration

16. Abstract
Cement stabilized soil base (so-called soil cement base) has been used in flexible pavement in Louisiana for more than 50 years. Soil cement has an excellent load carrying capacity and durability but is also well-known for developing shrinkage cracks, which can reflect through asphalt concrete surfaces and accelerate the deterioration of asphalt pavements. Micro-cracking is a special reflective cracking mitigation technique used in a cement-stabilized base construction. The objectives of the study were to determine if the micro-cracking technique is suitable for implementing on soil cement pavements in Louisiana and to evaluate the effectiveness of the micro-cracking on reducing the shrinkage/reflective cracking on soil cement pavements. To achieve the objectives, micro-cracked base sections were constructed on three selected pavement sites. Specifically, one pavement site was chosen at the Louisiana Pavement Research Facility (PRF), where six unsurfaced soil cement or cement treated base test sections were constructed including four of them micro-cracked. The PRF sections were used to investigate the shrinkage cracking performance considering various micro-cracking levels and cement contents. Two other pavement sites were selected on field pavement rehabilitation projects of LA 1003 and LA 599 through the support of DOTD project engineers, in which nine 1000-ft. long test sections were constructed including four micro-cracked soil cement base test sections. In general, two types of DOTD's soil cement base course design-cement stabilized design (CSD) and cement treated design (CTD) were considered in this study.

In-situ non-destructive tests (NDT) and cracking surveys were performed periodically on PRF test sections after construction. Substantial amounts of hairline-type shrinkage cracks were first observed on all test sections during the early curing periods, but the surface cracks all disappeared in approximately six months thereafter. Not a single, wide and deep shrinkage crack could be found after three and half years of monitoring on those PRF sections. Saw-cutting beams also indicated that no underneath severe shrinkage cracks had been developed at the end of monitoring. The measured base stiffness, however, did show an increasing trend over time on all sections tested. Similarly, in-situ NDT tests and cracking surveys were performed on the testing sites of LA 1003 and LA 599. Based on the test results, it was found that a micro-cracked, 8.5-in. soil cement pavement (i.e., the CSD base design) generally showed a similar early performance (approximately three years of service) as compared to a non-micro-cracked soil cement pavement in terms of the overall cracking performance as well as pavement performance of rutting and pavement smoothness. However, due to very few reflection cracks having been developed so far on both the control and micro-cracked sections, whether or not the micro-cracking technique is effective in mitigation of reflection cracks on an 8.5-in. soil cement pavements in Louisiana may be still too early to be drawn. On the other hand, the two 12-in. cement treated soil base pavements (i.e., the CTD base design) did not show better early performance than non-micro-cracked control sections, especially in the cracking performance. After three years of trafficking, more cracks were found on the micro-cracked test sections than the control ones indicating that the micro-cracking technique may be not effective when applied on a 12-in. cement treated soil base in Louisiana.

17. Key Words	18. Distribution Statement
Cement stabilized/treated base, Micro-cracking, Pavement performance	Unrestricted. This document is available through the National Technical Information Service, Springfield, VA 21161.

19. Security Classif. (of this report)	20. Security Classif. (of this page)	21. No. of Pages	22. Price
Unclassified	Unclassified	119	

ACKNOWLEDGMENTS

This study was supported by the Louisiana Transportation Research Center (LTRC) and the Louisiana Department of Transportation and Development (DOTD) under LTRC Research Project Number 12-3P. The authors would like to express thanks to all those who provided valuable help in this study. Specifically, the authors would like to acknowledge DOTD project engineers Aaron Elisar, Mattew French, and LTRC's Pavement Research Section: Kevin Gaspard, Mitchell Terrell, Shawn Elisar, and Terrell Gorham who coordinated and carried out field testing for this study.

IMPLEMENTATION STATEMENT

The early pavement cracking performance of eight micro-cracked test sections in this study generally indicate that the micro-cracking technique may be not suitable for implementing on soil cement pavements in Louisiana, especially when a 12-in. cement treated soil base (i.e, the CTD design) was used. Therefore, no implementation guidelines could be developed at this time. However, continuously monitoring of the micro-cracked 8.5-in. soil cement pavement sections on LA 599 and LA 1003 will be beneficial in determining if there is a long-term reflection-cracking-relief effectiveness of micro-cracking on 8.5-in soil cement pavements in Louisiana.

TABLE OF CONTENTS

LIST OF TABLES

LIST OF FIGURES

INTRODUCTION

Problem Statement

The Louisiana Department of Transportation and Development (DOTD) has been using cement stabilized soil bases (so-called soil cement) in flexible pavement construction for more than 50 years. This type of base course, although known for having an excellent loading carrying capacity and durability, is also well-known for developing shrinkage cracks, which can reflect through the asphalt concrete surface and accelerate the deterioration of the pavement. Common techniques employed by DOTD to reduce the shrinkage/reflective cracking problems on soil cement pavements include a lower-cement content/thicker-base-thickness design, a stone interlayer design, and an asphalt surface treatment (AST) design. Among the treatments, the thicker soil cement base design tends to have compaction problems for the bottom part of the base; whereas, the stone interlayer and AST designs both have a potential to increase the construction costs.

Micro-cracking is a special reflective-cracking mitigation technique used for an asphalt pavement with a cement-stabilized base during the construction. Micro-cracking aims to produce a fine network of hairline cracks in the cement stabilized base by applying several passes of heavy vibratory roller compaction (usually 10-12 tons) shortly after the base construction. The developed micro-cracks will help relieve the contracting stress of the cement stabilized layer during its drying process and prevent it from forming of wider shrinkage cracks, which are more likely to be reflected to the pavement surface. Several recent research studies by other state agencies *[1-8]* reported that micro-cracking did improve the field performance of pavement test sections with cement stabilized bases by reducing the crack width, crack length, or both, indicating a great potential of applying this technique on the soil cement pavement construction in Louisiana. To fully understand the micro-cracking technique and explore its implementation potential on Louisiana's soil cement pavements, field research is needed.

Literature Review

Cementitious stabilization is a common technique to increase the strength and stiffness of unbound base materials in pavement construction. In the existing literature, different terminologies have been used to refer to base courses stabilized with cement, such as cement stabilized base (CSB), cement treated base (CTB), soil cement base, etc., depending on the type of unbound materials and cement contents used. The cement-stabilized base is well known for generating shrinkage cracks during drying or temperature changing. Severe

shrinkage cracks can propagate and reflect through the asphalt concrete layer, as shown in Figure 1, and accelerate the deterioration of the pavement. The reflective cracking may also cause water infiltration in pavement layers, which would result in the loss of subgrade support by pumping of fines. Therefore, many efforts have been made to mitigate shrinkage cracking in cement-stabilized bases.

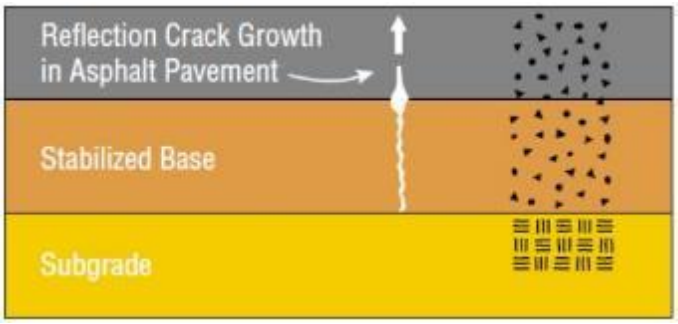

Figure 1
Propagation of reflection cracking *[9]*

Mechanism of the Generation of Shrinkage Cracks in Cement-Stabilized Bases

Drying or fluctuation changing can result in tensile strain in cement-stabilized bases that are restrained by the subbase or subgrade friction. When the cement-stabilized base is composed of fine-grained soil cement mixtures, it is believed that the tensile strain is mainly attributable to dry shrinkage *[10]*. When the tensile stress (corresponding to the tensile strain) in the cement stabilized base exceeds the tensile strength of the base material, shrinkage cracking will initiate from the preexisting flaws and further propagate along the transverse direction of the base. The crack spacing is mainly dependent on the subgrade friction and the tensile strength of the base, while the crack width is subject to the crack spacing and the ultimate shrinkage strain of the base material *[11, 12, 13]*.

Factors Influencing Shrinkage Cracking and Methods in Mitigating Reflective Cracking

The following factors including cement content, density, material type, mixing moisture content, and curing time may affect the shrinkage cracking performance of cement stabilized bases in various ways *[11]*. In these factors, an optimal cement content may exist to minimize shrinkage under a certain compaction condition. Granular materials with a low clay content and in a dry state are favorable in mitigating shrinkage. Additionally, a longer curing time is more beneficial to prevent shrinkage of the cement stabilized base since drying is the major cause of shrinkage as aforementioned.

Many methods have been investigated and implemented to minimize shrinkage cracking and reflective cracking, such as notch-cutting of the fresh cement-stabilized layer and adding interlayers *[9, 11]*. In these methods, adding the stress relief layer between the cement stabilized base and the top layer (as shown in Figure 2) were widely implemented by many agencies.

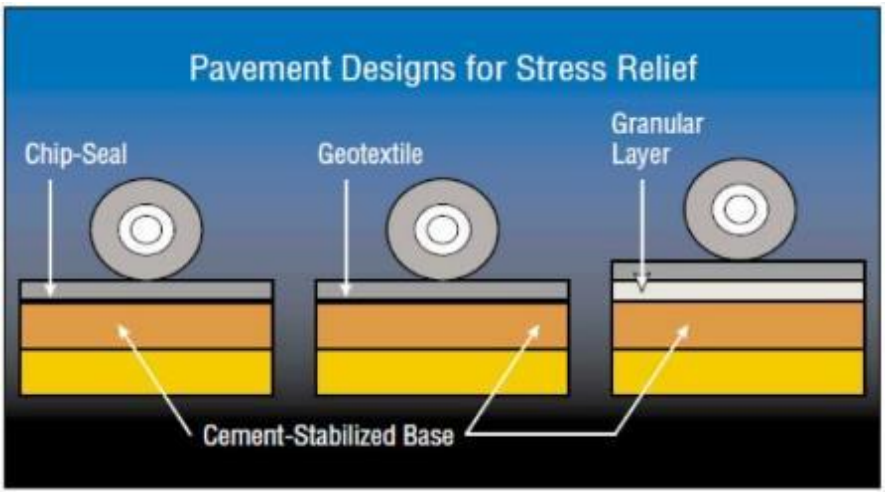

Figure 2
Installation of the stress relief layer *[9]*

Historical Research of DOTD in Mitigating Reflective Cracking

DOTD conducted a research project, which was reported in 2002, to evaluate variables related to the shrinkage crack mitigation of soil cement, including cement contents, base thicknesses, fibers, interlayers, curing membranes, and curing periods *[14]*. To address the influences of these variables, ten 1000-ft.-long test sections with soil cement bases, as described in Table 1, were constructed on LA 89 by DOTD.

In Table 1, two types of soil cement base designs were described, cement stabilized design (CSD) and cement treated design (CTD). CSD (in test sections 1, 2, 3, 7, 8, 9, and 10) refers to an 8.5-in.-thick soil cement design with a high cement content (9%) to achieve a 7-day compressive strength of 300 psi, while CTD (in test sections 4, 5, and 6) refers to a 12-in.-thick soil cement design with a low cement content (5%) to obtain a minimum 7-day compressive strength of 150 psi. In test sections 2, 3, 5, and 6, polypropylene fibers were properly mixed with soil cement at different contents, aiming to reduce shrinkage cracks. In test section 7, a 0.5-in.-thick asphalt surface treatment layer (ASTL) was constructed as a crack relief layer to prevent shrinkage cracks propagating into the asphalt surface layer. In test section 8, a thicker emulsified asphalt curing membrane topped by a 0.25-in.-thick sand layer was constructed as another type of interlayer. Test section 10 was cured in an extended

period to investigate the impact of the curing period on the shrinkage cracking performance of the test section. Test sections 1, 4, and 9 were served as control sections.

Crack mapping surveys were conducted before and after the soil cement base course was overlaid with asphalt concrete. The survey results were used to determine the influence of the variables in mitigating shrinkage cracking and reflective cracking. Within two weeks after construction, the crack mapping results showed that shrinkage cracks appeared on all the sections that were surveyed. During the two years of monitoring, no reflective cracks were observed on any test sections.

Laboratory tests were conducted to evaluate the mechanistic properties of the soil cement mixtures with fibrillated polypropylene fibers, including durability, unconfined compressive strength (UCS), indirect tensile strength and strain (ITS), and indirect tensile resilient modulus (ITM_r) *[15]*. The results indicated that the addition of the fibers to the soil cement mixtures increased the indirect tensile strength, the indirect tensile strain, and the toughness index. The layer coefficients and resilient moduli of the soil cement layers of all the test sections were also tested. The results met or exceeded design guides and were consistent with other projects in Louisiana.

Table 1
Test section descriptions

Test Section	Thickness Inches	Cement Content	Fiber Content	Overlay Period	Description/ Station location
1	8.5	9%	N/A	<7 days	**Control Section-CSD** Sta. (5+00 to 15+00)
2	8.5	9%	0.1%	<7 days	**CSD with fibers** Sta. (15+00 to 25+00)
3	8.5	9%	0.05%	<7 days	**CSD with fibers** Sta. (25+00 to 35+00)
4	12	5%	N/A	<7 days	**CTD** Sta. (35+00 to 45+00)
5	12	5%	0.1%	<7 days	**CTD with fibers** Sta. (45+00 to 55+00)
6	12	5%	0.05%	<7 days	**CTD with fibers** Sta. (55+00 to 65+00)
7	8.5	9%	N/A	<7 days	**Crack Relief Layer-CSD** Sta. (65+00 to 75+00)
8	8.5	9%	N/A	<7 days	**E.A. Curing Layer w/sand CSD** Sta. (75+00 to 85+00)
9	8.5	9%	N/A	<7 days	**Control Section-CSD** Sta. (85+00 to 95+00)
10	8.5	9%	N/A	14 to 30 days	**E.A. Curing Layer w/sand CSD** Sta. (95+00 to 105+00)

Note: CSD: Cement Stabilized Design; CTD: Cement Treated Design; E.A.: emulsified asphalt

Micro-Cracking

Micro-cracking is a special construction technique used to mitigate the severity of shrinkage cracking and reflective cracking in flexible pavements with cement stabilized bases. Micro-cracking aims to produce a fine network of hairline cracks to the cement stabilized base layer by a few passes of vibratory roller compaction shortly after the base construction. The micro-cracks produced in this process will help relieve the contracting stress in the cement stabilized base during drying and prevent the forming of wider shrinkage cracks, as illustrated in Figure 3. As a result, the reflection of shrinkage cracks can be prevented or delayed.

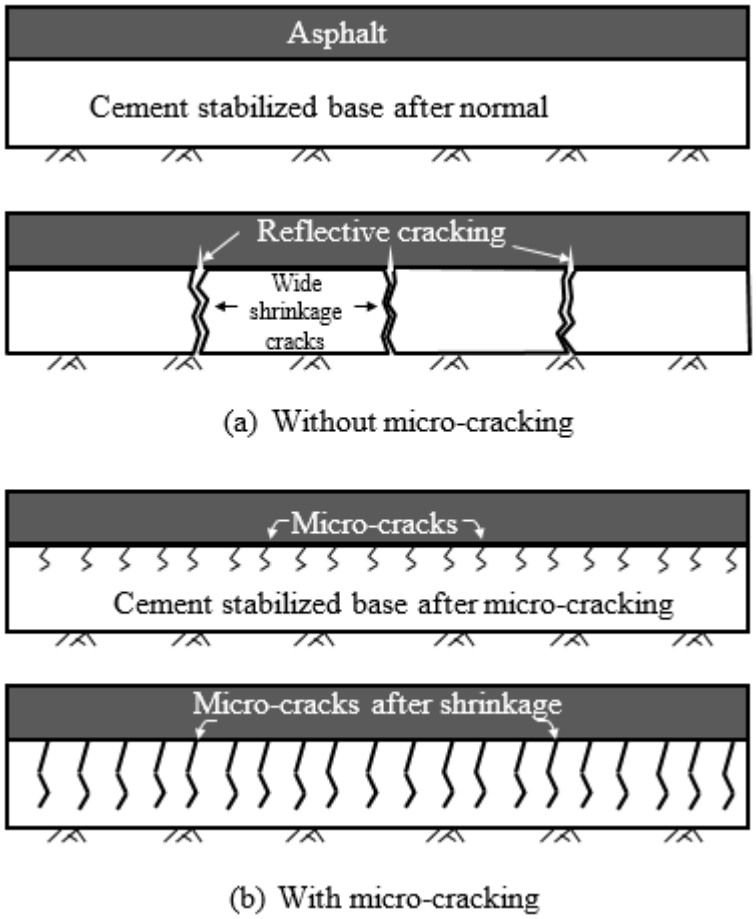

Figure 3

Mechanism of the micro-cracking technique to prevent severe shrinkage cracking

The micro-cracking technique was developed in Austria in the 1990s and has been used in several other European countries *[2, 3]*. Litzka and Haslehner reported an application of micro-cracking in a rural road rehabilitation project in Austria *[2]*. In the project, the existing

asphalt concrete (AC) and stone base of the road were removed and the sublayer was treated with cement to form a 12-in. thick stabilized base with a 7-day design UCS of 435 psi. To minimize the development of wide shrinkage cracks, micro-cracking was performed by five passes of a 10-ton vibratory roller compactor on the cement stabilized base after 24 to 72 hours of the base construction.

Largely based on the Austrian experience, Mississippi and Texas DOTs constructed field test sections to evaluate the effectiveness of the micro-cracking technique. In 2000, MDOT constructed an 800-ft. test section with a pavement structure of 8.8-in. asphalt concrete over a 6-in. cement stabilized sand clay (with a cement content of 5.5% by weight) *[4, 5]*. In the same year, TxDOT constructed three field test sections with a pavement structure of 2-in. asphalt concrete over a 6-in. cement stabilized river gravel *[6]*. The cement content used in the test sections was 6 to 8% to achieve a 7-day design UCS of 500 psi. In 2002 – 2003, more test sites were constructed in two pavement rehabilitation projects in Texas, while a reduced cement content (2 to 3%) was used to achieve a 7-day design UCS of 300 psi.

Due to the promising field performance of the test sections in Mississippi and Texas, the micro-cracking technique was later implemented by several other North American agencies, including agencies in Utah, Wyoming, Maine, New Hampshire, and Canada *[16-18]*. In these implementations, micro-cracking was generally applied to cement stabilized RAP-stone (RAP stands for recycled asphalt pavement) blending bases with a thickness of 8 to 12 in.

Generally, findings from the previous studies on micro-cracking can be summarized into two categories: (1) the performance of micro-cracked road sections and (2) the optimum construction procedure of micro-cracking.

Performance of micro-cracked road sections. As aforementioned, the purpose of micro-cracking in previous studies was to reduce the shrinkage cracking in cement stabilized bases and the consequential reflective cracking in the asphalt concrete.

Both Mississippi and Texas compared the cracking performance of the un-surfaced cement stabilized base sections with and without micro-cracking *[5-8, 19]*. In Mississippi, the shrinkage cracks appeared in the micro-cracking section were monitored in a 28-day period after construction. It was found that the micro-cracked section outperformed the control section with the corresponding percentages of the cracked area of 4.8 and 17.4%, respectively *[5]*. In Texas, two un-surfaced test sites (both 350 ft. long) were constructed with cement contents of 4% and 8%, respectively. A visual survey conducted two years after construction indicated that micro-cracking reduced both the total length and the width of shrinkage cracking (as shown in Figure 4) *[19]*. The cracking performance on the asphalt

concrete surface of micro-cracked pavements was also monitored and compared with the control sections in several field projects in Texas. Overall, the long-term field performance of the micro-cracked sections was satisfying based on the observation *[8]*. For the test sections constructed in another project, the total length of the surface cracking appeared on the micro-cracked section was only 1/5 to 1/10 of that on the control section in a 6-month period *[6]*.

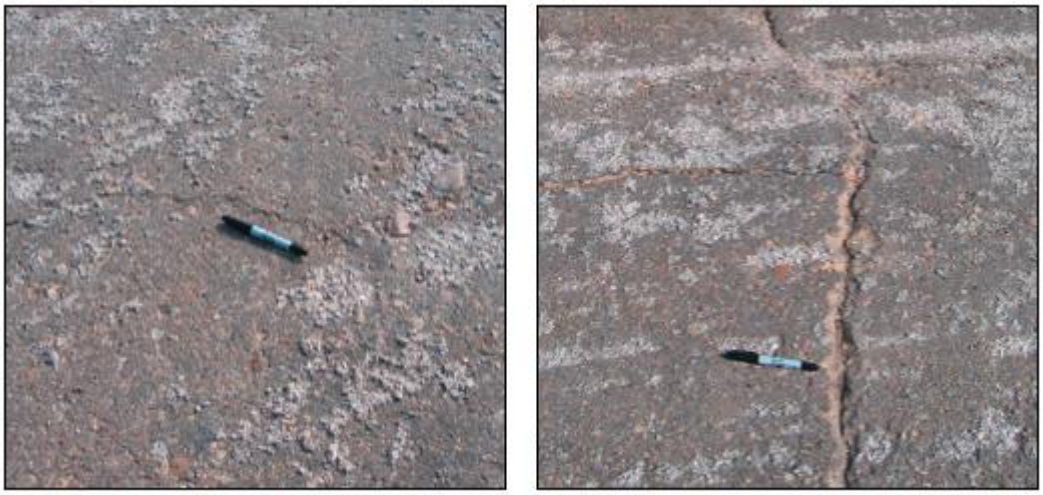

Figure 4
Shrinkage cracks in a micro-cracked section and an untreated section *[8]*

The California Department of Transportation (Caltrans) also reviewed the current implementations of micro-cracking in several other states and put together a technical memorandum *[20]*. In this technical memorandum, micro-cracking projects in Texas, Utah, and New Hampshire were reviewed. The longer-term monitoring on a range of projects in Texas and other state indicated that micro-cracking might not always be successful in preventing reflective cracking. It was concluded that additional research is necessary to better understand the mechanism of micro-cracking and to identify the key factors influencing the performance of micro-cracking sections.

Previous field test studies provided valuable experiences in implementing the micro-cracking technique. Due to varying environmental conditions and soils available, however, cautions should be taken for other agencies when considering the findings from these studies. In most of the previous studies, the base materials were either cement stabilized river gravel (as used in Texas) or a blended base of RAP (produced by cold in-place recycling) and stone stabilized with cement *[1, 6-8, 16-19]*. In Louisiana, a wide range of natural soils can be used for the construction of cement stabilized bases, including soils with a high fine content (e.g.,

A-4 and A-6). The increased fine content may result in a higher shrinkage potential for the cement stabilized base during drying *[13, 21]*.

Optimum Construction Procedure. To apply micro-cracking in the construction of cement stabilized bases properly, several factors need to be considered: (1) curing time and curing method of cement stabilized bases, (2) weight of the roller compactor used in the application of micro-cracking, and (3) the number of compaction passes or the criteria to stop the compaction.

In the original Austrian field test, the cement stabilized layer was wet-cured for 24 to 72 hours after construction and micro-cracking was then performed with five-passes by a 10-ton roller compactor *[2]*.

MDOT applied a similar micro-cracking procedure based on the Austrian study but used an 8-ton roller compactor. The author of the study, Dr. George, suggested that a proper micro-cracking should not reduce the base modulus by more than 25% *[13]*.

Early field experiments conducted in Texas suggested that micro-cracking should be conducted with three full passes by a vibratory roller compactor (at least 12-ton) operated at a low speed (2–3 mph) and a high vibration amplitude. In addition, a 40% reduction in the modulus cement stabilized base was recommended (based on the test results of a falling weight deflectometer) *[6]*. In a later study in Texas, this target number was increased to 60% *[7]*. The optimum initial curing procedure of cement stabilized bases was extensively studied by the Texas Transportation Institute (TTI) *[7, 8, 19]*. A number of un-surfaced base sections were constructed and micro-cracked with different initial curing ages (one to three days) and varying curing methods (dry, prime coat, and moist curing). By monitoring the shrinkage cracking of these test sections for two years, it was concluded that micro-cracking after two days of wet curing generated the best performance. In recent years, the recommended construction procedure by Texas, which can be found in Appendix A, was also adopted by several other agencies in their field applications *[16-18]*.

The micro-cracking procedure was also investigated in Utah and Wyoming *[16]*. The percentage reduction achieved by a single number of roller pass varied from site to site. In general, two to four passes of a vibratory roller compactor were applied during the application of micro-cracking.

Due to the difficulty in the visual inspection of micro-cracks, non-destructive testing (NDT) devices were used to control the micro-cracking process. As mentioned previously, after the application of micro-cracking, the stiffness of the cement stabilized layer will decrease as a

result of the development of micro-cracks. Therefore, the micro-cracking process can be controlled by monitoring the change of pavement stiffness. For this purpose, the falling weight deflectometer (FWD) was widely used in the early field studies *[4-8, 19]*. However, the FWD test is relatively expensive and may not be readily available during the construction. In recent years, several states have investigated the use of portable NDT devices to replace the FWD, such as the light falling weight deflectometer (LFWD) and geogauge *[8, 16]*.

The correlation between different test devices was investigated by several states. Test data from Texas (presented in Figure 5) suggested that back-calculated moduli from the FWD and PFWD (Portable Falling Weight Deflectometer, which is synonymous to LFWD) can be correlated to each other using equation (1) *[7]*.

$$E_{FWD} = 0.137(E_{LFWD})^{1.69}, R^2 = 0.75 \quad (1)$$

where, E_{FWD} and E_{LFWD} are the back-calculated moduli from the FWD and LFWD, respectively. Meanwhile, the changes of back-calculated moduli from the two devices seem to have a linear correlation *[7]*:

$$\Delta E_{FWD} = 1.4305(\Delta E_{LFWD}) - 6.6277, R^2 = 0.95 \quad (2)$$

where, ΔE_{FWD} and ΔE_{LFWD} are the changes (in percentage) of back-calculated moduli from the FWD and LFWD, respectively, compared to the initial modulus of the cement stabilized base before micro-cracking. Based on equation (2), a 60% modulus reduction indicated by the FWD is equivalent to a 40% obtained from the LFWD *[7]*.

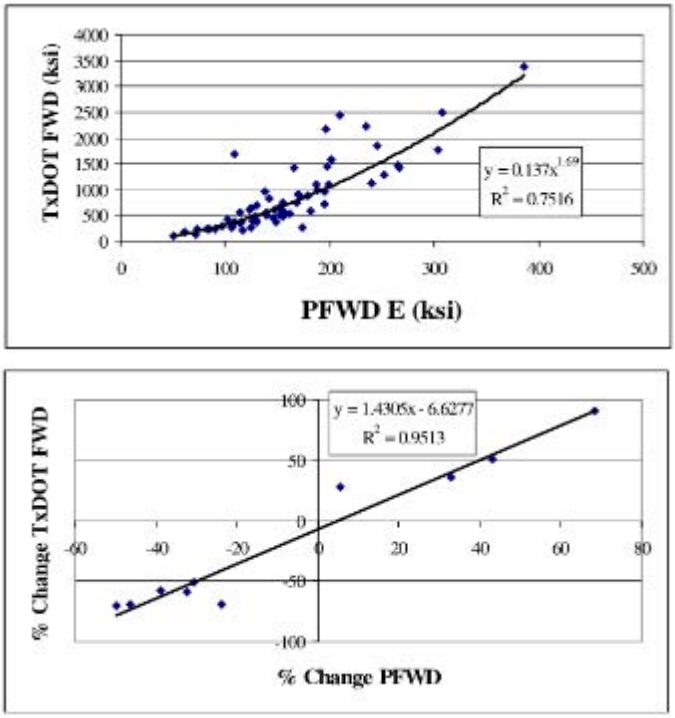

Figure 5
Correlation between FWD and LFWD measurements *[7]*

Field test results from Utah and Wyoming suggested that both the LFWD and geogauge can be used to monitor and control the micro-cracking process *[12]*. The correlation between the LFWD and geogauge measurements was given by equation (3).

$$\Delta E_{SSG} = 0.58(\Delta E_{LFWD}) + 3.65\,, R^2 = 0.56 \quad (3)$$

where, ΔE_{SSG} is the changes (in percentage) of back-calculated moduli based on a geogauge.

Miller et al. found that heavy clegg impact soil tester (CIST) was able to characterize the modulus reduction of the cement stabilized base and the CIST measured moduli of the cement stabilized base dropped by 21 to 24% after micro-cracking *[17]*. CIST was also investigated in Utah and Wyoming but the test results indicated that this instrument is not sensitive to micro-cracking *[26]*.

Prediction Model for Shrinkage and Reflective Cracking

Although field test results demonstrated the effectiveness of the micro-cracking technique, no analytical model is available to quantify the effect of micro-cracking on the cracking performance of the pavement. In order to develop such a prediction model, it is necessary to understand (1) the relationship between crack width and spacing under a constant volumetric

shrinkage condition and (2) the relationship between the crack width on the underlying layer and the reflective cracking development.

George proposed a 1-D model to estimate the spacing and the width of shrinkage cracks *[22]:*

$$L_{max} = \frac{2\sigma_u}{\mu\gamma} \quad (4)$$

where, L_{max} is the maximum spacing of shrinkage cracking, σ_u is the ultimate tensile strength of the cement stabilized base, μ is the is the coefficient of sliding friction between the cement stabilized base and the subgrade, and γ is the unit weight of the cement stabilized material.

George also proposed the relationship between the actual spacing and the width of a shrinkage cracking, as expressed in equation (5) *[22]*.

$$\delta_T = \varepsilon_c L - \frac{\mu\gamma L^2}{4E_t} \quad (5)$$

where, δ_T is the width of a shrinkage cracking, L is the actual spacing, ε_c is the shrinkage strain of the cement stabilized material, and E_t is the elastic modulus of the cement stabilized material in tension.

Based on equations (4) and (5), reducing the spacing of shrinkage cracks by micro-cracking will reduce the width of shrinkage cracks, which confirms the field observation of Sebesta *[7-8,19]*. Theoretically, a wide shrinkage crack in a cement stabilized base is more likely to reflect through the asphalt concrete layer than a narrow one *[23]*. However, the relationship between the potential of a reflective cracking and the crack width on the underlying layer has not been well established.

The current reflective cracking model in the MEPDG is empirical-based and cannot address the effect of the crack width of the underlying layer. In a recent NCHRP project, Lytton et al. developed a new reflective cracking model for the MEPDG *[24]*. The proposed model was developed based on Paris' Law *[25]*:

$$\frac{dc}{dN} = A(\Delta K)^n \quad (6)$$

where, c is the crack length, N is the number of load application, A and n are material properties of the AC layer, and ΔK is the stress intensity factor (SIF). According to equation

(6), with an identical AC material property, the rate of crack propagation in the AC layer is a function of the SIF. The magnitude of the SIF is affected by many factors, such as load levels, pavement structures, and cracking geometries. Therefore, to quantify the effect of micro-cracking on reducing reflective cracking, the relationship between the SIF and the width/length of the shrinkage cracking may need to be considered first.

OBJECTIVES

The objectives of this research were two-fold: (1) to determine if the micro-cracking technique is suitable for implementing on pavements with soil cement bases in Louisiana and (2) to evaluate the effectiveness of the micro-cracking technique in reducing the shrinkage/reflective cracking on pavements with soil cement bases.

SCOPE

Eight sections with micro-cracked cement stabilized or treated soil bases were constructed and monitored in this study. In these eight sections, four were constructed at LTRC's Pavement Research Facility (PRF) site and the rest of the sections were at the sites of two selected state pavement projects. The micro-cracking procedure used was similar to the one developed by the Texas Transportation Institute (TTI). In the micro-cracking application, a vibratory roller compactor (at least 12 ton) was used to achieve a stiffness reduction of 30% to 50% of the cement bases. Pavement performance after micro-cracking was monitored through the in-situ visual cracking survey, high-speed digital vehicle survey, FWD, LFWD, heavy weight deflectometer (HWD), and field coring. Statistical analyses were performed based on the pavement performance data collected from both the control sections and the micro-cracked sections.

METHODOLOGY

DOTD has two types of soil cement base course designs in the construction of flexible pavement: cement stabilized design (CSD) and cement treated design (CTD). The current practice of the CSD uses a high cement content (generally greater than 6% by volume) for soil aggregate or recycled base materials to achieve a minimum 7-day UCS of 300 psi, whereas the CTD uses a low cement content (4% to 6% by volume) and requires a minimum 7-day UCS of 150 psi. Typically, both the CSD base (so-called soil cement base in Louisiana) and the CTD base are in-place mixed and compacted, but the final thicknesses of the two bases are 8.5 in. and 12 in., respectively. In this study, the effectiveness of the micro-cracking technique in mitigating the shrinkage cracking and reflective cracking on both the CSD and CTD bases was investigated based on the field monitoring results of the test sections. In total, 15 test sections were constructed, including six sections (four micro-cracked sections and two control sections) at LTRC's Pavement Research Facility (PRF) site, five sections (two micro-cracked sections and three control sections) in the LA 1003 pavement project, and four sections (two micro-cracked sections and two control sections) in the LA 599 pavement project. The base courses in this study were categorized as Class II according to the *Louisiana Standard Specifications for Roads and Bridges*. In terms of the site locations, the three groups of test sections were referred to as PRF test sections, LA 1003 test sections, and LA 599 test sections.

PRF Test Sections

Figure 6 presents a plan view of the six test sections at the PRF constructed in December 2013. Each test section consisted of only a newly-built base layer and an existing embankment subgrade. All the test sections were not surfaced (i.e., no asphalt surfacing) and endured no traffic loading during the study. The PRF sections were used for examining the feasibility of the micro-cracking procedure applying to the typical CSD and CTD layers and directly observing cracks on the bases due to shrinkage. Table 2 provides the factorial design of all the test sections, including individual base design criteria and base thicknesses.

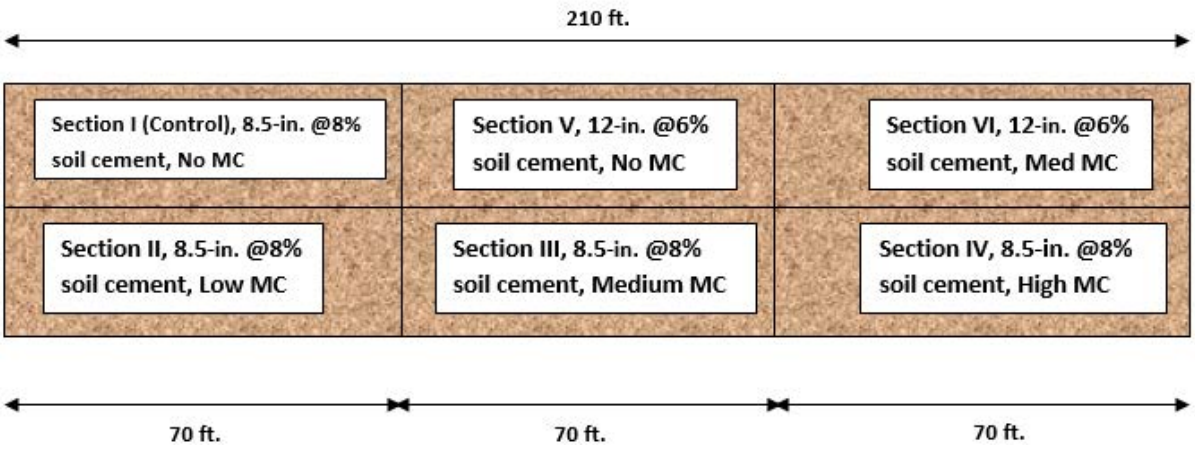

Figure 6
Layout of PRF sections

Table 2
PRF micro-cracking test section design

Section No.	Length (ft.)	Base Course thickness (in.)	Base Course 7-day UCS (psi.)	Micro-cracking
I	70	8.5	≥300	No micro-cracking
II	70	8.5	≥300	Low MC*
III	70	8.5	≥300	Medium MC
IV	70	8.5	≥300	High MC
V	70	12	≥150	No micro-cracking
VI	70	12	≥150	Medium MC

*MC = Micro-cracking

As listed in Table 2, the dimension of the PRF test sections was approximately 70-ft. long and 11-ft. wide. Sections I, II, III, and IV had an 8.5-in. CSD base designed with a minimum 7-day UCS of 300 psi. In these sections, section I served as a control section and the rest of the sections were subjected to different levels of micro-cracking (i.e., low, medium, and high) in terms of the magnitude of modulus (or stiffness) reduction. Sections V and VI had a 12-in. CTD base designed at a minimum 7-day UCS of 150 psi. In the two sections, Section VI was subjected to a medium level of micro-cracking, while Sections V served as a control section.

In the construction of the PRF test sections, a silty-clay soil consisting of 47.7% silt and 30% of clay was used in the base construction. The liquid limit (LL) and the plasticity index (PI) of the soil were 32 and 14, respectively. The optimum moisture content of the soil was 18.5% corresponding to a dry density of 104 pcf. Figure 7 shows the unconfined compressive

strength test results of the soil cement mixtures with varying cement contents. Based on the AASHTO soil classification, it was classified as an A-6 soil. According to the DOTD's roadway design specification, the minimum 7-day UCSs for a cement treated soil base and a soil cement base should be 150 and 300 psi, respectively. To meet the specification, the cement treated soil bases in Sections V and VI had a 6% cement content by volume, while those in Sections I-IV had a cement content of 8%.

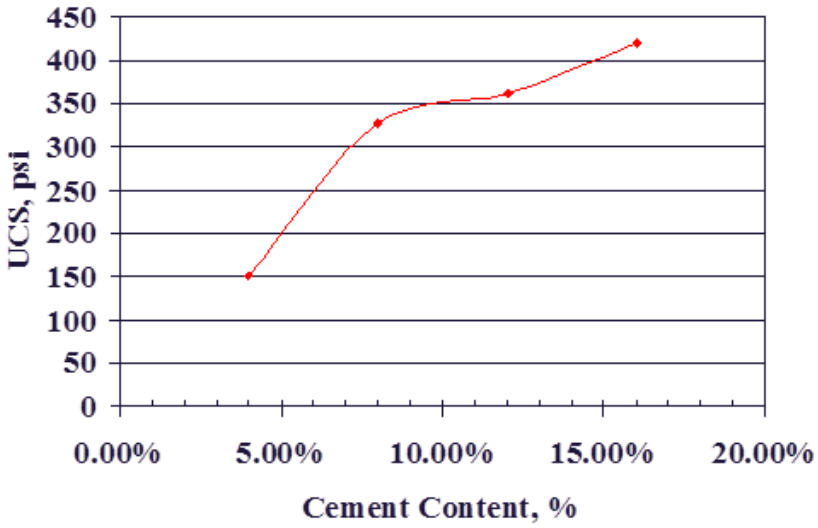

Figure 7
7-day UCS of soil-cement mixtures with varying cement contents

After the construction, all the sections were sprayed with water and covered by a plastic sheet for a 65-hour curing. On the day of micro-cracking, the plastic sheet was removed so that the test sections could be dried for a few hours.

The research team used an FWD to monitor the reduction in base modulus due to micro-cracking [Figure 8 (a)]. In addition, two other portable devices, LFWD [Figure 8(b) and 8(c)] and Humboldt Geogauge [Figure 8(d)], were also employed during the application of micro-cracking to investigate the feasibility of using a portable device for controlling the quality of the micro-cracking process.

(a) Falling weight deflectometer (FWD)

(b) Light falling weight deflectometer (LFWD), DYNATEST

(c) Light falling weight deflectometer (LFWD), ZORN

(d) Geogauge

Figure 8
Monitoring stiffness reduction of bases using FWD, LFWD, and Geogauge

Micro-Cracking

The micro-cracking process was carried out using a 12-ton vibrating roller, CAT CB54, as shown in Figure 9. As the roller was 5.5-ft. wide and the width of each test section was 11 ft., two passes of compaction were applied in parallel to cover the whole surface of a test section and were considered as one full pass of micro-cracking. The number of passes

applied to each micro-cracking section was determined by the modulus (or stiffness) reduction back-calculated according to the FWD results after each roller pass.

Figure 9
Roller compactor used for the micro-cracking process at PRF

At the beginning, sections II, III, and IV all underwent three full passes of compaction with a low amplitude and a high speed. The reduction in modulus, however, was insignificant. The roller compactor was then operated at a high amplitude and a low speed (about 0.42 mph) for the remaining number of passes. In total, both the sections II and III received six passes of compaction, whereas, sections IV and VI had ten and four passes, respectively. Table 3 shows the average stiffness reductions of all the micro-cracking sections monitored by the FWD before and after the roller compaction. As shown in the table, after the application of micro-cracking, none of the sections achieved a modulus reduction higher than 50%. There may exist a certain limit in the modulus reduction of the cement bases under roller compaction. After six to ten passes of compaction, no additional modulus reduction could be achieved for the 8.5-in. soil cement base. This is the reason that the research team chose a six-pass of compaction for both the sections II and III, and a ten-pass for the Section IV. In other words, the original research plan to achieve different levels of micro-cracking on sections II, III and IV was not able to be fulfilled due to a possible limit in the base modulus reduction. A similar situation happened on the 12-in. cement treated base after four passes of compaction. Four passes of low amplitude and high vibration rolling were conducted on Section VI and achieved a medium reduction in base modulus of 46.4%. It should be noted that the average initial modulus of section VI (i.e., a 12-in. cement treated soil base) was

higher than those of sections II, III, and IV, all of which had an 8.5-in. soil cement base. Figure 10 shows the surface of Section IV after the application of micro-cracking.

Table 3
Base modulus reduction of PRF test sections determined by FWD results

Section	Base Modulus (Before micro-cracking), ksi	Base Modulus (After micro-cracking), ksi	Reduction, %
II	86.9	58.4	32.8
III	87.5	55.0	37.1
IV	111.5	75.9	32.0
VI	192.0	102.8	46.4

Figure 10
Surface of Section IV after 10 passes of micro-cracking

Table 4 shows the average modulus reductions before and after the micro-cracking monitored by the LFWD. The LFWD results listed in Table 4 are somewhat different from those in Table 3, which were back-calculated based on the FWD results. One issue associated with the LFWD measurement was its repeatability. Although the LFWD did not provide a consistent modulus reduction after each roller pass as the FWD did, the LFWD did show a similar reduction trend for the four micro-cracked sections. Therefore, because of its portability and easy to operate, it is suggested to use an LFWD device in monitoring the

modulus reduction of soil cement bases during the application of micro-cracking in the field when an FWD device is not readily available.

Table 4
Base modulus reduction of PRF test sections determined by LFWD results

Section	Base Modulus (Before micro-cracking), ksi	Base Modulus (After micro-cracking), ksi	Reduction, %
II	148.3	137.6	7.2
III	135.5	118.0	12.9
IV	282.0	141.4	49.9
VI	301.1	204.8	32.0

Note that using a geogauge in monitoring the modulus reduction was not successful in this study due to its significantly unstable measurements.

After the application of micro-cracking, all the PRF sections were covered by a plastic sheet for curing of three months. During the curing, FWD, LFWD, and visual cracking survey were continuously conducted and the corresponding data were recorded. After removal of the Visqueen plastic sheet, LFWD and cracking survey were performed more frequently. In the end of the project (approximately after three and half years of construction), beams were cut from the selected sections to investigate the cracking pattern, if any, along the wall of the cut-out beams.

LA1003 Test Sections

A rehabilitation project (state project number H.010533.5) located in LA 1003 of Assumption Parish was selected as one of the field micro-cracking projects in this study. This project was originally called for a pavement structure of 3.5-in. asphalt concrete over 12-in. cement-treated soil base for a design annual daily traffic (ADT) of 850 and design ESAL of 604,977 in 20 years. The project construction plan was then modified to construct four 1000-ft. long test sections (Section I through IV) and an 818-ft. long section (Section V) as illustrated in Figure 11. It should be noted that the following terminologies were used in Figure 11:

- Cement stabilized design (CSD): an 8.5-inch-thick cement stabilized base with a minimum 7-day USC of 300 psi;
- Cement treated design (CTD): a 12-inch-thick cement treated base with a minimum 7-day USC of 150 psi;

- Asphalt surface treatment (AST);
- Micro-cracking (Mcrack).

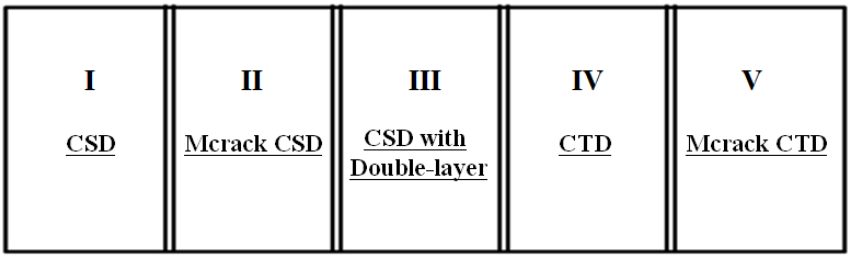

I - Control Section: CSD
II - Treatment Section 1: Mcrack CSD
III - Treatment Section 2: CSD with double-layer AST
IV - Control Section: CTD
V - Treatment Section 3: Mcrack CTD

Figure 11
Micro-cracking test section plan

A non-plastic silty soil, classified as A-4 according to the AASHTO soil classification, was used in the base construction, which consisted of 48% silt and 14% of clay. The base construction followed a common procedure used in Louisiana. Note that sections I, II and III used an 11% of cement content to achieve a minimum value of 7-day UCS of 300 psi, whereas both the sections IV and V used an 8% of cement content to achieve a minimum 7-day UCS of 150 psi. Figure 12 shows the layout of the constructed test sections on LA 1003.

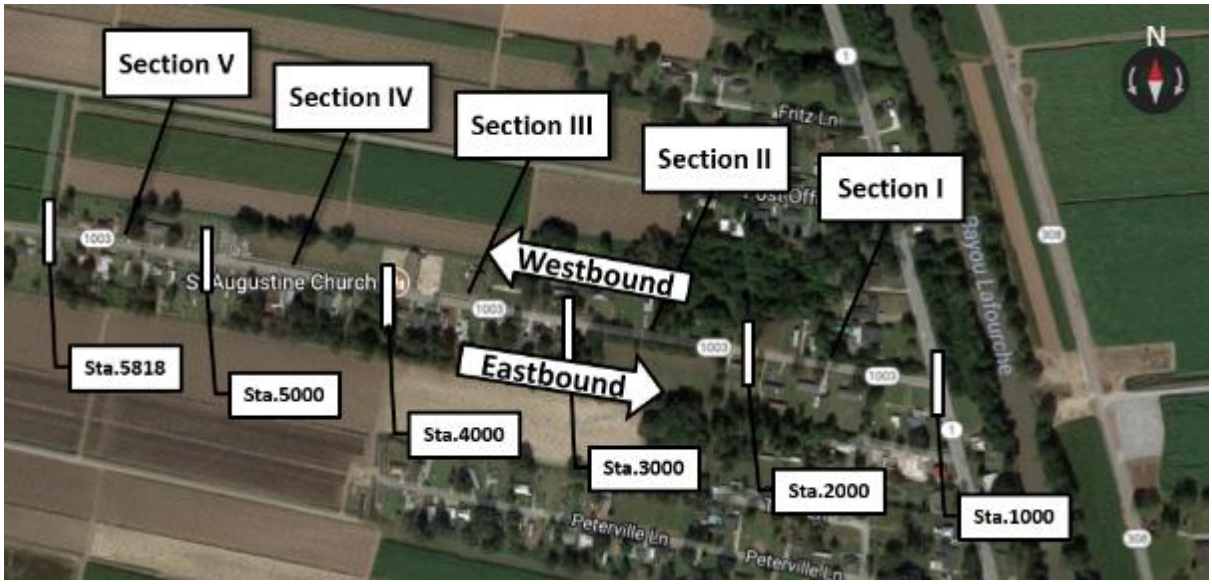

Figure 12
Constructed test section on LA 1003

Micro-Cracking

To monitor the application of the micro-cracking process, the research team visited the LA1003 project site on September 26, 2014, which was three days after the completion of the base construction. No curing membrane was used to cover the bases prior to the micro-cracking. Instead, the contractor was instructed to water the constructed bases at least once a day. In this project, a 14.5-ton RR-24 Hamm HD-140 vibratory roller as shown in Figure 13(a) was used for micro-cracking of the two base layers. Both the bases in the sections II and V underwent the micro-cracking process. For each of the micro-cracking test section, a preliminary testing was conducted on a 200-ft. portion to determine the number of roller passes required to reduce the base modulus by approximately 40% to 60%. After the number of passes was determined, the contractor performed the determined number of roller passes on the rest portion of each test section. Since the FWD devices were not available at the time of the micro-cracking application, an LFWD (ZORN -ZFG 2000) was used to monitor the base modulus reduction, as shown in Figure 13(b).

(a) (b)

Figure 13
(a) Roller for micro-cracking (b) LFWD used on LA1003

Based on the experience of the PRF test sections, the micro-cracking procedure was accomplished by operating the roller over the base course at a low speed but the highest frequency and amplitude of the machine. After each pass (a pass consisted of one forward rolling and one backward rolling), the LFWD readings were recorded at three selected locations with 50-ft. spacing to obtain an average base modulus value after micro-cracking. This sequence was continued until the desired modulus reduction was achieved. In the end, it was found that Section II (the 8.5-in. soil cement base with a cement content of 11%) required 10 roller passes to achieve a modulus reduction of 37%. Section V (the 12-in. cement treated base with a cement content of 8%) underwent 12 passes but achieved a modulus reduction of 31%. Table 5 shows average LFWD modulus values before and after the micro-cracking on both sections II and V of LA1003.

Table 5
Base modulus reduction of the LA 1003 sections determined by LFWD results

Section	Base Modulus (Before micro-cracking), ksi	Base Modulus (After micro-cracking), ksi	Reduction, %
II	132.88	84.02	36.77
V	122.83	84.38	31.30

Figure 14 shows a base surface after the micro-cracking. In general, only a few fine cracks were observed on the surface of the micro-cracked base courses. No surface break-ups were

found after the micro-cracking. This may indicate that the micro-cracking technique did not result in pavement damage during the construction.

Figure 14
Typical base surface after the micro-cracking

LA 599 Test Sections

A pavement reconstruction project (state project number H.009535.6) on LA 599, near Monroe, LA, was selected as another field micro-cracking test site in this study. The entire roadway reconstruction was 9.5-mile long, including bridges and curves. A change order was then made by the DOTD to construct three 1000-ft. long test sections (Section I, IV and V) and a 1077-ft. section (Section II) between station 71+95 and station 123+30 as illustrated in Figure 15. Each of the four test sections consists of a pavement structure of a 3.5-in. asphalt concrete over either a 12-in. cement-treated base or an 8.5-in. soil cement base over an existing subgrade. Note that the soil materials used in the construction of test sections were recycled from the soil cement bases underneath the top aged asphalt concrete. The pulverized existing soil cement layer was mixed with fresh cement by a cement content of 6% for the construction of the 12-in. cement treated bases (in sections I and II) and at a

cement content of 9% for the construction of the 8.5-in. soil cement bases (in sections IV and V), as shown in Figure 15.

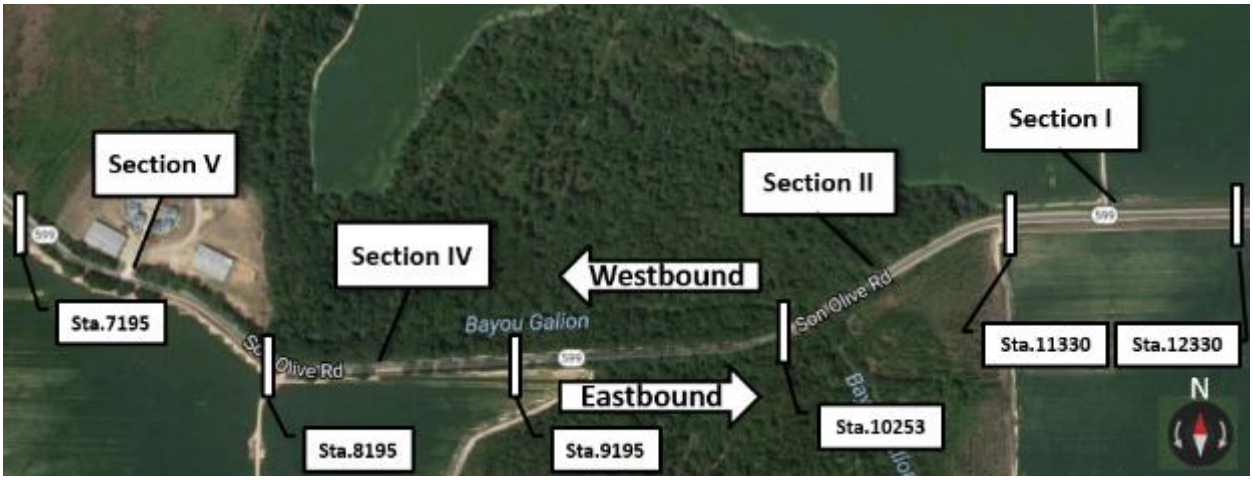

Figure 15
Section arrangement of project LA 599

Micro-Cracking

To perform and monitor the implementation of the micro-cracking, the research team visited the LA 599 project site on August 3, 2015, which was three days after the completion of the base construction. Similar to the curing of the LA 1003 test sections, curing membrane was not used to cover the completed base courses but the base surfaces were watered at least once a day. In this project, the same type vibratory roller (i.e., 14.5-ton RR-24 Hamm HD-140 roller) as that used for the LA 1003 test sections was operated for the application of micro-cracking, as shown in Figure 16. At this test site, micro-cracking was performed on both the bases in sections II and IV. FWD and LFWD were employed to monitor the base modulus reduction and readings were taken at five stations on each of the micro-cracking sections. Similar to the LA 1003 test sections, a preliminary testing was conducted on a 200-ft. portion of each micro-cracking section to determine the number of roller passes required to reduce the base modulus by the desired percent reduction (usually 40% to 60%).

Micro-cracking was first performed on a 200-ft. portion of Section II. The base modulus decreased consistently only in the initial four passes with a total modulus reduction of less than 10% and no surface fine (or micro) cracks were observed at the time. After the initial passes, the base moduli back-calculated by both the FWD and LFWD at varying stations and passes became unstable and fluctuated irregularly with a variation of approximately 20%. Because no additional modulus reduction could be obtained with the increasing rolling passes and the base course seemed unchanged after each roller pass, the micro-cracking rolling process ceased at 17 roller passes and the corresponding modulus reduction determined by

the FWD was found to be 33.6%. Figure 17 shows the surface of Section II after the application of micro-cracking. The research team did not observe any base damage or surface break-ups but a few fine cracks as shown in Figure 17. Based on the results, micro-cracking was performed on the rest of Section II by using 17 full roller passes. A similar micro-cracking procedure was adopted in Section IV. However, the back-calculated modulus of Section IV (i.e., the 8.5-in soil cement base) showed a more consistent trend of decreasing as compared with that of Section II. It was found that the base modulus was reduced by 35.2% after 18 passes in the preliminary test and additional passes became relatively ineffective in the modulus reduction. Thus, 18 passes were recommended for the remaining part of Section IV.

Figure 16
Micro-cracking with vibratory roller (HD 140)

Figure 17

Section II after 17 passes

Table 6 presents the average modulus values of Sections II and IV back-calculated based on the FWD results measured before and after the micro-cracking. It should be pointed out that the LFWD readings were found not sensitive enough to measure the modulus reduction of the LA 599 test sections. The possible reasons may include (1) the surface of the bases was not smooth and level, causing errors in the LFWD readings and (2) the LFWD load was too small to detect a change in the base modulus. Table 7 lists the general information of the test sections at these three sites.

Table 6

Base modulus reduction of the LA 599 sections determined by FWD results

Section	Base Modulus (Before micro-cracking), ksi	Base Modulus (After micro-cracking), ksi	Reduction, %
II	30.7	20.4	33.6
IV	45.4	29.4	35.2

Table 7

Information of all the test sections

Characteristics	PRF test sections	LA 1003 test sections	LA 599 test sections
Type	Uncovered base and newly built	Covered and reconstructed	Covered and reconstructed
Thickness	8.5" (CSD), 12" (CTD)	8.5" (CSD), 12" (CTD)	8.5" (CSD), 12" (CTD)
Cement Content	8% (CSD), 6% (CTD)	11% (CSD), 8% (CTD)	9% (CSD), 6% (CTD)
Soil (Base)	A-6	A-4	Recycled soil cement
Top Asphalt Layer	-	2" binder course, 1.5" wearing course**	2" binder course, 1.5" wearing course
ADT	-	850 (2013), 950 (2023)	375 (2015), 400 (2025)
Traffic Char.	-	D = 55%, K = 10%, T = 8%	D = 55%, K = 10%, T = 12%
Initial modulus, ksi	86.9, 87.5, 111.5 (CSD), 192 (CTD)	36.9 (CSD), 35.7 (CTD)*	45.4 (CSD), 30.7 (CTD)
Roller Weight	11.9 Ton	14.5 Ton	14.5 Ton
Roller Passes	6,6, 10 (CSD) and 4 (CTD)	10 (CSD), 12 (CTD)	18 (CSD), 17 (CTD)
Roller Type	CAT CB54	HAMM HD+ 140 VV HF	HAMM HD+ 140 VV HF

Roller Speed	0.42 mph	1.05 mph	1.8 mph
Roller Width	67”	84.3”	84.3”
Roller Frequency		Full	3000 vpm
Curing Time (before Micro-cracking)	65 hours	48-72 hours	70-76 hours
Curing Method	Covered by a Visqueen plastic membrane after water spraying	Water Spraying	Water Spraying

* converted from the LFWD results.

** Section III of LA 1003 is CSD with Double Layer AST

In-Situ Tests Performed

Road Surface Profiler

The modified Dynatest Road Surface Profiler technology 5051 Mark III (RSP III) was used to survey the field projects, as shown in Figure 18. The operator interface of the RSP III is a Windows-based control program installed on a laptop. The data processing unit (DPU) consists of a single-board computer and one or more Profiler System Boards (PSB) attached to a backplane. The DPU collects data, processes data, and sends the processed data to the terminal via an Ethernet connection.

The RSP III collected data of International Roughness Index (IRI), ride number with precise transverse/longitudinal inertial, and profile elevations. The longitudinal profile was measured based on the South Dakota method. An accelerometer and a laser sensor were employed to acquire the vertical inertial movement of the vehicle and the distance between the road surface and the vehicle. More than five laser sensors were used to detect the transverse profile and rutting. The RSP III can also be used to collect data regarding pavement textures and faulting.

The measurement of the RSP III was in compliance with the AASHTO R 56-14 “Standard Practice for Certification of Inertial Profiling Systems” and the ASTM E950/E950M-09 “Standard Test Method for Measuring the Longitudinal Profile of Traveled Surfaces with an Accelerometer Established Inertial Profiling Reference”. During the survey, the IRI and rutting values were collected every 25 ft.

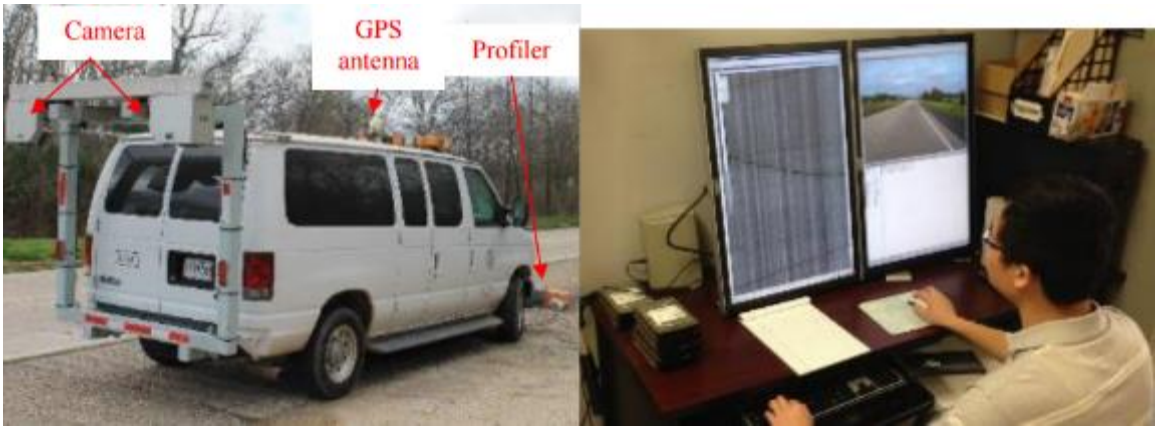

Figure 18
Dynatest RSP III and workstation

Cracking Survey

The visual crack survey was conducted on both the PRF sections and field test sections (LA 1003 and LA 599) to record the types, lengths, widths, and locations of the cracks appeared on the surface of the bases or asphalt layers. The crack survey was performed at several time intervals to observe the initiation and propagation of cracking. Figure 19 shows one longitudinal crack observed on the pavement surface of LA 1003.

Figure 19
Crack survey on LA 1003

Pavement Sampling

Coring was conducted on the selected cracking locations to collect samples for the investigation of the cracking behavior of the micro-cracked sections and control sections. The SIMCO 255 PTC drilling rig, as shown in Figure 20, was utilized and cores with a 6-in. diameter for both the asphalt and base layers were drilled and collected.

Figure 20
Pavement sampling on LA 599

The locations of coring were marked on both the longitudinal cracks and transverse cracks during the crack survey. The coring barrel was located accurately on the marked locations to intersect with the cracks so that the mechanism of the cracks can be investigated based on the cores. In addition, effort was made to assure that the drilling depth would be at least 10 in. so that the entire asphalt concrete and the base layer will be drilled through. The cores were retrieved from the coring barrel with extra caution to obtain integrated samples. After the coring, the drilling holes were backfilled with hot asphalt mixes and then compacted manually.

Falling Weight Deflectometer (FWD) and Heavy Weight Deflectometer (HWD)

The Falling Weight Deflectometer (FWD) and Heavy Weight Deflectometer (HWD) are devices that closely approximates the effect of a moving wheel load, both in magnitude and duration. The FWD and HWD devices are configured to have a 9-sensor array, with sensors spaced at 0, 8, 12, 18, 24, 36, 48, 60, and 72 in. away from the load plate. Different load magnitudes can be generated by changing the mass of weight and drop height. Once the load is applied, the deflections are measured by a precise heavy-duty load cell installed above the

loading plate. By means of high-speed transducers, the deflection data measured from the 9 sensors (D1-D9) are acquired and stored. Through a back-calculation process or tool, for instance, ELMOD6 (a back-calculation software developed by Dynatest), the resilient modulus (elastic modulus) of each layer can be back-calculated.

In this study, Dynatest model 8000 FWD and Dynatest 8081 HWD test systems were used to measure the stiffness of pavement structures. A 9,000-lb. load was applied through a circular plate to cause the deflecting of the pavement. ELMOD6 was used for the back-calculation of the FWD raw data. Deflection basin analysis was also carried out. The deflection values of overall pavement structure (D1) and deflections related to the base layer (D3-D5) on all test stations were used to compare the performance of micro-cracked sections and their control sections. The pavement effective structure numbers were then analyzed based on the FWD data. The HWD test was also conducted near cracking locations to investigate the cracking behavior of pavement structures.

Light Falling Weight Deflectometer (LFWD)

LFWD is a portable NDT device as an alternative to the FWD, as shown in Figure 8(b) and 8(c). As the falling weight drops onto the loading plate, the impact force and the deflection of the loading plate are measured by built-in sensors. Compared with the FWD, LFWD has a much lower load capacity and is much less expensive. The mass of the dropping weight and the size of the loading plate vary in terms of product models. There are two types of commonly-used LFWD devices, Dynatest 3031 and ZFG 2000 (Zorn LFWD), which have different working procedures. Dynatest 3031 gives stiffness values for each drop, while ZFG 2000 requires three preloading drops and then three more drops are required to provide three deflection values and an average modulus [Average modulus = 1.5×150×0.1/ (Average deflection)].

In this study, both the two types of LFWD devices were used. Three deflection values for a single station were read for consistency checking. If the variation of the three deflection readings was higher than 15%, the LFWD test was repeated.

Geogauge

Geogauge is a type of portable device to measure the stiffness (in force per length) and the modulus (in force per area) of the ground. Unlike LFWD, Geogauge applies a vertical load by vibration (at 100 to 200 Hz) rather than the weight of the device. The vibration imparts very small displacements to the ground (usually less than 0.00005 in.), which provides a good estimation of the resilient behavior of the pavement under typical traffic loads. To make sure that the foot of the Geogauge has a good contact with the test material, a very thin sand

layer has to be used to prepare a flat surface. The thickness of the sand layer is relatively small compared to the tested layer thickness and its influence can be neglected. The entire measurement takes about one minute. Note that the Geogauge test was only applied on PRF test sections but did not yield good results.

Back-Calculation of Flexible Pavement

NDT deflection testing has been widely used for structure evaluation on constructed pavements and it is also recommended in the AASHTO 1993 design procedure *[26-28]*. FWD test is one of the widely used NDT techniques for this purpose. The FWD data can be applied to calculate subgrade resilient modulus and structural number to estimate the structure condition of the pavement sections with micro-cracked CSD/CTD base layers.

In an FWD test, when the distance of a displacement transducer from the load center is sufficiently large, it is supposed that the measured deflection from pavement surface is most entirely due to the subgrade deformation. The subgrade resilient modulus can be back-calculated by equation (7).

$$M_R = \frac{0.24P}{D_r r} \tag{7}$$

where,

M_r = the back-calculated subgrade resilient modulus, psi;

P = the applied load, lb;

r = the distance of the displacement transducer from the center of the load plate, in.;

D_r = the deflection measured by the transducer, in.;

In this study, both the FWD and HWD tests were conducted with an applied load of 9000 lbs. The obtained deflection of D6 with a distance of 36-in. away from the center of the loading plate was normalized and then used in equation (7). Temperature adjustment was not conducted since the measured deflection was subject to the subgrade layer, of which the deformation is not influenced by temperature.

With the determined M_r, equation (8) was then employed to determine the effective modulus (E_p) of all pavement layers above subgrade.

$$D_1 = 1.5Pa \left[\frac{1}{M_r \sqrt{1+[\left(\frac{D}{a}\right) * \sqrt[3]{\frac{E_p}{M_r}}]^2}} + \frac{1-\frac{1}{\sqrt{1+(\frac{D}{a})^2}}}{E_p} \right] \quad (8)$$

where,
D_1 = the deflection measured at the center of the FWD/HWD plate (adjusted to 68°F), in.;
a = the radius of the FWD/HWD load plate, in.;
D = total thickness of pavement layers above the subgrade, in.;
E_p = the effective modulus of all pavement layers above subgrade, psi.

In equation (8), E_p was determined by trial and error in Excel software. The effective structural number was then calculated according to equation (9).

$$SN_{eff} = 0.0045 D \sqrt[3]{E_p} \quad (9)$$

where, SN_{eff} = the effective structural number of an existing pavement.

DISCUSSION OF RESULTS

PRF Sections

Figure 21 shows the overview of the constructed sections at PRF. After the micro-cracking, in-situ cracking survey including FWD and LFWD tests were performed periodically on these sections.

Figure 21
Overview of PRF test sections

Figure 22 presents the average LFWD moduli measured by the Dynatest LFWD device at various durations after three months of construction. It is known that LFWD moduli generally reflect an overall stiffness of a pavement structure. Considering the possible unavailability of the FWD device and the simple pavement structures of all the PRF sections (CSD/CTD base courses over the same existing subgrade), the LFWD modulus reading was chosen as the stiffness indicator of the six soil cement sections. As shown in Figure 22, the moduli of all the micro-cracked base sections (sections II, III, IV and VI) increased significantly due to curing over time after micro-cracking. As shown in the figure, the base course in Section I (the 8.5-in. control section) was stiffer than the micro-cracked bases of Sections II and III before and after the micro-cracking. This result could be attributed to the construction variation since Sections II and III were built on a different lane as compared to

Section I, as shown in Figure 21. On the other hand, Sections V and VI, constructed on the same lane, demonstrated similar stiffness values after 69 days, indicating that, as other studies have reported, the micro-cracking process would not damage the base in the long run *[4, 6]*.

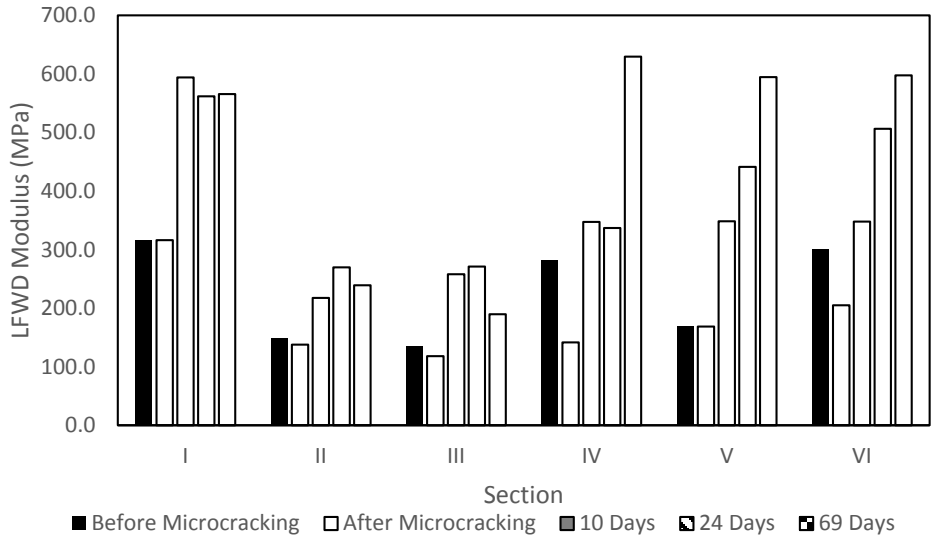

Figure 22
Average LFWD moduli of PRF test sections

The test sections were monitored continuously for shrinkage cracks after the construction. Figure 23 shows the crack-mapping results of the six sections surveyed on April 25, 2014. As seen in Figure 23, many closely spaced short hairline cracks appeared on the surfaces of all micro-cracked sections (i.e., Sections II, III, IV and VI). Those cracks are likely to be the shrinkage cracks due to cement hydration. For the control sections, Sections I and V, the number of fine network cracks was relatively low. Instead, a couple of longitudinal cracks were observed. These cracking performance results indicate that the micro-cracking method seems to be able to reduce or eliminate long shrinkage cracks on both the CSD and CTD bases.

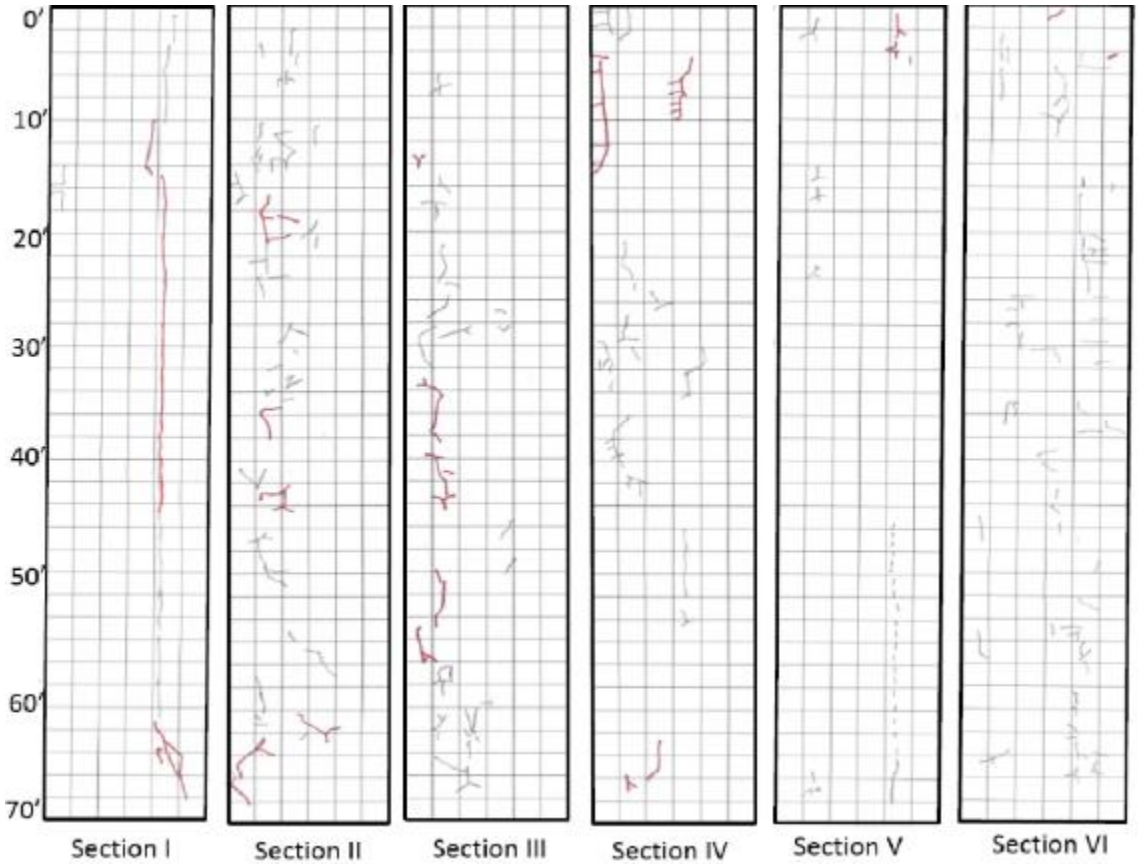

Figure 23

PRF Crack-mapping as of April 25, 2014

However, a further crack survey found that the crack density and patterns observed earlier on each of the test section changed significantly after in-situ loose materials on the surface (e.g., soils, cement dust, and small aggregates) were removed by broom. Figure 24 shows the crack-mapping results obtained on June 12, 2014. As shown in the figure, the crack patterns were completely different to those in Figure 23. The length of the longitudinal cracks on Sections I and V became shorter, while transverse cracks became more visible on the micro-cracked sections. However, almost all the short hairline type cracks were disappeared. An additional crack survey conducted later found that all previously observed surface shrinkage cracks were gone after the surfaces were cleaned up. This result indicates that all the cracks observed on the PRF test sections may be thin and shallow.

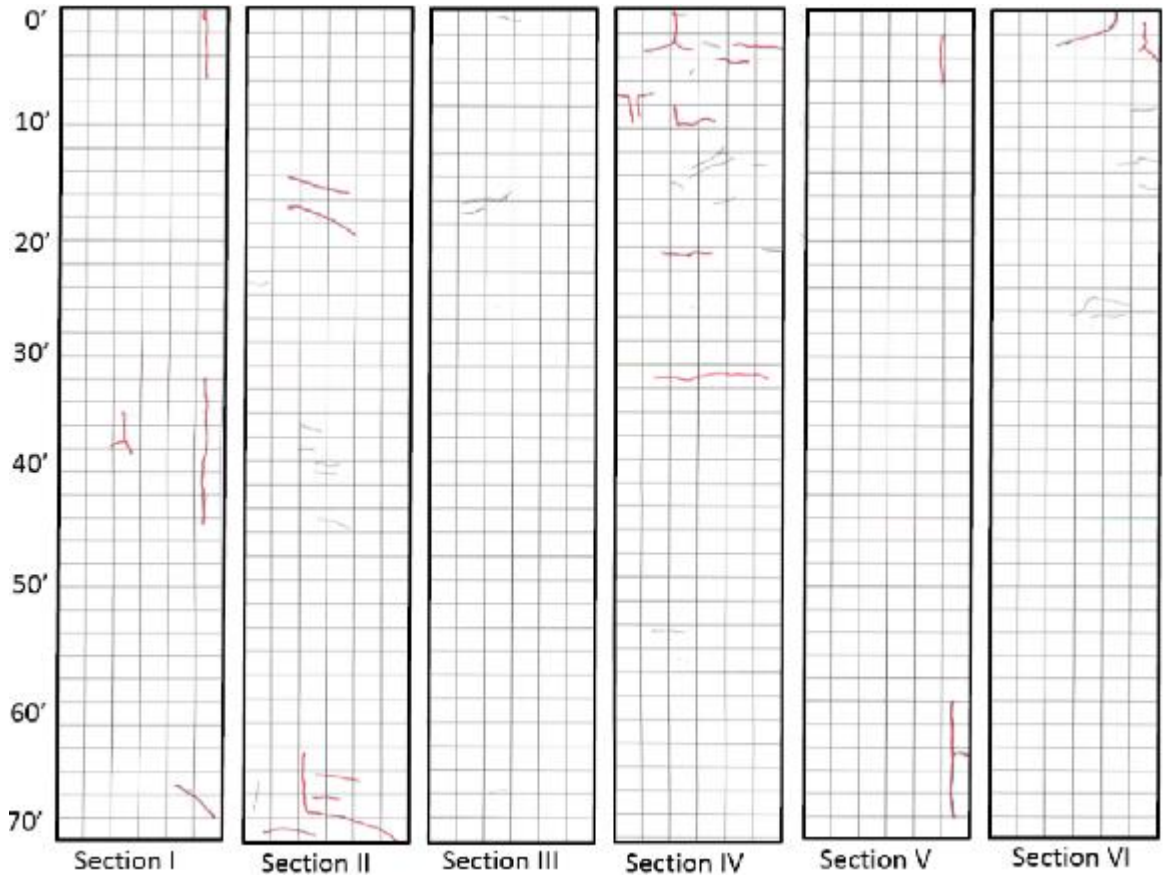

Figure 24
PRF crack-mapping as of June 12, 2014

To determine if any shrinkage cracks might hide from the surface or propagate downward, saw-cut beams were collected on several selected locations on the soil cement sections (section I, II, and III). Figures 25 and 26 show the saw-cut beams on Sections I and III, respectively.

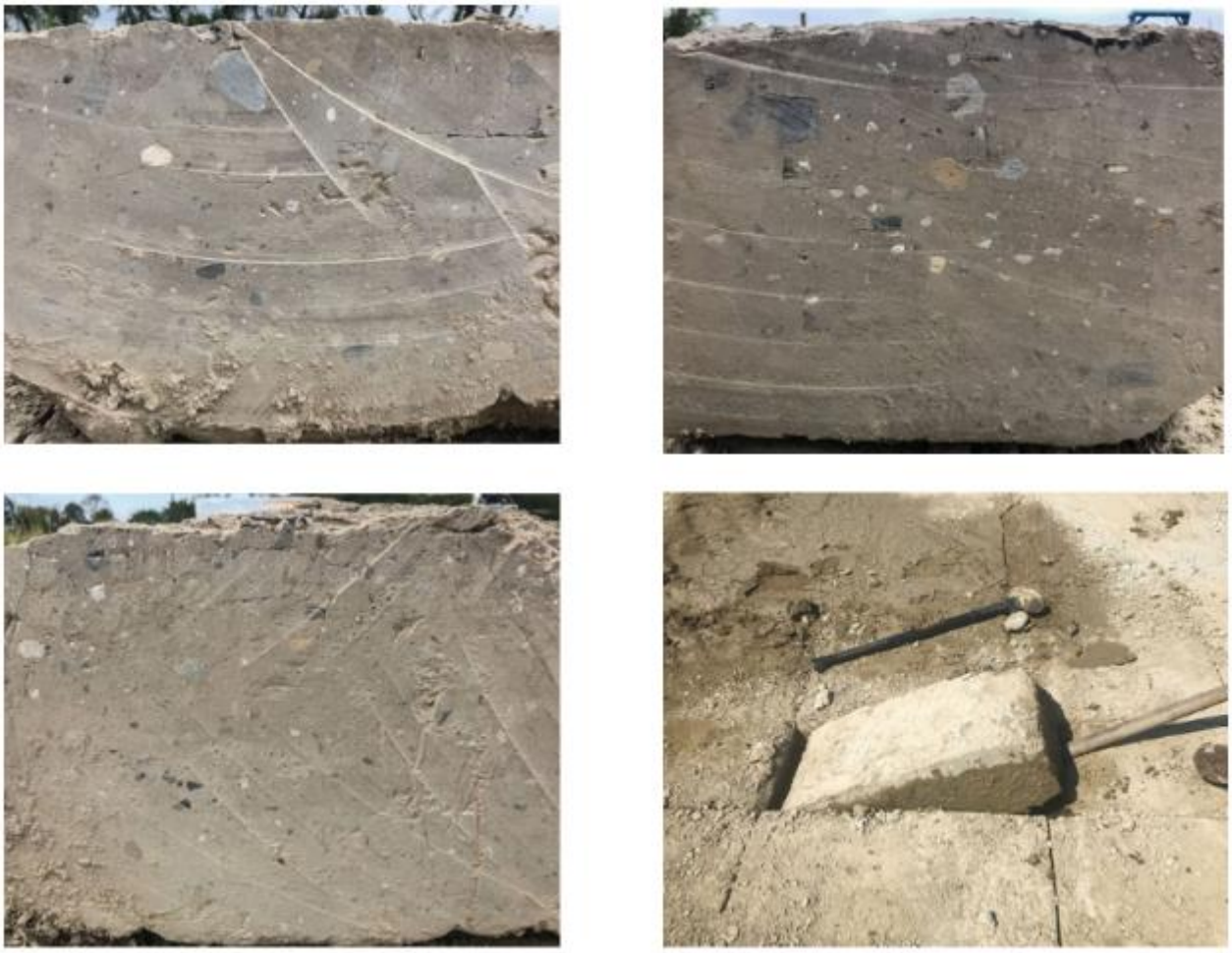

Figure 25
Saw-cut beam in Section I

Figure 26
Saw-cut beam in Section III (micro-cracked section)

To evaluate the long-term base stiffness after micro-cracking, additional FWD tests were performed in May 2015, approximately eighteen months after construction. The back-calculated moduli of all the PRF sections are presented in Figure 27. As expected, the base moduli were found similar to each other for the same type of base courses. In general, the average base moduli were 464 ksi for the soil cement bases and 231 ksi for the cement treated soil bases.

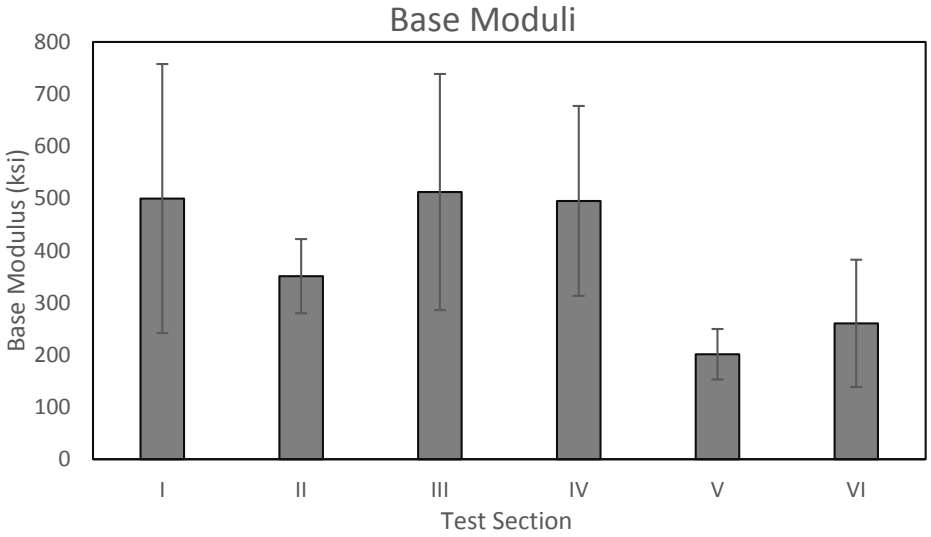

Figure 27
Back-calculated moduli of PRF bases as of May 2015.

In summary, no major shrinkage cracks developed on the PRF sections and the possible reasons are as follows:

- Sufficient curing time and moisture;
- Abnormal micro-cracking process;
- Short section length; and
- No traffic loading.

LA 1003 Test Sections

Figure 28 shows the plan view of the five test sections constructed in LA 1003. Each test section is approximately 1000-ft. long and 24-ft. wide, including one westbound (WB) lane and one eastbound (EB) lane. All the sections have a surface layer of 3.5 in. HMA. Especially, Section I (control) and Section II (micro-cracked) include an 8.5-in. soil cement base; whereas Sections IV (control) and V (micro-cracked) consist of a 12-in. cement treated base. Section III is a special section with a double chip seal layer over an 8.5-in. soil cement base. Micro-cracking was accomplished with a 14.5-ton roller on September 26, 2014. More details can be found in the Methodology section of this report.

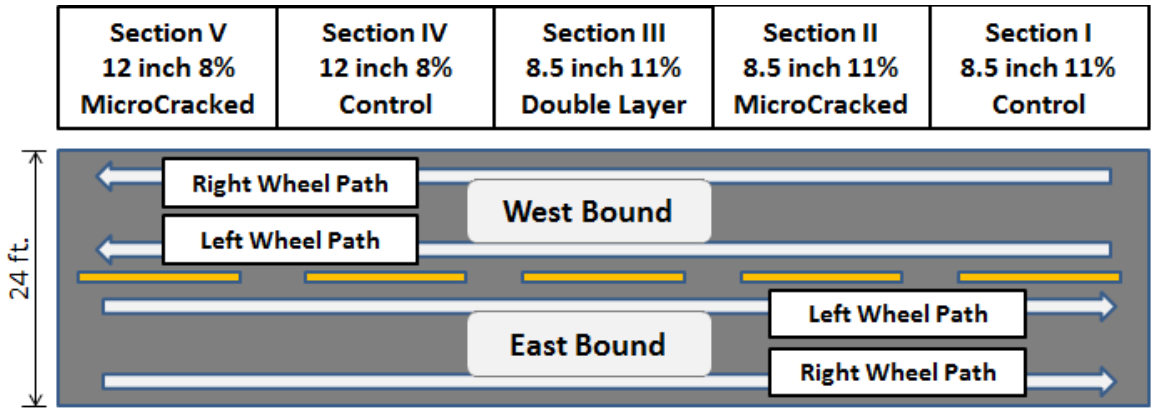

Figure 28
Plan view of LA1003 test sections

On July 10, 2017, the research team performed the final inspection of crack performance as well as the high-speed digital pavement surface survey on LA1003. The cracking survey results are summarized in Tables 8 and 9. Overall, all sections except Section II exhibited a certain amount of cracks after three years of pavement service. As indicated in Table 8, most of the cracks may be considered as hairline-type, fine cracks (width < 3 mm), and the majority are along the longitudinal (or traffic) direction. However, Sections I, IV, and V (the micro-cracked 12-in. cement treated section) did show some transverse cracks, which appear to be the reflective cracks related to the shrinkage cracks of the cement stabilized or treated bases.

Table 8

Total crack length and number of cracks (in parentheses) of sections on LA 1003

Section	Severity (mm)	Transverse Cracks Total Length (No. of cracks)		Longitudinal Cracks Total Length (No. of cracks)	
		Eastbound	Westbound	Eastbound	Westbound
I	0-1				
	1-3	2 ft. (1)			
	3-5	4 ft. (1)	3 ft. (1)		
II	0-1				
	1-3				
	3-5				
III	0-1			44 ft. (2)	19 ft. (2)
	1-3			61 ft. (3)	48 ft. (3)
	3-5				
IV	0-1		4 ft. (1)	24 ft. (1)	59.5 ft. (9)
	1-3		4 ft. (1)		99 ft. (6)
	3-5				
V	0-1	17 ft. (3)	3 ft. (1)	90 ft. (4)	33 ft. (2)
	1-3	8.5 ft. (2)	5.5 ft. (2)		53 ft. (4)
	3-5				

Table 9

Summary of total cracking density (LA1003)

Section No.	Crack Length in feet per 100 ft. of pavement (1200 sq.ft.)		Total Crack Length in feet per 100 ft. of pavement (2400 sq.ft.)
	EB	WB	
I (8.5 in. control)	0.6	0.3	0.9
II (8.5 in. MC)	0	0	0
III (8.5 in.+ double layer)	10.5	6.7	17.2
IV (12 in. control)	2.4	16.7	19.1
V (12 in. MC)	14.1	11.6	25.7

Section I vs. Section II (8.5-in. Soil Cement Base)

Crack performance. Figures 29-31 show the eastbound and westbound views of Section I. Note that 'S1+715' means that the beginning of a crack on Section I is 715-ft. away from the starting point of the section. The locations of other cracks in this report

followed the same format. Only two transverse cracks were noticed on Section I as shown in Figure 29 and they are possibly reflective cracks due to the shrinkage of the soil cement base. Figures 32-33 show the pavement views of Section II and no surface cracks were found on Section II.

Figure 29

Transverse cracks near S1+715 on Section I of LA1003

Figure 30

Westside view of Section I on LA1003

Figure 31

Eastside view of Section I on LA1003

Figure 32

Westbound lane of Section II (first part) on LA1003

Figure 33

Westbound lane of Section II (second part) on LA1003

The cracking performances above may indicate that the micro-cracked soil cement section (Section II) performed slightly better than the non-micro-cracked section (Section I) in term of the reflective cracking. However, due to the relatively low crack density of the two test sections and the short duration (only three years) of low-volume roadway service, it may be too early to draw a conclusion.

Rutting and IRI performance. Pavement rut depth and longitudinal profiles were collected by LTRC's digital highway data vehicle (Figure 18 in Methodology). Figure 34 plots the measured rut depths along the length of each 1000-ft. section of both traffic directions. As shown in Figure 35, the measured rut depths of all the pavement sections in Figure 34 are relatively low, except the first 500-ft. long portion of Section I WB.

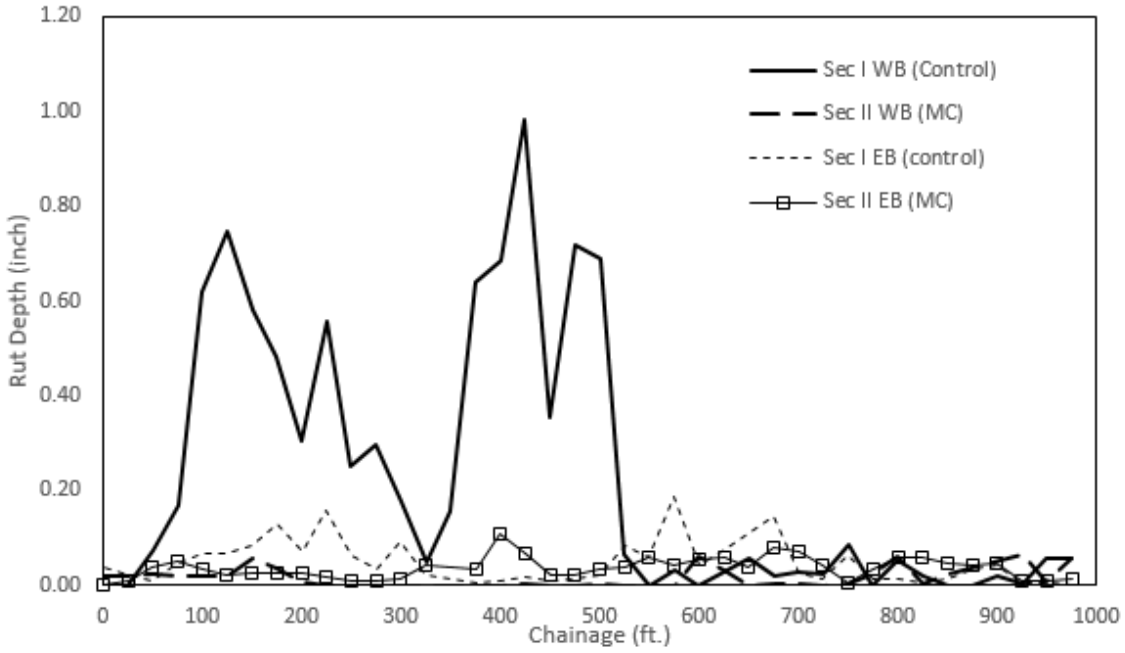

Figure 34
Measured rut depths of Section I & II on LA1003

A student's T-test was conducted to examine if there exists a significant difference between the average rut depth of the control and micro-cracked sections. The results are summarized in Table 10. In general, a p-value less than 0.05 indicates that the means of the two comparing datasets are significantly different from each other. As expected, Table 10

confirms that the average rut depth of Section I WB is significantly higher than that of other section in the comparison.

Table 10
Average rut depths of Sections I & II (8.5-in. control and micro-cracked sections) on LA 1003

Sections	Section I WB	Section II WB	Section I EB	Section II EB
Properties	8.5 in. 11% soil cement, Control section	8.5 in. 11% soil cement, MC section	8.5 in. 11% soil cement, Control section	8.5 in. 11% soil cement, MC section
Rutting Ave. (inch)	0.23	0.02	0.05	0.04
Standard Deviation	0.28	0.02	0.05	0.02
p-value	<0.0001		0.2239	

Figure 35 plots the measured IRI values obtained on the right-wheel paths of Sections I and II on both traffic directions. Similar to the rutting measurements, the first portion of Section I WB showed higher IRI values than its second portion. T-test results, as shown in Table 11, indicate that there is no significant difference between Section I and Section II in terms of IRI. The average IRI values of Section I WB, Section I EB, Section II WB, and Section II EB are 76.9, 83.5, 68.3, 73.7 in./mile, respectively.

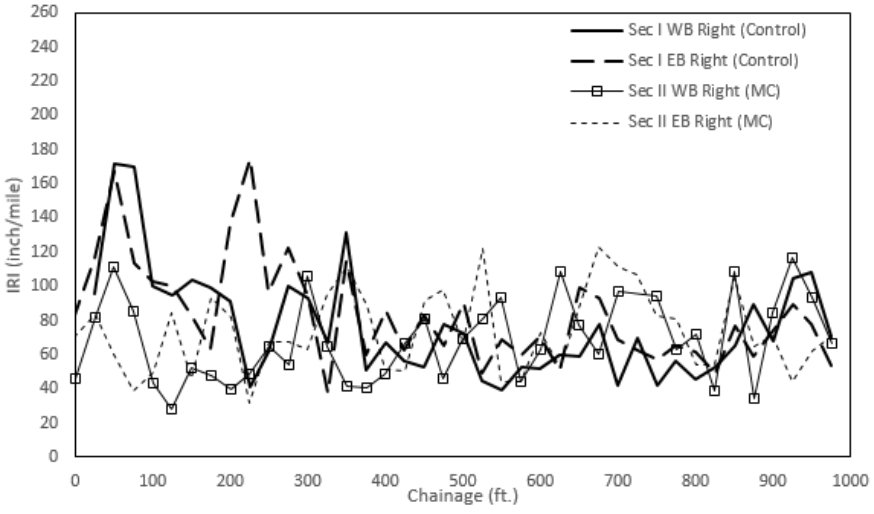

Figure 35
IRI values of Sections I & II on the right wheel paths

Table 11
Average IRIs of Section I & II on LA 1003

Bound and Lane	WB		EB	
Sections	I Control	II MC	I Control	II MC
IRI Ave. (inch/mile)	76.9	68.3	83.5	73.7
Standard Deviation	31.8	24.5	30.4	23.8
p-value	0.1863		0.1105	

FWD tests. Three FWD tests were conducted on LA 1003 on March 29, 2016, October 13, 2016, and July 12, 2017, which correspond to 553, 751, and 1,023 days after the base construction, respectively. The FWD tests were conducted at a 100-ft. interval on each test section. The obtained FWD deflection data were then normalized to 9000 lbs. loading and no temperature correction was made.

The FWD measured deflections are presented in Figure 36. In general, the higher D1 is, the lower of the pavement overall load carrying capacity is. A Higher D3-D5 indicates a lower base stiffness. As shown in Figure 36(a), the FWD deflection results generally confirm that the pavement structure of the Section I WB is weaker than other sections. The weakness may be directly related to its weaker soil cement base layer, as indicated in Figure 36(b).

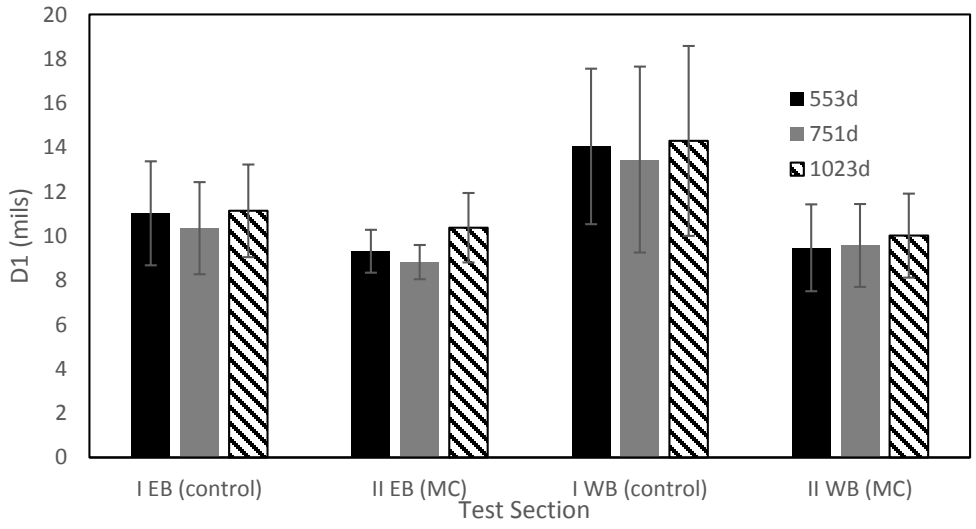

(a)

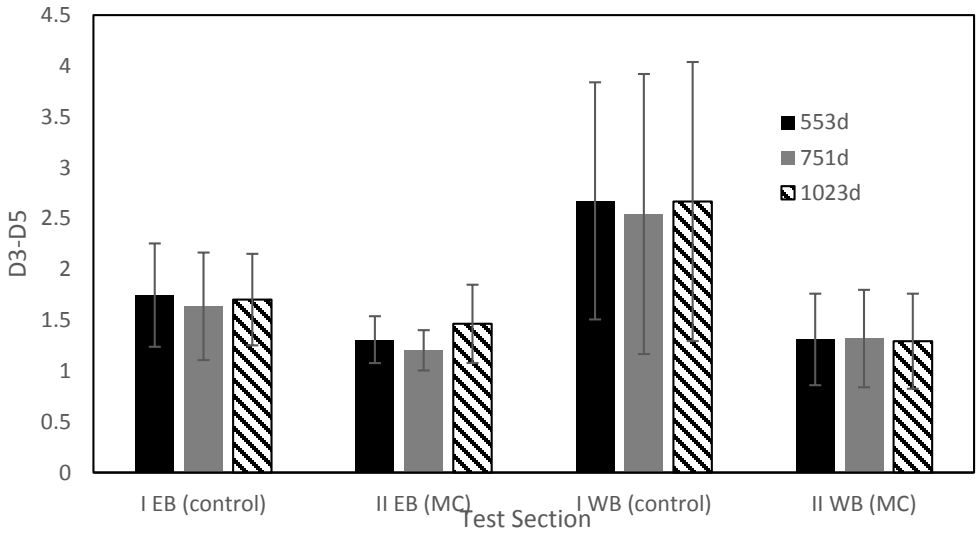

(b)

Figure 36

(a) Average overall deflections and (b) average (D3-D5) values of 8.5-in. control and micro-cracked sections (Section I & II)

Table 12 presents the T-Test results of the FWD deflections of Sections I and II. The results showed that Section II had consistently lower D1 and D3-D5 than those of Section I, indicating the micro-cracked soil cement base of Section II becomes stiffer over time after the micro-cracking than the non-micro-cracked one of Section I.

Table 12

Average overall deflection and (D3-D5) of 8.5-in. control section (Section I) and micro-cracked section (Section II) on LA 1003

FWD-LA 1003	Date	Days after Constr.	T-test				
			Control Sec.Ave	Standard Dev.	MC Sec. Ave	Standard Dev.	p-value
D1: SecI-II EB	3/29/2016	553	11.02	2.35	9.31	0.97	0.0562
	10/13/2016	751	10.35	2.08	8.82	0.77	0.0513
	7/12/2017	1023	11.14	2.09	10.37	1.57	0.3781
D1: SecI-II WB	3/29/2016	553	14.04	3.51	9.47	1.96	0.0046
	10/13/2016	751	13.45	4.20	9.57	1.87	0.0271
	7/12/2017	1023	14.30	4.29	10.0	1.90	0.0189
D3-D5: SecI-II EB	3/29/2016	553	1.75	0.51	1.58	0.89	0.0292
	10/13/2016	751	1.64	0.53	1.20	0.20	0.0326
	7/12/2017	1023	1.70	0.45	1.46	0.38	0.2317

FWD-LA 1003	Date	Days after Constr.	T-test				
			Control Sec.Ave	Standard Dev.	MC Sec. Ave	Standard Dev.	p-value
D3-D5: SecI-II WB	3/29/2016	553	2.67	1.17	1.31	0.45	0.0080
	10/13/2016	751	2.54	1.38	1.32	0.48	0.0302
	7/12/2017	1023	2.66	1.37	1.29	0.47	0.0176

In summary, based on the crack performance results, high-speed pavement profile survey, and FWD testing, it may be concluded that Section II with an 8.5-in. micro-cracked cement soil base layer performed slightly better than or similar to Section I with an 8.5-in. non-micro-cracked soil cement base layer. The high rut depths of Section I WB may be related to its weak base stiffness as indicated by its high D3-D5 value. On the other hand, the construction difficulty in the residential area (as shown in Figure 37), where high rut depths are usually observed, could possibly result in the worse rutting performance of the section.

Figure 37
View of section I WB in front of residential entrances

Section IV vs. Section V (12-in. Cement Treated Soil Base)

Crack performance. In total, two transverse cracks and 16 longitudinal cracks were observed on Section IV (the control section). Figures 38 and 39 show the transverse crack locations on Section IV, which are approximately 4 ft. long and 1-2 mm wide.

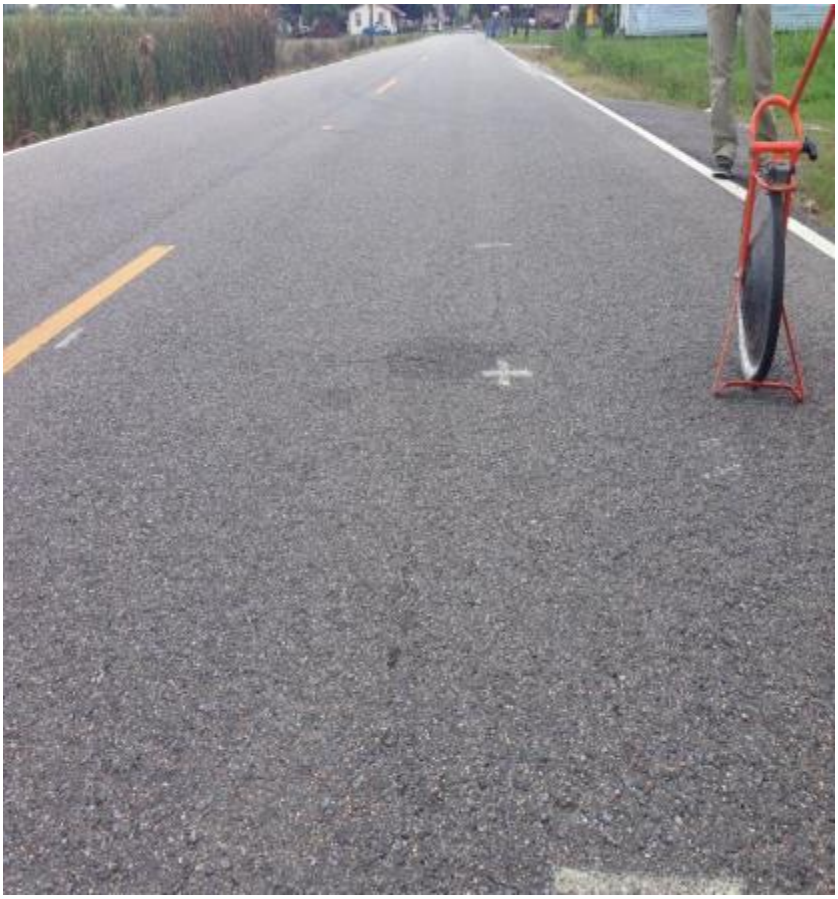

Figure 38

Transverse cracking, westbound lane, 4 ft. long, 1 mm wide. (S4+575)

Figure 39

Transverse cracking, westbound lane, 4 ft. long, 2 mm wide (S4+500)

Figures 40 through 42 present typical longitudinal cracks on Section IV. Most of the longitudinal cracks (less than 10 ft. long and about 2 mm wide) occurred in the middle of a lane between wheel paths.

Figure 40

Longitudinal cracking, westbound lane, 8 ft. long, 2 mm wide (S4+380 approx)

Figure 41

Longitudinal cracking, westbound lane, 26 ft. long, 2 mm wide (S4+639 approx)

Figure 42
Longitudinal cracking, eastbound lane, 24 ft. long, 1 mm wide (S4+640 approx.)

In total, eight low-severity transverse cracks and 10 longitudinal cracks were observed on Section V (the micro-cracked section of 12-in. cement treated base) after approximately three years of traffic loading.

Figures 43-45 show three major transverse cracks on Section V. Although this section has been micro-cracked during its base construction, it did show slightly more transverse cracks than the control section IV in terms of both the cracking occurrence frequency and the total length, as listed in Table 8.

Figure 43

Transverse cracking, westbound lane, 4 ft. long, 2 mm wide (S5+448)

Figure 44

Transverse cracking, eastbound lane, 12 ft. long, 1 mm wide (S5+500 approx)

Figure 45
Transverse cracking, eastbound lane, 7 ft. long, 2 mm wide (S5+350 approx)

Figures 46 and 47 present typical longitudinal cracks on Section V. The longitudinal cracks observed on Section V are also located in the middle of a lane between the two wheel paths. Most of the cracks are less than 3-mm wide. It is worth mentioning that a 46-ft. long longitudinal crack was found on the eastbound lane at S5+541 (as shown in Figure 46). The longitudinal crack seems like a top-down cracking, resulted from the bending of the top asphalt concrete layer under heavy truck loading. The bending stress in the asphalt layer might also be exaggerated due to the weakened support caused either by the differential subgrade settlement or by a base failure, which was potentially caused by an over-compaction during the micro-cracking.

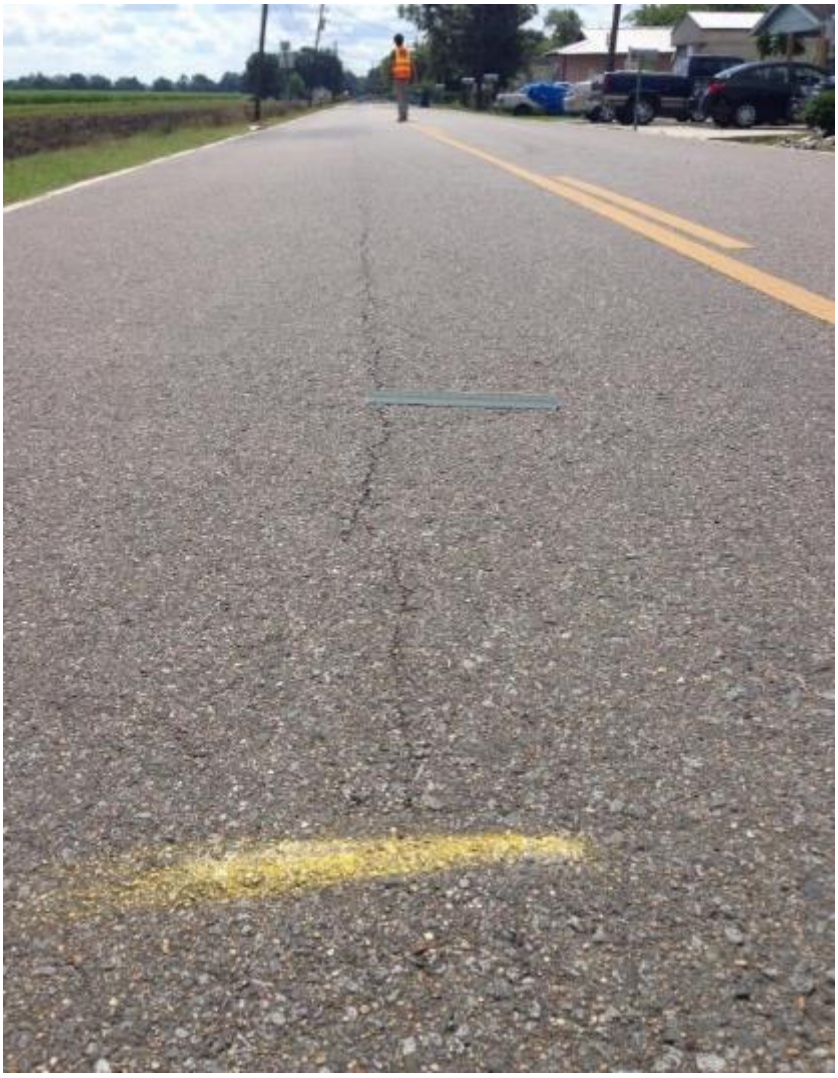

Figure 46

Longitudinal cracking, eastbound lane, 46 ft. long, 1 mm wide (S5+541)

Figure 47
Longitudinal cracking, westbound lane, 12 ft. long, 2 mm wide (S5+122)

In general, the total crack densities of Section IV and Section V are 19.1 ft. and 21.1 ft. per 2400 sq. ft. pavement, respectively (Table 9). The transverse cracks could be related to the shrinkage of the 12-in. cement treated soil base. However, the longitudinal cracks may be caused mainly by the pavement bending under heavy traffic loads, as most of the longitudinal cracks were found in the middle of traffic lanes, not close to construction joints. These cracks may be top-down cracking. The bending of the pavement could also be exaggerated by the differential settlement of a weak subgrade embankment and/or the base compaction issues during the construction.

Based on the above discussion of the cracking performance, it is found that the micro-cracked 12-in. cement treated soil base (Section V) did not show a better cracking resistance as compared to the non-micro-cracked control section (Section IV) in terms of the transverse and longitudinal cracking performance. Therefore, the effect of using the micro-cracking technique on a 12-in. cement treated soil base under a typical subgrade condition in southern Louisiana is still questionable.

Rutting and IRI performance. Rut depth values were also measured and the results of Section IV and Section V are compared in Figure 48.

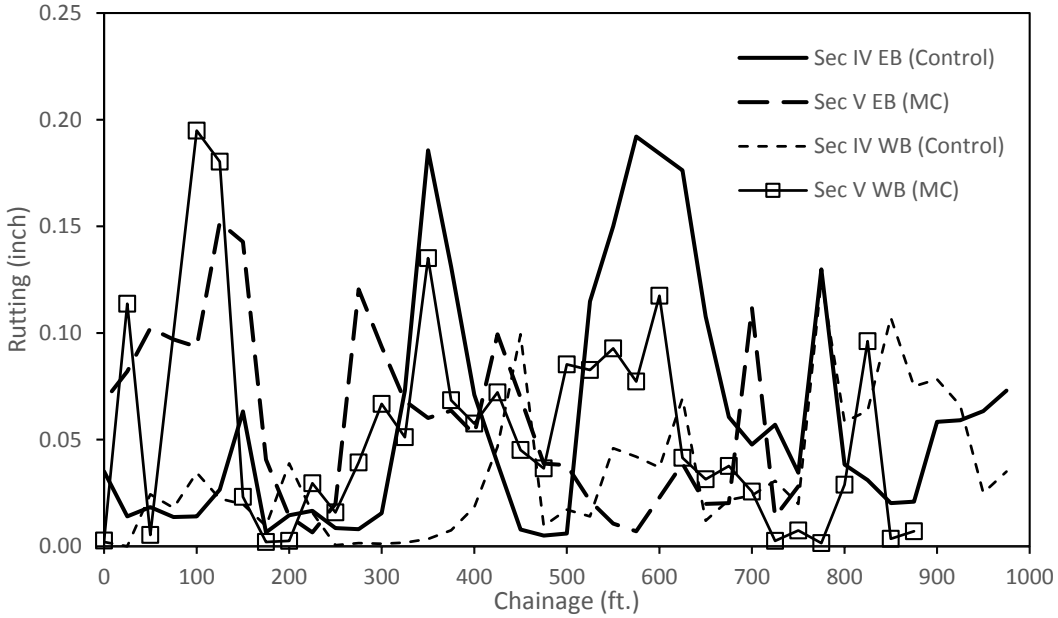

Figure 48

Measured rut depths of Section IV & V on LA1003

The student's T-test was conducted to examine the difference of rut depth values of Section IV and V and the results are shown in Table 13. It is found out that there is no significant difference between the eastbound sections, even though the difference of westbound sections is statistically significant. However, the average values are very close to each other (0.03 and 0.05 in.).

Table 13

Average rut depth of Section IV & V (12-in. control and micro-cracked sections), LA 1003

Sections	Section IV WB	Section V WB	Section IV EB	Section V EB
Properties	12-in. 8% cement treated, Control section	12-in. 8% cement treated, MC section	12-in. 8% cement treated, Control section	12-in. 8% cement treated, MC section
Rutting Ave.(in.)	0.03	0.05	0.06	0.06
Standard Deviation	0.03	0.05	0.05	0.04
p-value	0.04473		0.9198	

The IRI test results on the right wheel paths of Sections IV and V are shown in Figure 49. For the right wheel paths of these two lanes, the average IRI values of micro-cracked sections are larger than those of their corresponding control sections. Table 14 summarizes the average IRI values and the results of the statistical analysis. It is found out that the difference is statistically significant in the westbound lane. The possible reason is that a residential area close to the westbound lane may have a higher influence on the westbound pavement surface, similar to the situation of Sections I and II (Figure 37).

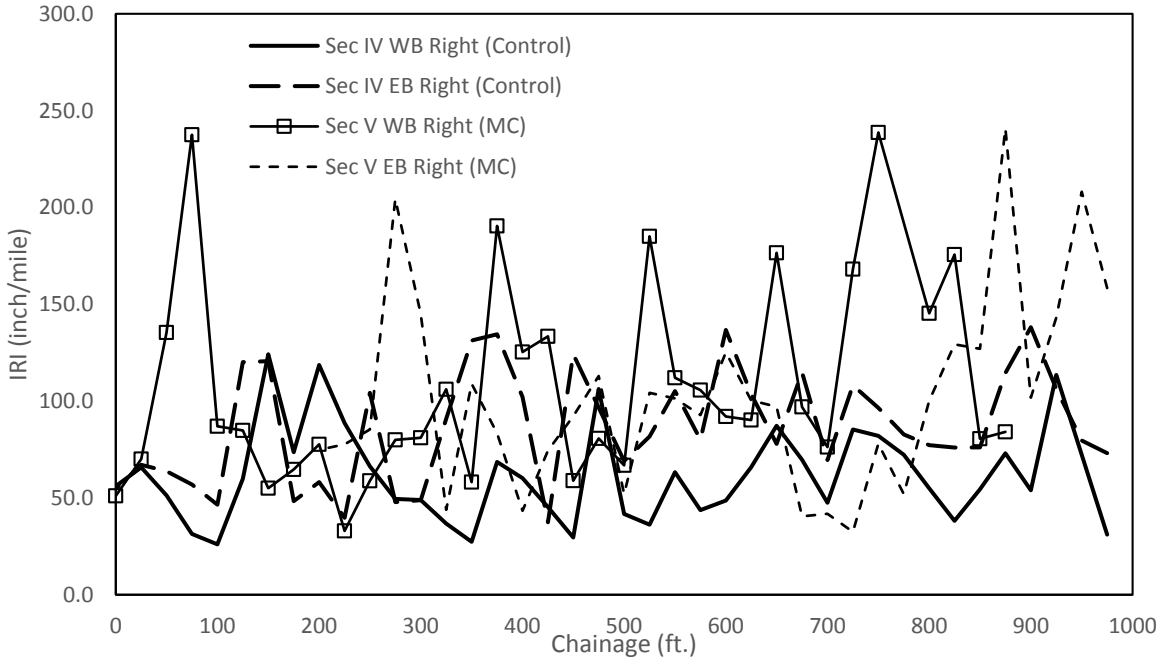

Figure 49
IRI values of Sections IV & V on the right wheel paths

Table 14
Average IRI values of Sections IV & V (12-in. control and micro-cracked sections), LA 1003

Bound and Lane	WB Right		EB Right	
Sections	IV Control	V MC	IV Control	V MC
IRI Ave. (inch/mile)	61.5	107.5	86.3	102.3
Standard Deviation	25.1	52.5	29.2	49.9
p-value	<0.001		0.1158	

FWD Tests. Three FWD tests were conducted on the two test sections on LA 1003. On each test section, FWD tests were performed at 10 equally-spaced test stations. The latest D1 and (D3-D5) obtained from the FWD test conducted on July 12 2017 (1023 days after construction) are plotted in Figures 50 (a) and (b). Table 15 summarizes the T-Test results and Figures 51 (a) and (b) compare the average D1 and D3-D5 of the two test sections. In general, the difference between the micro-cracked section and the non-micro-cracked section is not statistically significant.

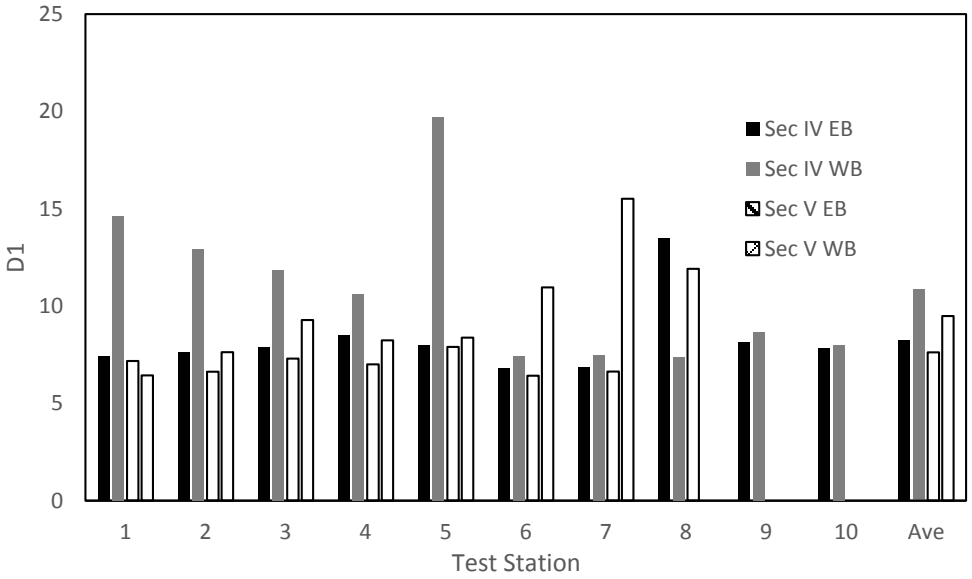

(a)

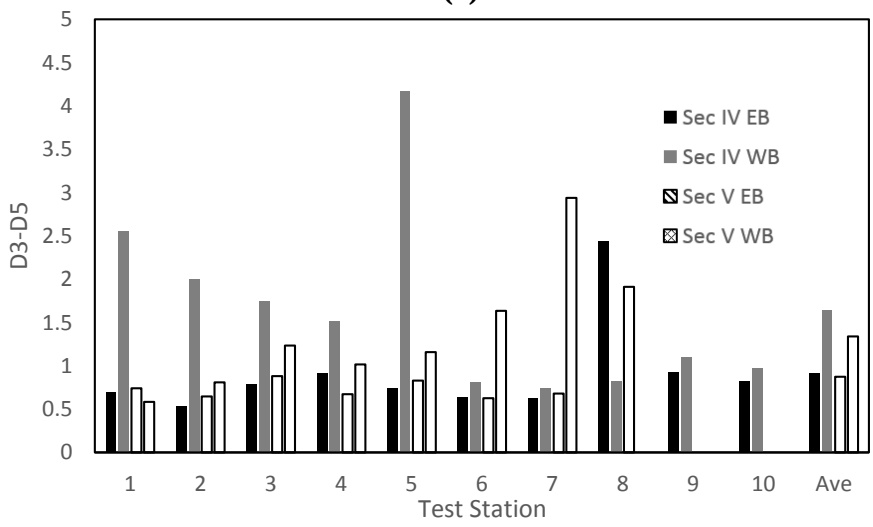

(b)

Figure 50

Deflection values of Sections IV & V (a) D1 (b) (D3-D5)

Table 15

Average D1 and (D3-D5) of Section IV (12-in. control section) and Section V (micro-cracked section) on LA 1003

FWD-LA 1003	Date	Days after Constr.	T-test				
			Control Sec.Ave	Standard Dev.	MC Sec. Ave	Standard Dev.	p-value
D1: SecIV-V EB	3/29/2016	553	7.26	1.79	6.30	0.93	0.1666
	10/13/2016	751	7.78	2.58	7.49	2.26	0.8025
	7/12/2017	1023	8.26	1.92	7.63	1.80	0.4777
D1: SecIV-V WB	3/29/2016	553	10.11	3.59	7.55	1.58	0.0647
	10/13/2016	751	10.20	2.62	7.89	1.75	0.0409
	7/12/2017	1023	10.86	4.04	9.49	3.00	0.4361
D3-D5: SecIV-V EB	3/29/2016	553	0.83	0.43	0.75	0.30	0.6449
	10/13/2016	751	0.94	0.75	0.90	0.53	0.8973
	7/12/2017	1023	0.91	0.55	0.87	0.43	0.8689
D3-D5: SecIV-V WB	3/29/2016	553	1.69	1.29	0.99	0.39	0.1284
	10/13/2016	751	1.55	0.69	1.04	0.49	0.0892
	7/12/2017	1023	1.64	1.07	1.34	0.78	0.1284

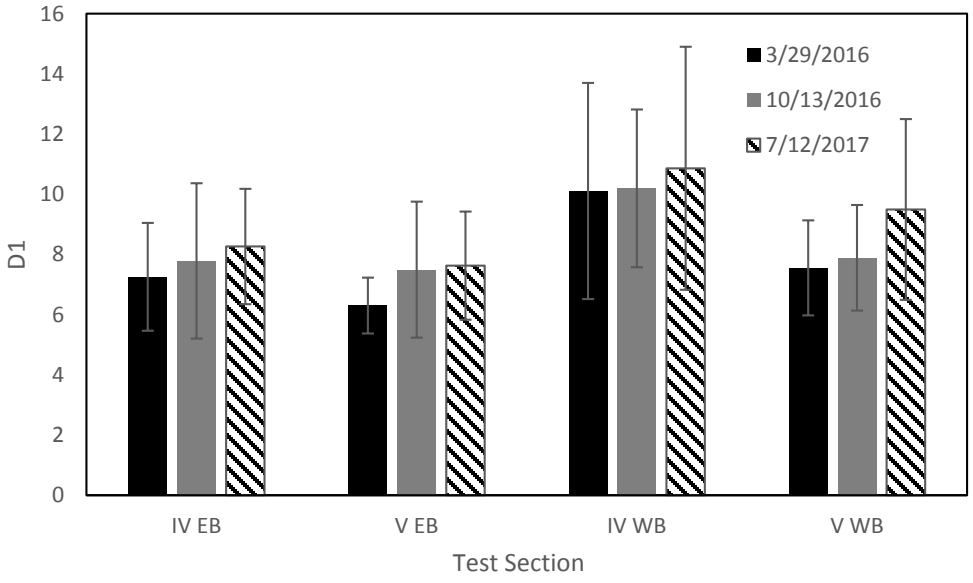

(a)

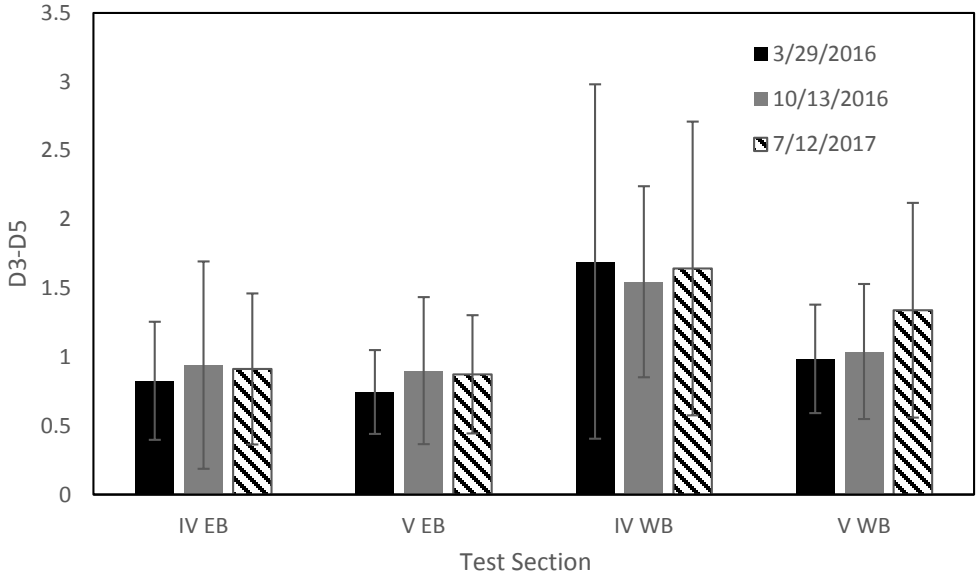

(b)

Figure 51

(a) Average overall deflection and (b) average (D3-D5) value of 12-in. control and micro-cracked sections (Section IV & V)

Based on the test results of crack mapping, visual survey, road surface profiling, and FWD, it can be concluded that the 12 in. micro-cracked cement treated section have not performed better than its control section in the past service period. The possible reasons are that the low cement content did not provide sufficient bonding among soil particles so that the process of micro-cracking damaged the base layer.

Section I vs. Section III (8.5-in. Control Section and 8.5-in. Double Layer Section)

Crack Performance. The typical cracks observed on Section III are shown in Figures 52-55.

Figure 52

Longitudinal cracking, eastbound lane, 18 ft. long, 1 mm wide. (S3+307)

Figure 53

Longitudinal cracking, eastbound lane, 30 ft. long, 2 mm wide. (S3+358)

Figure 54

Longitudinal cracking, westbound lane, 26 ft. long, 2 mm wide. (S3+555)

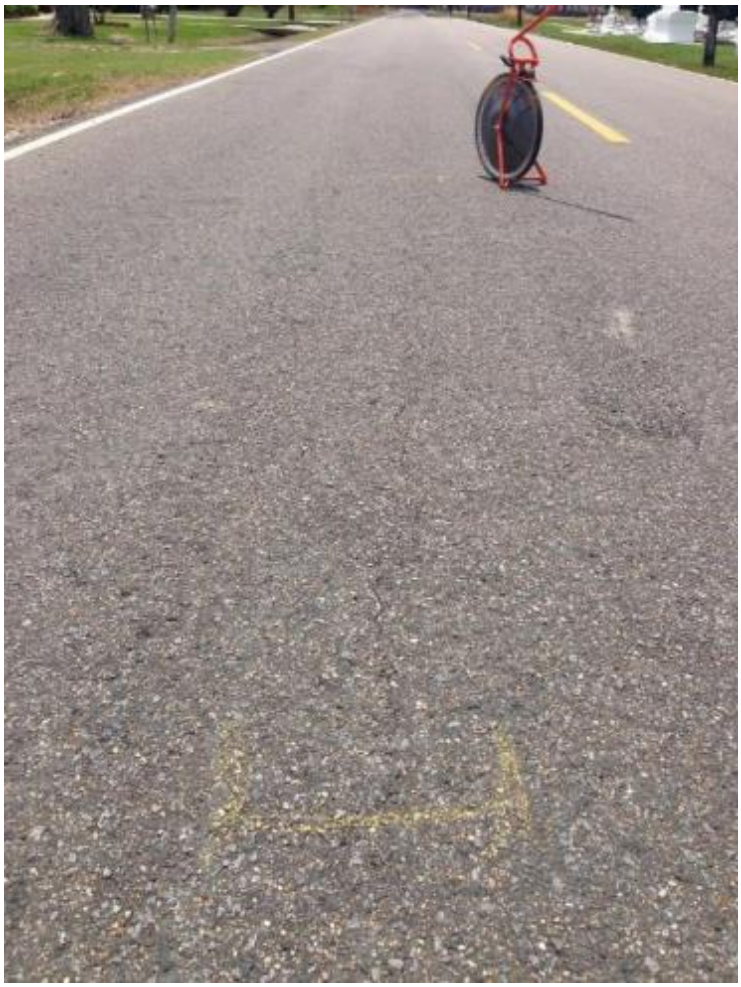

Figure 55
Longitudinal cracking, westbound lane, 11 ft. long, 1 mm wide. (S3+741)

Only longitudinal cracks were found on Section III. The total lengths of the longitudinal cracks on the eastbound lane and westbound lane are 105 ft. and 67 ft., respectively. Most of these cracks are 10-30 ft. long and 1-2 mm wide. The cracking density (17.2 ft. per 100 ft. pavement) of the double layer section (Section III) is significantly higher than that (0.9 ft. per 100 ft. pavement) of the 8.5-in. Control Section (Section I). The phenomenon that no transverse cracking was observed on Section III may indicate that double layer was effective in reducing the reflective cracking.

Rutting and IRI Performance. Rut depths were measured and the results of the two sections are compared in Figure 56.

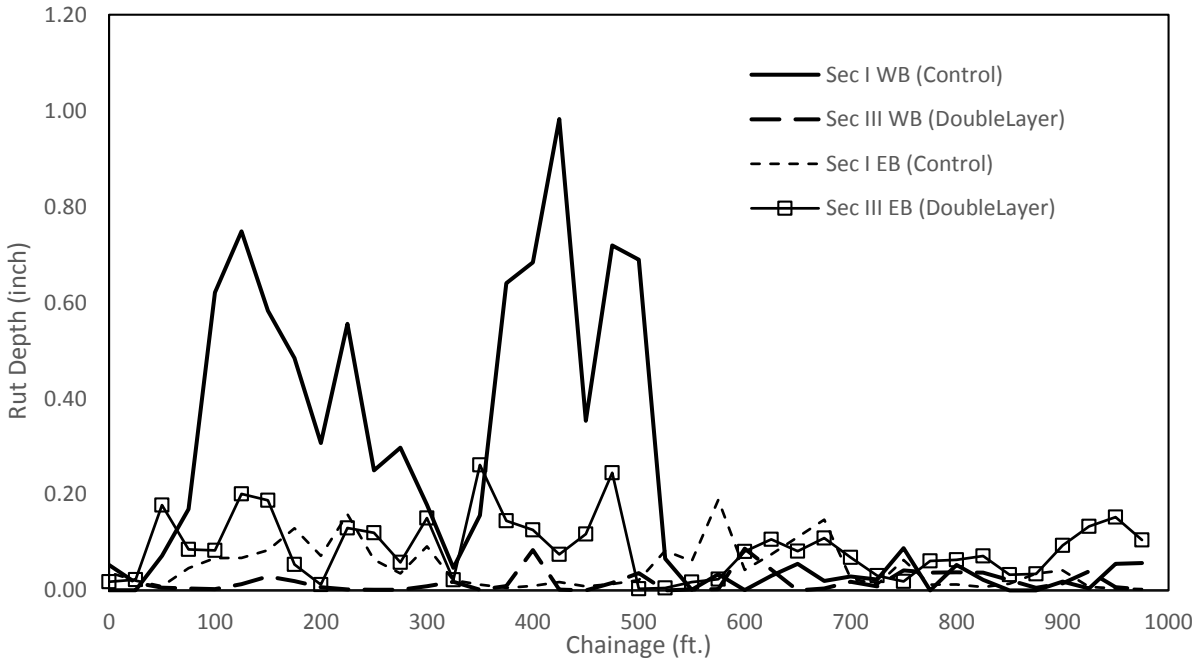

Figure 56
Measured rut depths of Sections I and III on LA1003

It can be seen that the rut depth of Section I westbound lane is significantly large on the first 500 ft., while the double layer section (Section III) has relatively high rut depths on the eastbound lane. These observations were confirmed by T-Test. Table 16 summarizes the average values and the results of T-Test.

Table 16
Average rut depth of Section I and III, LA 1003

Sections	Section I WB	Section III WB	Section I EB	Section III EB
Properties	8.5 inch 11% soil cement, Control section	8.5 inch 11% Double Layer	8.5 inch 11% soil cement, Control section	8.5 inch 11% Double Layer
Rutting Ave. (inch)	0.23	0.02	0.05	0.09
Standard Deviation	0.28	0.02	0.05	0.07
p-value	<0.0001		0.0012	

Figure 57 plots the IRI results obtained from the two sections. As shown in Figure 57, IRI results of Section I are slightly higher than those of Section III on the westbound lane, while Section III shows substantially high IRI values on the first 500 ft. section on the eastbound lane. These observations demonstrate similar trend as those of rut depths. The results of T-Test summarized in Table 17 confirms these observations.

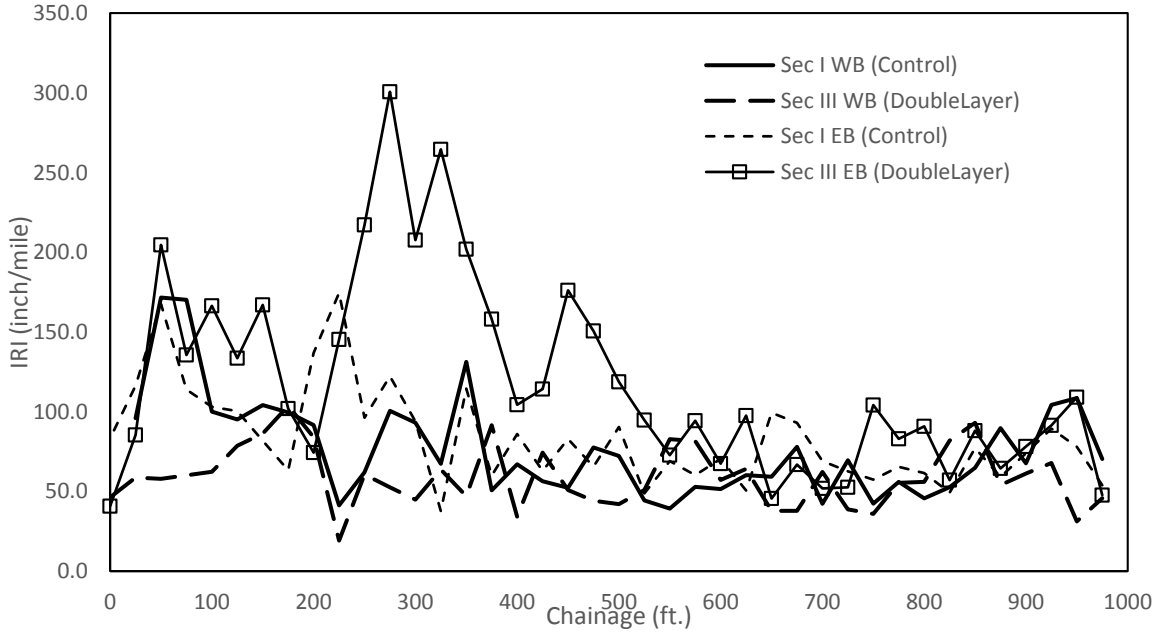

Figure 57
IRI value of Section I and III on LA 1003

Table 17
Average IRI of Section I & II of LA 1003

Bound and Lane	WB		EB	
Sections	I Control	III Double Layer	I Control	III Double Layer
IRI Ave. (inch/mile)	76.92	58.95	83.55	118.17
Standard Deviation	31.82	19.32	30.37	61.65
p-value	0.0037		0.0023	

FWD Tests. Figure 58 plots the overall pavement deflection (D1) and (D3-D5) of the two sections.

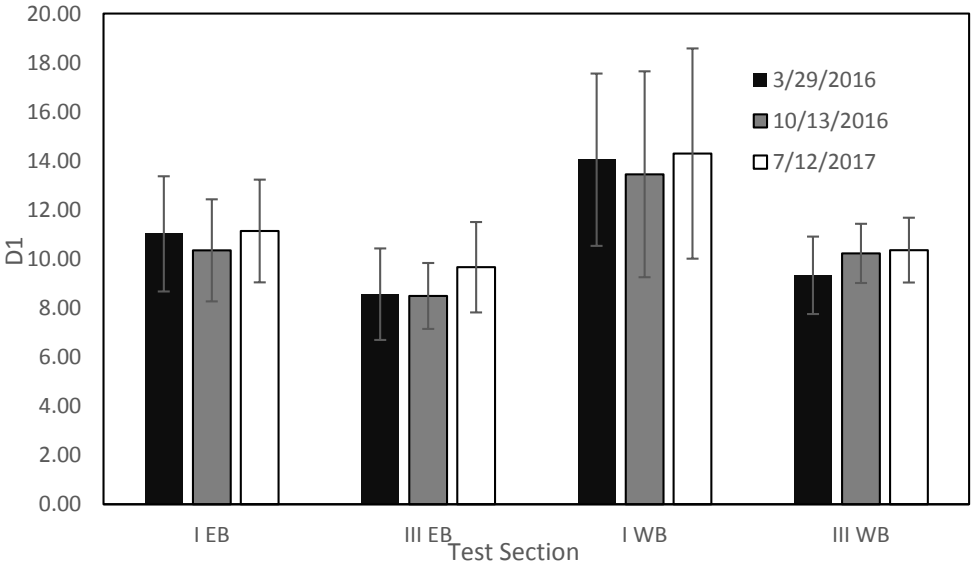

(a)

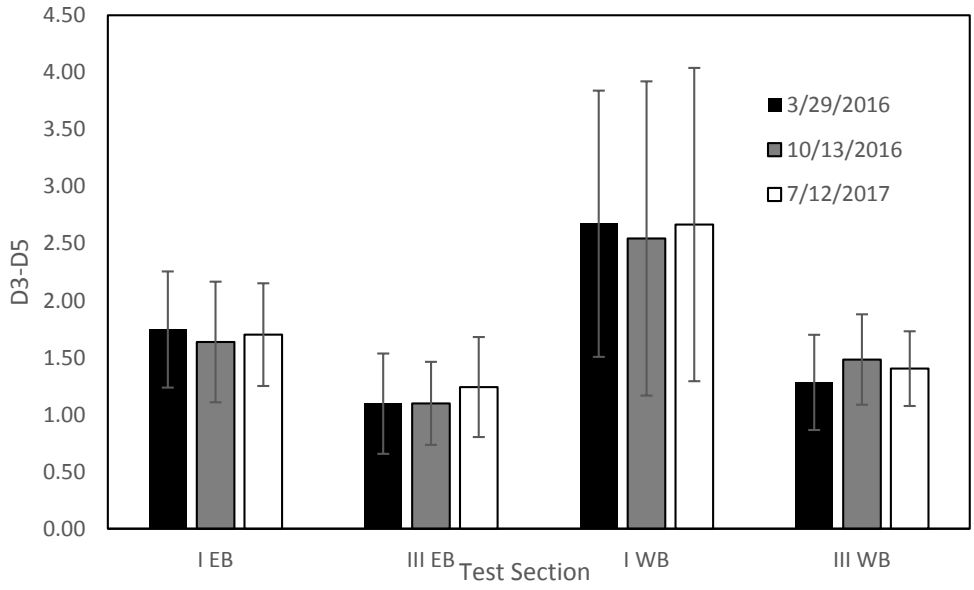

(b)

Figure 58

(a) Average D1 and (b) average (D3-D5) values of Section I and Section III

Figure 58 (a) shows the overall deflections (D1) of the 8.5-in. control section and double layer section on both lanes. It can be seen that the overall deflections of the westbound lane are higher than those of the eastbound lane. The results from T-Test listed in Table 18 supports this observation. (D3-D5) shows a similar trend as D1.

Table 18
Average overall deflection (D1) and (D3-D5) of Section I and Section III on LA 1003

FWD-LA 1003	Date	Days after Constr.	T-test				
			SecI .Ave	Standard Dev.	SecIII. Ave	Standard Dev.	p-value
D1: SecI-III EB	3/29/2016	553	11.02	2.35	8.56	1.87	0.0189
	10/13/2016	751	10.35	2.08	8.49	1.34	0.0312
	7/12/2017	1023	11.14	2.09	9.66	1.84	0.1118
D1: SecI-III WB	3/29/2016	553	14.04	3.51	9.33	1.58	0.0036
	10/13/2016	751	13.45	4.20	10.22	1.21	0.0529
	7/12/2017	1023	14.30	4.29	10.36	1.32	0.0259
D3-D5: SecI-III EB	3/29/2016	553	1.75	0.51	1.10	0.44	0.0070
	10/13/2016	751	1.64	0.53	1.10	0.36	0.0175
	7/12/2017	1023	1.70	0.45	1.24	0.44	0.0327
D3-D5: SecI-III WB	3/29/2016	553	2.67	1.17	1.28	0.42	0.0071
	10/13/2016	751	2.54	1.38	1.48	0.40	0.0525
	7/12/2017	1023	2.67	1.37	1.40	0.33	0.0252

Summary of Test Results. Based on the test results of the crack performance, road surface profiling, and the FWD, it can be concluded that 8.5-in. control section is better than the double layer in terms of the crack performance. For the current service period, it may conclude that Double Layer section did not show a better performance than the control section.

LA 599 Test Sections

Figure 59 shows the plan view of five test sections constructed on LA 599. Each test section is approximately 1000-ft. long and 24-ft. wide, including one westbound (WB) lane and one eastbound (EB) lane. The sections have a 3.5-in. HMA layer. As shown in Figure 59, Section I (control) and Section II (micro-cracked) consist of a 12-in. cement treated base, whereas Section IV (micro-cracked) and Section V (control) include an 8.5-in. soil cement base. Section III is a 12-in. thick soil cement section. Due to a construction mistake of Section III, the section was not discussed in this report. Micro-cracking was performed by a 14.5-ton roller on August 3, 2015. More details may be found in the Methodology section of this report.

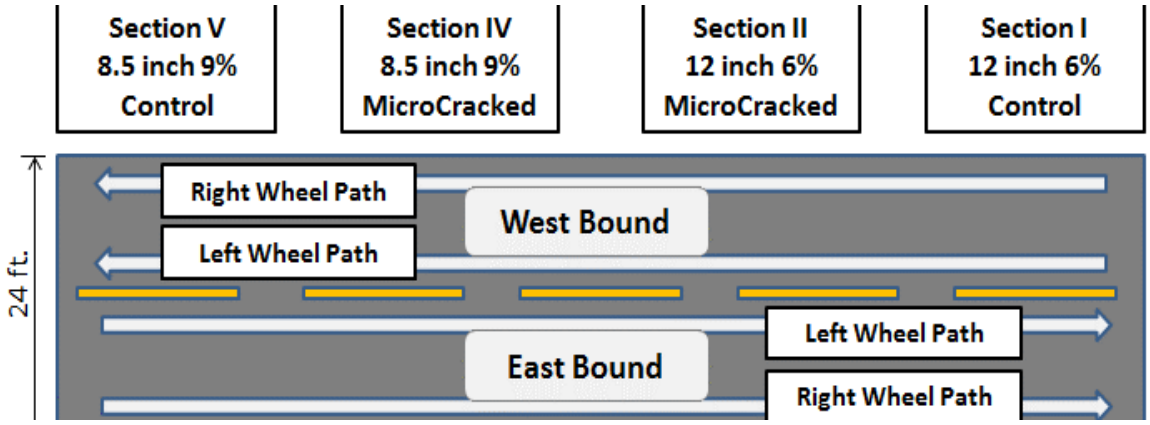

Figure 59
Section plan view of LA599

In July 2017, the research team performed a final inspection of test sections on LA599 including cracking survey, FWD, and high-speed digital surface profiling. The cracking survey results are summarized in Table 19. Overall, both the control sections (Sections I and V) had fewer amounts of cracks than their counterpart, i.e., micro-cracked sections (Section II and IV). The total crack lengths per 2400 ft^2 of pavement area on Sections I-V are 1.8-ft, 24.3-ft, 13.8-ft, 6.4-ft, and 0-ft, respectively (Table 20) and these results are not as expected. Detailed analyses of the pavement performance are presented below.

Table 19
Total length and number of cracks (in parentheses) of sections on LA 599

Section	Severity (mm)	Transverse Cracks Total Length (No. of cracks)		Longitudinal Cracks Total Length (No. of cracks)	
		Eastbound	Westbound	Eastbound	Westbound
I	0-6				18 ft. (2)
	6-19				
	>19				
II	0-6	9 ft. (1)		27 ft. (2)	81 ft. (4)
	6-19			64 ft. (1)	81 ft. (3)
	>19				
III	0-6		12 ft. (2)	23 ft. (2)	13 ft. (1)
	6-19			21 ft. (1)	79 ft. (1)
	>19				
IV	0-6				46 ft. (2)
	6-19				18 ft. (1)

	>19				
V	0-6				
	6-19				
	>19				

Table 20

Summary of the total cracking densities of sections on LA 599

Section No.	Crack Length in feet per 100 ft. of pavement (1200 sq. ft.)		Total Crack Length in feet per 100 ft. of pavement (2400 sq. ft.)
	EB	WB	
I (12" control)	0	1.8	1.8
II (12" MC)	9.3	15.0	24.3
III (12"SC control)	4.1	9.7	13.8
IV (8.5" MC)	0	6.4	6.4
V (8.5" control)	0	0	0

Section I vs. Section II (12-in. Cement Treated Base)

Crack Performance. Only two hair-line type longitudinal cracks were found on Section I, as shown in Figure 60. These cracks, developed along the centerline of the westbound lane of Section I, were too fine to be observed in a photo. No transverse cracks were found in this section.

(a)

(b)

Figure 60

Eastside view of Section I on LA599 (a) first part (b) second part

On the other hand, one transverse crack and nine longitudinal cracks were found on Section II on LA 599. Figure 61 shows the transverse crack observed and Figures 62-65 present typical longitudinal cracks found.

Figure 61

Transverse cracking with 9 ft. long and 2 mm wide on eastbound lane (S2+261)

Figure 62

Longitudinal crack with 23 ft. long and 6 mm wide on eastbound lane (S2+327)

Figure 63

Longitudinal crack with 64 ft. long and 8 mm wide on eastbound lane (S2+267)

Figure 64

Longitudinal cracking with 20 ft. long and 5 mm wide on westbound lane (S2+486)

Figure 65
Two longitudinal cracks with 22 & 43 ft. long and 10 mm wide on westbound lane (S2+269 & S2+243)

On Section I (control section), transverse cracking was not observed, but longitudinal cracking with a total length of 18 ft. was found in the westbound lane. On the micro-cracked section (Section II), transverse cracking with a total length of 9 ft. was observed on the eastbound lane; longitudinal cracks with a total length of 91 ft. and 162 ft. were found in the eastbound lane and westbound lane, respectively.

Three cores were taken on the selected cracked locations on Section II. Figure 66 shows the retrieved cores. As expected, all cores showed that there was no bonding between the asphalt and the base layer. Core #1, taken at a transverse crack location on Section II, clearly shows

that the crack is a reflective one. On the other hand, Cores #2 and #3 were taken from two longitudinal crack locations, and both of them seemed to be top-down cracks. In addition, only the top 3-in. portion of the 12-in. cement treated soil base was able to core out for Cores #2 and #3, indicating a weak cement bonding at the bottom portion of the base layer, at least at the locations of the two cores. No cores were taken from Section I, as no cracks were found in the visual crack survey. It should be noted that longitudinal cracks on Section I were detected by the road surface profiler during the subsequent survey.

(a)

(b)

(c)

Figure 66

Cores collected from Section II (a) Core #1 from transverse crack (b) Core #2 from longitudinal crack and (c) Core #3 from longitudinal crack

Rutting and IRI Performance. Rut depth and IRI values were measured by the Road Surface Profiler. Figure 67 compares the rut depths obtained from the micro-cracked section (Section II) and the control section (Section I).

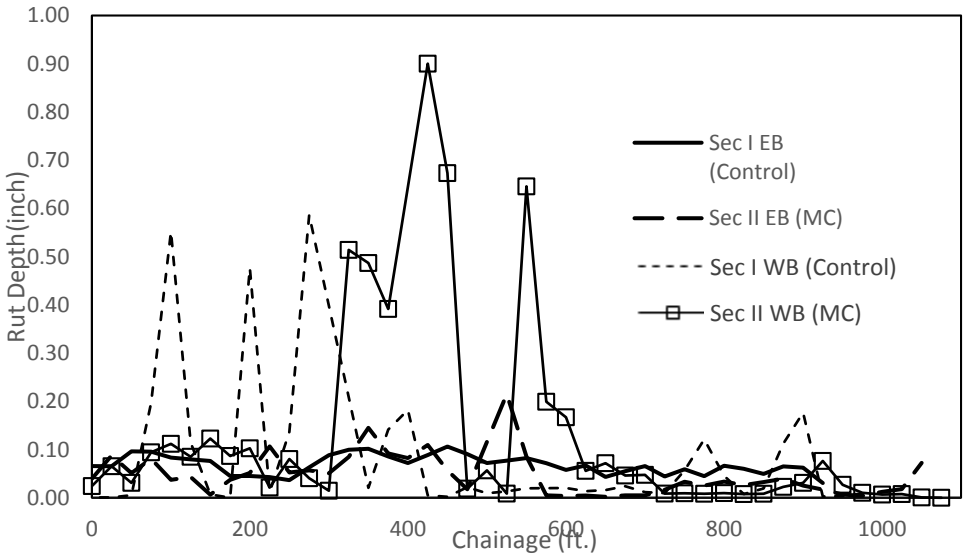

Figure 67

Measured rut depths of Sections I & II on LA 599

Table 21 lists the averaged rutting values and the T-Test results of the micro-cracked section and its control section. Both the section I WB and Section II WB have high localized rut depths. However, on the eastbound lane, the rut depth is relatively low.

A t-test was conducted to examine the significance of the difference of the rut depth values of the control section and micro-cracked section. It can be seen that the rutting value of the control section is significantly larger than that of the micro-cracked section on the eastbound lane; on the westbound lane, although the average rutting values of the two sections have a difference of 0.07 in., the difference is not statically significant.

Table 21
Average rut depths of Sections I & II on LA 599

Sections	Section I EB	Section II EB	Section I WB	Section II WB
Properties	12-in. 6% cement treated, Control section	12-in. 6% cement treated, MC section	12-in. 6% cement treated, Control section	12-in. 6% cement treated, MC section
Rutting Ave. (inch)	0.07	0.05	0.08	0.15
Standard Deviation	0.02	0.04	0.15	0.21
p-value	<0.0001		0.2932	

From IRI results shown in Figure 68, it can be seen that Section II is rougher than Section I on both the westbound and eastbound lanes, especially on some portion of the westbound lane in Section II.

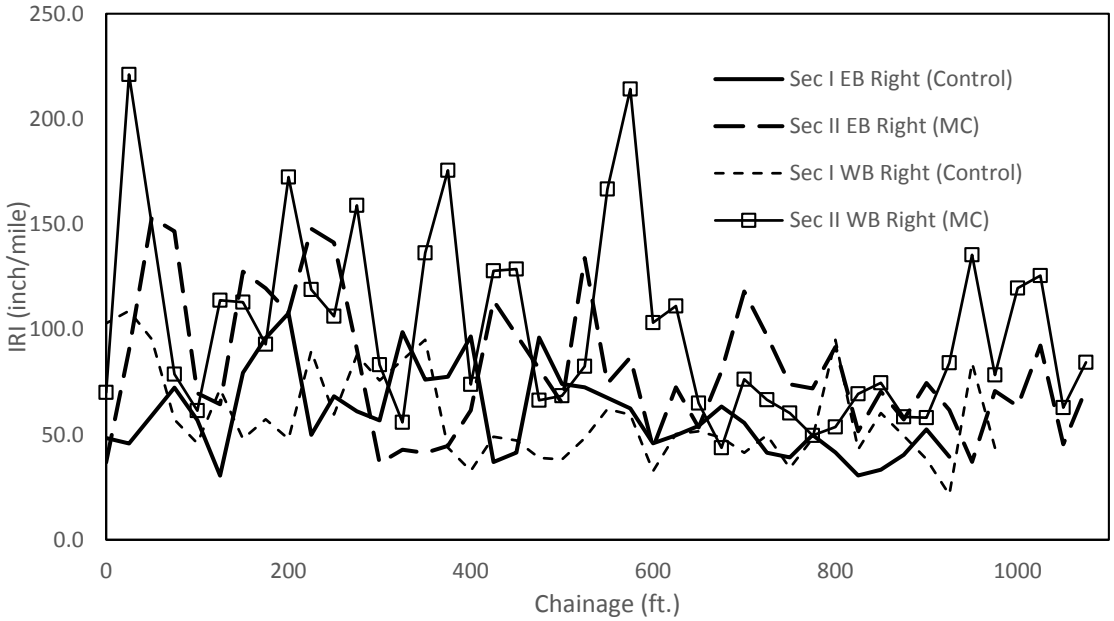

Figure 68

IRI values of Sections I & II on the right wheel path of LA599

The average IRI test results and the T-test results are summarized in Table 22. It can be concluded that, during the current service period, all the micro-cracked sections had larger average IRI values than their control sections and the differences are significant.

Table 22

Average IRI of Section I & II, LA 599

Bound and Lane	EB Right		WB Right	
Sections	I Control	II MC	I Control	II MC
IRI Ave. (inch/mile)	59.5	76.1	57.8	100.5
Standard Deviation	20.7	33.2	21.8	43.8
p-value	<0.001		<0.001	

FWD Tests. Four FWD tests were conducted on the westbound lane of the sections on LA 599 on October 28, 2015; April 20, 2016; December 14, 2016; and July 19, 2017, which correspond to 89, 264, 502 and 719 days after construction. Only one FWD was performed in the eastbound lane on August 15, 2017, which is 746 days after construction. FWD tests were conducted at 22 stations on each test section. The obtained FWD deflection data were then normalized to 9000 lbs. loading and no temperature correction was conducted.

The latest overall pavement deflection (D1) and deflections related to the base layer (D3-D5) are plotted in Figure 69 and Figure 70, respectively. Table 23 lists the averaged D1 and (D3-D5) as well as the results of the T-Test.

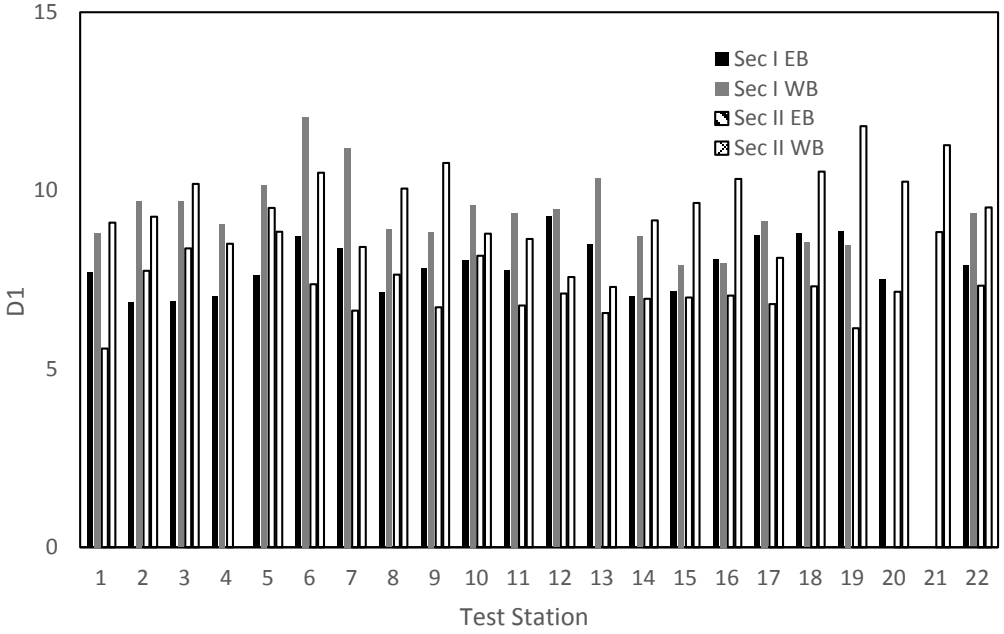

Figure 69

Overall deflection values of Section I (control section) and Section II (12-in. micro-cracked)

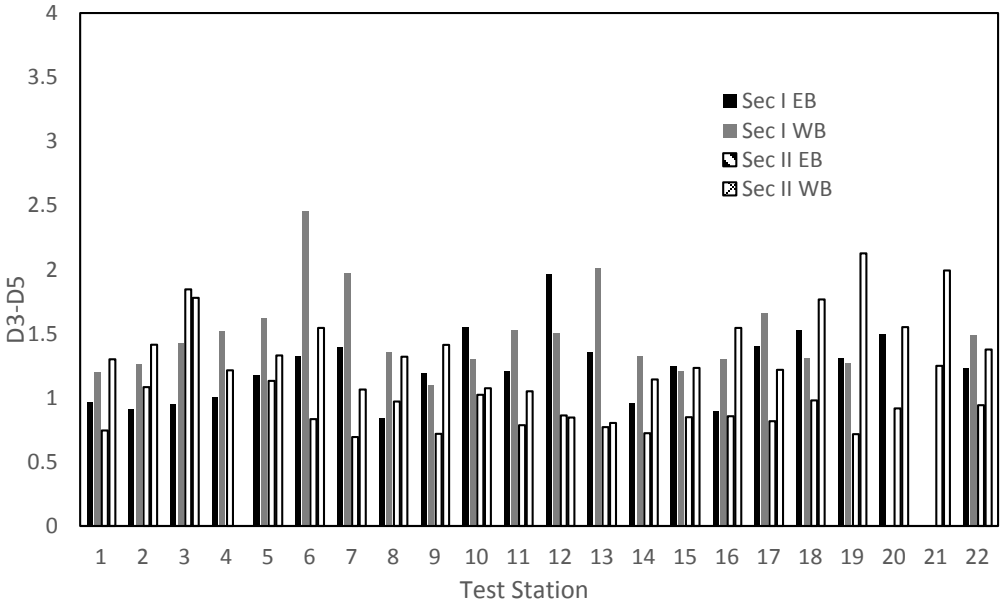

Figure 70

(D3-D5) values of Section I (control) and Section II (12-in. micro-cracked)

Table 23
Average overall deflection (D1) and (D3-D5) of Section I (control) and Section II (12-in. micro-cracked section) on LA 599

FWD-LA 599	Date	Days after Constr.	T-test				
			Control Sec. Ave	Standard Dev.	MC Sec. Ave	Standard Dev.	p-value
D1: Sec I-II EB	8/15/2017	746	7.90	0.74	7.34	0.93	0.9738
D1: Sec I-II WB	10/28/2015	89	13.62	1.74	13.51	3.28	0.9739
	4/20/2016	264	10.92	1.07	9.57	2.38	0.9437
	12/14/2016	502	8.29	1.19	8.47	3.69	0.9468
	7/19/2017	719	9.37	1.04	9.53	1.21	0.9727
D3-D5: Sec I-II EB	8/15/2017	746	1.23	0.28	0.94	0.26	0.9739
D3-D5: Sec I-II WB	10/28/2015	89	3.67	0.81	3.29	1.35	0.9738
	4/20/2016	264	2.33	0.53	1.60	0.72	0.9439
	12/14/2016	502	1.77	0.52	1.54	1.05	0.9467
	7/19/2017	719	1.49	0.34	1.38	0.35	0.9726

From the test results listed in Table 23, it can be seen that, for overall deflection (D1) and (D3-D5), the 12-in. micro-cracked sections are similar to their control sections on both lanes. The obtained p-value indicates that neither the difference of the overall deflection (D1) nor that of (D3-D5) between the micro-cracked section and control section is statistically significant.

Summary of Test Results. In terms of the cracking, Section I (control section) has a better performance than Section II. Both the Section I and Section II has a similar rutting performance on the westbound lane; on the eastbound lane, however, Section II has a better performance. The control section has lower IRI values on both lanes. In general, the micro-cracked section (Section II) did not perform well in terms of cracking resistance and more cracks were found on the micro-cracked section. This result is consistent with those of LA 1003. It is concluded that the micro-cracking technique was not effective in mitigating the reflective cracking on the 12-in. cement treated soil base layer. Possible reasons are that (1) the low cement content resulting in less bonding in the bottom part of the layer and (2) extra roller compaction potentially damaged the base layer due to its low cement content.

Section IV vs. Section V (8.5-in. Soil Cement Base)

Crack Performance. Three longitudinal cracks, 11-35 ft. long and 5-10 mm wide, were observed on the westbound lane of Section IV (the micro-cracked section), as shown in Figures 71-73.

Figure 71

Longitudinal cracking, westbound lane, 18 ft. long, 7 mm wide (S4+441).

Figure 72

Longitudinal cracking, westbound lane, 11 ft. long, 5 mm wide (S4+374).

Figure 73

Longitudinal cracking with 35 ft. long and 5 mm wide on the westbound lane (S4+163).

There was no cracking observed on Section V (control section). Figures 74 and 75 show two pavement views from Section V.

Figure 74

Westbound lane of Section V (first part) on LA599

Figure 75

Eastbound lane of Section V (second part) on LA599

From the cracking performance above, it seems that the 8.5-in. non-micro-cracked control section (Section V) has a better performance than the micro-cracked section (Section IV). However, because Section IV is located in a swamp area the longitudinal cracks may be caused by the expansive soils of the subgrade. Additionally, as the roadway has serviced only for two years with a low daily traffic volume, further investigation is necessary before drawing a conclusion.

Rutting and IRI Performance. Rutting and IRI values of Sections IV and V were measured as well in this study and the results are shown in Figures 76-77.

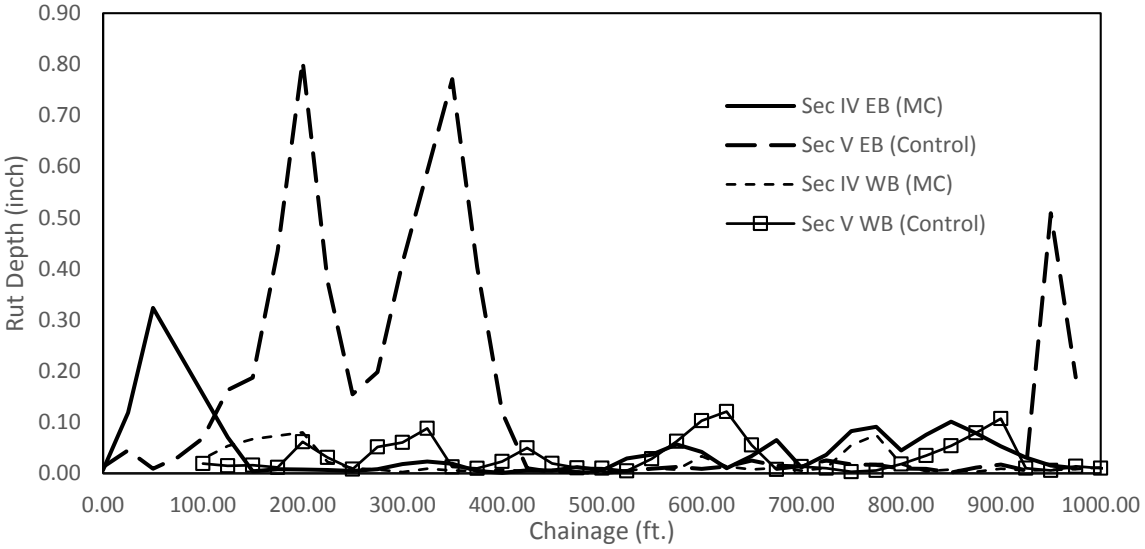

Figure 76
Measured rut depths of Section IV & V

On the first 400 ft. and the last 100 ft. of Section V Eastbound lane, high rut depths were measured and collected as shown in Figure 76. Table 24 lists the averaged rut depths of the 8.5-in. micro-cracked section and its control section and the results of the T-Test. The averaged rut depths on the eastbound lanes of the two sections are substantially different, while those on the westbound lanes are comparable. However, the rut depths on both the eastbound and westbound lanes of the two sections are statistically different.

Table 24

Average rut depths of Section IV & V (8.5-in. micro-cracked and control sections) on LA 599

Sections	Section IV EB	Section V EB	Section IV WB	Section V WB
Properties	8.5-in. 9% soil cement, MC section	8.5-in. 9% soil cement, Control section	8.5-in. 9% soil cement, MC section	8.5-in. 9% soil cement, Control section
Rutting Ave. (inch)	0.04	0.13	0.02	0.03
Standard Deviation	0.06	0.21	0.02	0.03
p-value	<0.0001		<0.0001	

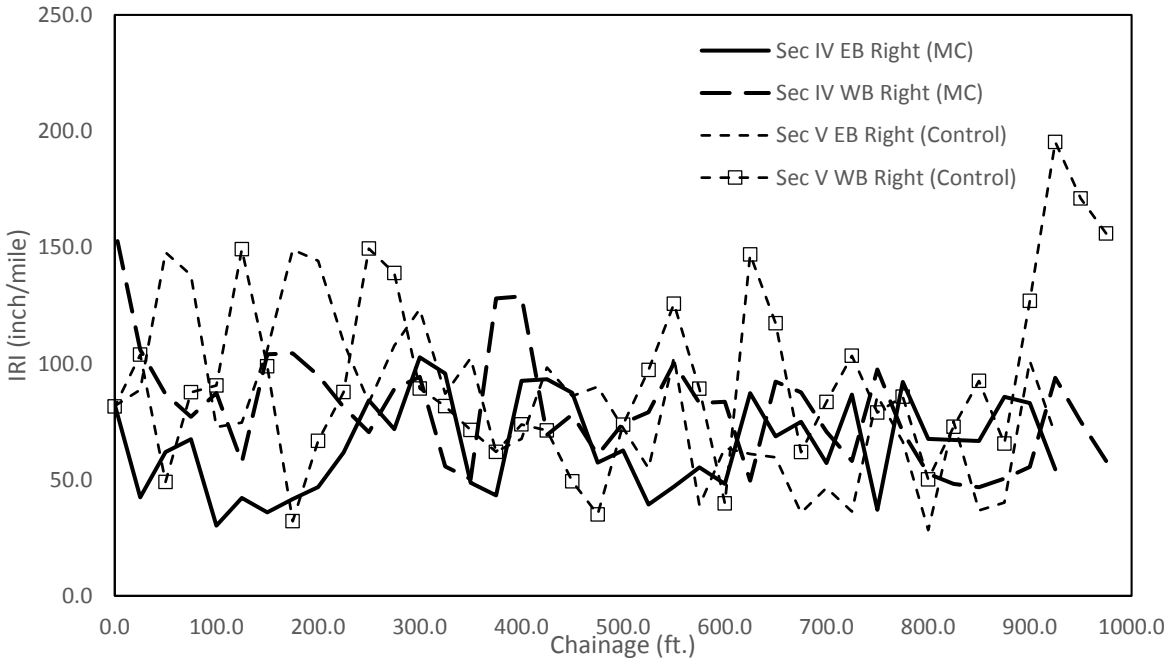

Figure 77

IRI values in the right wheel paths of Sections IV & V on LA 599

The T-Test results of IRI values (in the Right Wheel Path) is summarized in Table 25. It can be concluded that, in the current service period, all the micro-cracked sections have lower average IRI values than their control sections. However, in the right wheel path of the westbound lane, the difference is not significant.

Table 25
Average IRI values in the right wheel paths of Sections IV & V on LA 599

Bound and Lane	EB Right		WB Right	
Sections	IV MC	V Control	IV MC	V Control
IRI Ave. (inch/mile)	65.1	80.7	80.2	92.5
Standard Deviation	20.9	32.3	24.5	38.1
p-value	0.01295		0.09013	

FWD Tests. Four FWD tests were conducted on the westbound lane of LA599 on October 28, 2015; April 20, 2016; December 14, 2016; and July 19, 2017, which correspond to 89, 264, 502 and 719 days after construction. Only one FWD was performed in the eastbound lane on August 15, 2017, which is 746 days after construction. FWD tests were conducted at 22 stations on each test section. The obtained FWD deflection data were then normalized to 9000 lbs. loading and no temperature correction was conducted. The latest overall pavement deflection (D1) and deflections related to the base layer (D3-D5) are plotted in Figures 78-79. Table 26 summarizes the averaged deflections and the results of T-tests.

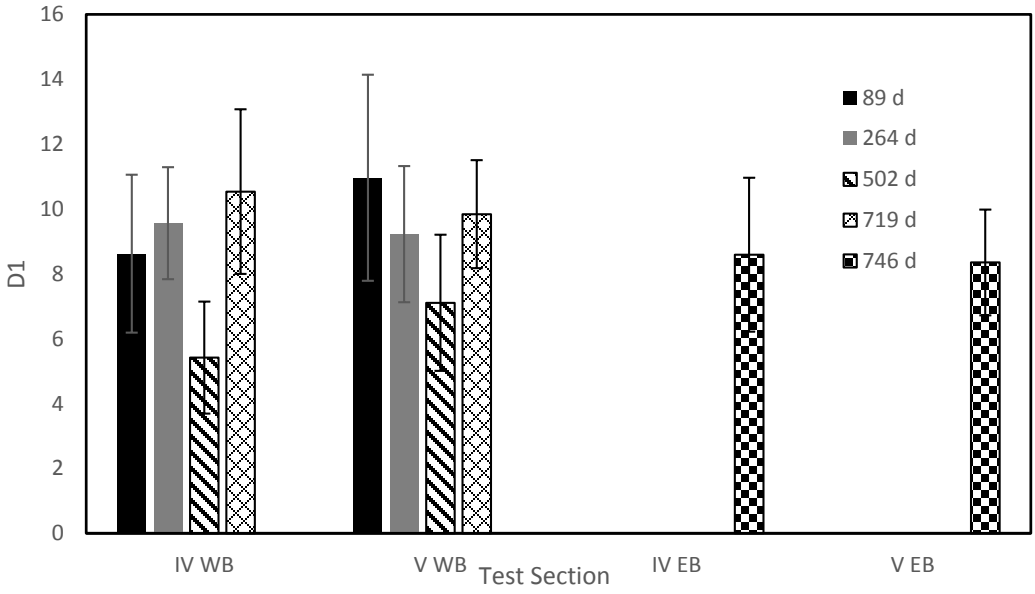

Figure 78
Overall deflection values of Section IV (8.5-in. micro-cracked) and Section V (control sections)

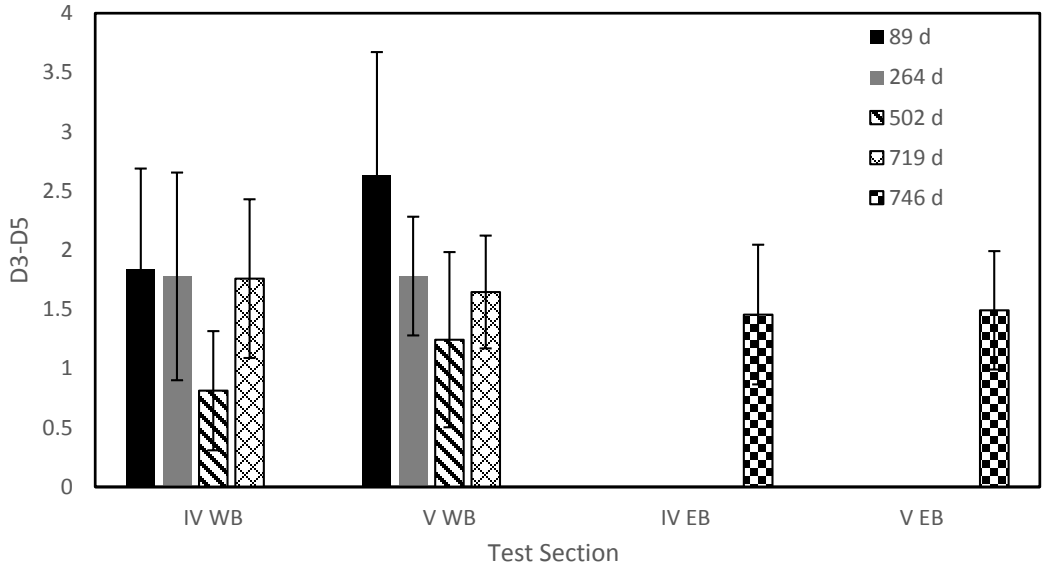

Figure 79
(D3-D5) values of Section IV (8.5 in. micro-cracked) and Section V (control sections)

Table 26
Average overall deflection and (D3-D5) of Section IV (8.5-in. micro-cracked section) and Section V (control section), LA 599

FWD-LA 599	Date	Days after Constr.	T-test				
			Control Sec.Ave	Standard Dev.	MC Sec. Ave	Standard Dev.	p-value
D1: Sec IV-V EB	8/15/2017	746	8.35	1.63	8.59	2.37	0.7118
D1: Sec IV-V WB	10/28/2015	89	10.96	3.18	8.62	2.43	0.0103
	4/20/2016	264	9.22	1.81	9.56	2.56	0.6358
	12/14/2016	502	7.11	2.10	5.42	1.73	0.0086
	7/19/2017	719	9.84	1.67	10.54	2.54	0.3061
D3-D5: Sec IV-V EB	8/15/2017	746	1.49	0.50	1.46	0.59	0.8306
D3-D5: Sec IV-V WB	10/28/2015	89	2.63	1.04	1.84	0.85	0.0095
	4/20/2016	264	1.78	0.50	1.78	0.88	0.9895
	12/14/2016	502	1.24	0.74	0.81	0.50	0.0386
	7/19/2017	719	1.65	0.48	1.76	0.67	0.5371

From the test results listed in Figure 78-79 and Table 26, it can be seen that the deflections of the micro-cracked sections are comparable to those of the control sections and the differences are not statistically significant.

Summary of Test Results. The micro-cracked section has a 64.5 ft. long longitudinal cracking and there was no transverse cracking observed on both sections. The micro-cracked section has a better performance in terms of the rutting and IRI. The deflections obtained from the micro-cracked section are similar to those from the control section, most of the differences are not significant. Considering the different subgrade conditions of the two sections, as well as the low traffic volume and the short service life (only two years), it is difficult to conclude if the micro-cracking technique is effective for the 8.5-in. soil cement base.

Structural Number (SN) Analysis

The FWD results were used to determine the subgrade resilient modulus M_r and the effective structural number SN_{eff} of the sections on LA 1003 and LA 599, according to the 1993 AASHTO NDT deflection-based procedure. For each test section, M_r and SN_{eff} were back-calculated in terms of the earliest and latest FWD/HWD test results to investigate the change of structural condition during the current service life. The obtained M_r and SN_{eff} of the micro-cracked sections were also compared with those of their control sections to investigate the influence of micro-cracking on pavement structural conditions.

LA 1003

Measured deflections from two FWD/HWD tests conducted on March 29, 2016 (553 days after the construction of bases) and July 12, 2017 (1023 days after the construction of bases) were selected for the back-calculation of the subgrade resilient moduli and effective structural numbers. The subgrade resilient moduli of test sections on LA 1003 are shown in Figure 80.

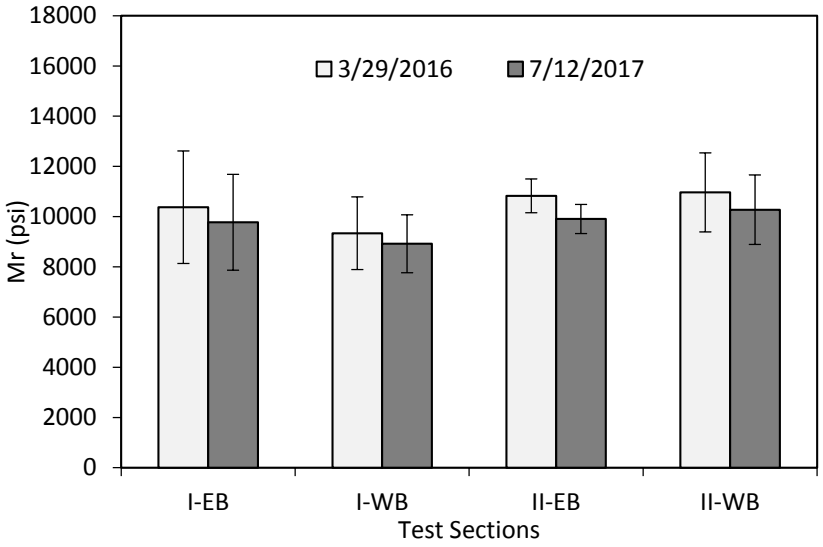
18000
16000
14000
12000
10000
8000
6000
4000
2000
0
Mr (psi)
3/29/2016
7/12/2017
I-EB
I-WB
II-EB
II-WB
Test Sections

(a)

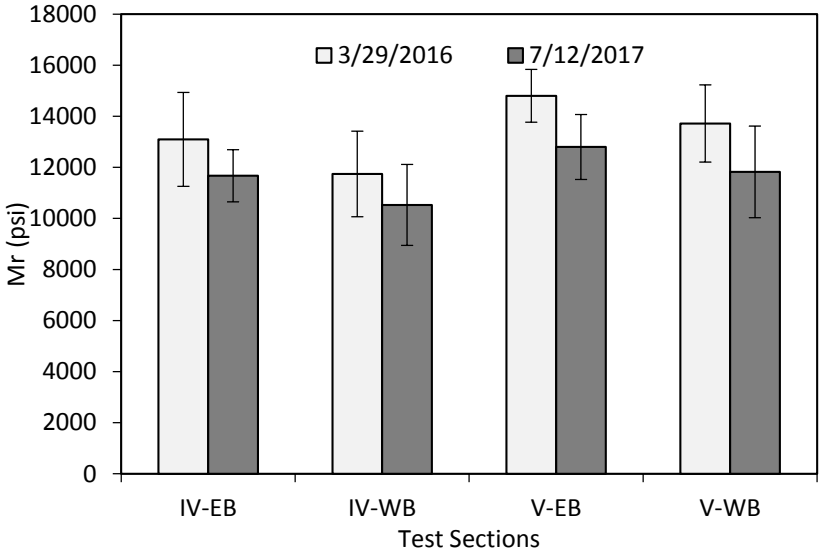
18000
16000
14000
12000
10000
8000
6000
4000
2000
0
Mr (psi)
3/29/2016
7/12/2017
IV-EB
IV-WB
V-EB
V-WB
Test Sections

(b)

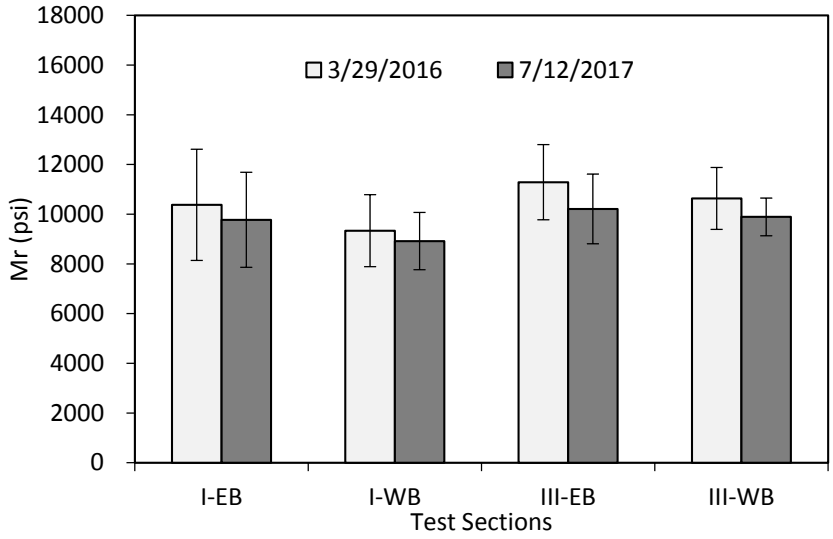

(c)

Figure 80

Subgrade resilient moduli of LA 1003 (a) Section I vs. Section II (b) Section IV vs. Section V (c) Section I vs. Section III

From Figure 80, it can be seen that on micro-cracked and control sections, subgrade resilient moduli M_r decreased with the increase of the service life. For the Sections I and II with 8.5-in. CSD bases, M_r values of traffic lanes in the micro-cracked section (Section II) were higher than those in the control section (Section I), but this difference is significant only on the westbound lane according to the statistical analysis (Table 27).

For the Sections V and IV with 12-in. CTD bases, the M_r values of traffic lanes in the micro-cracked section (Section V) were also higher than those in the control section (Section IV). However, the higher M_r values did not result in a better cracking performance on Section V.

For Sections I and III, the double layer section has greater M_r values than Section I on both Eastbound and Westbound; however, according to the T-Test results in Table 27, the difference is not significant.

Table 27
Subgrade resilient moduli of the LA 1003 test sections

Mr LA 1003	Date	Days after Constr.	T-test				
			Control Sec. Ave	Standard Dev.	MC/DL Sec. Ave	Standard Dev.	p-value
SecI-II EB	3/29/2016	553	10375	2238	10825	674	0.5572
	7/12/2017	1023	9775	1910	9905	580	0.8408
SecI-II WB	3/29/2016	553	9336	1447	10963	1571	0.0311
	7/12/2017	1023	8919	1155	10273	1384	0.0328
SecIV-V EB	3/29/2016	553	13093	1840	14803	1031	0.0254
	7/12/2017	1023	11671	1022	12798	11823	0.0626
SecIV-V WB	3/29/2016	553	11740	1676	13718	1508	0.0183
	7/12/2017	1023	10528	1584	11823	1797	0.1314
SecI-III EB	3/29/2016	553	10375	2238	11286	1514	0.3025
	7/12/2017	1023	9775	1910	10212	1402	0.5673
SecI-III WB	3/29/2016	553	9336	1447	10635	1245	0.0534
	7/12/2017	1023	8919	1155	9892	758	0.0504

* DL=Double Layer

Figure 81 shows the back-calculated effective structural number SN_{eff} of the LA 1003 test sections. As shown in Figure 81(a), for the Sections I and II with 8.5-in. CSD bases, the micro-cracked section (II) had higher SN_{eff} values as compared with the control section. The difference is significant in the westbound lane, confirmed by the t-test results summarized in Table 28.

For the Sections IV and V with 12-in. CTD sections, the micro-cracked section (V) also had greater SN_{eff} values than the control one (IV) as shown in Figure 81(b), though the control section (Section IV) had a better crack performance than the micro-cracked section (V) after a 3-year service period. However, the SN_{eff} values were not significantly different according to the statistical analysis.

The double layer section had larger effective structural numbers than the 8.5-in. control section and the difference is significant based on the T-Test results (Table 28). However, the significance decreased after one and half year.

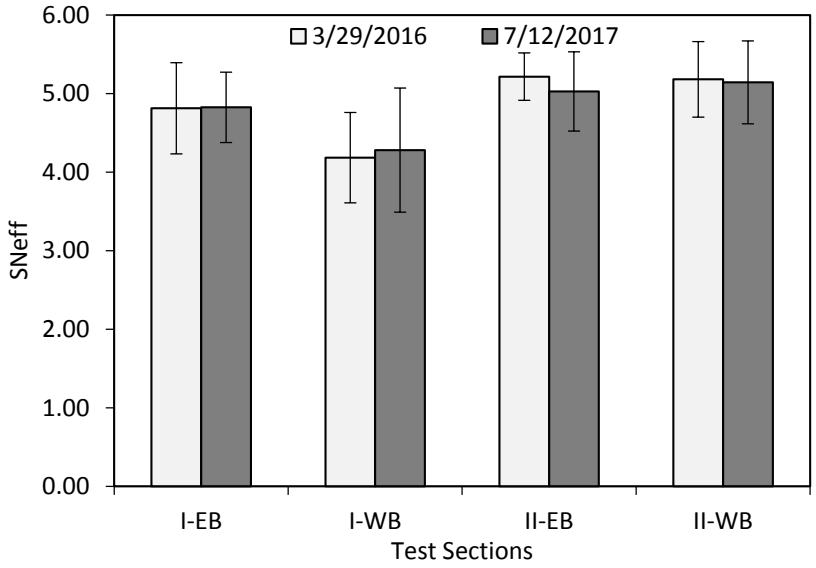
6.00
5.00
4.00
3.00
2.00
1.00
0.00
SNeff
3/29/2016
7/12/2017
I-EB
I-WB
II-EB
II-WB
Test Sections

(a)

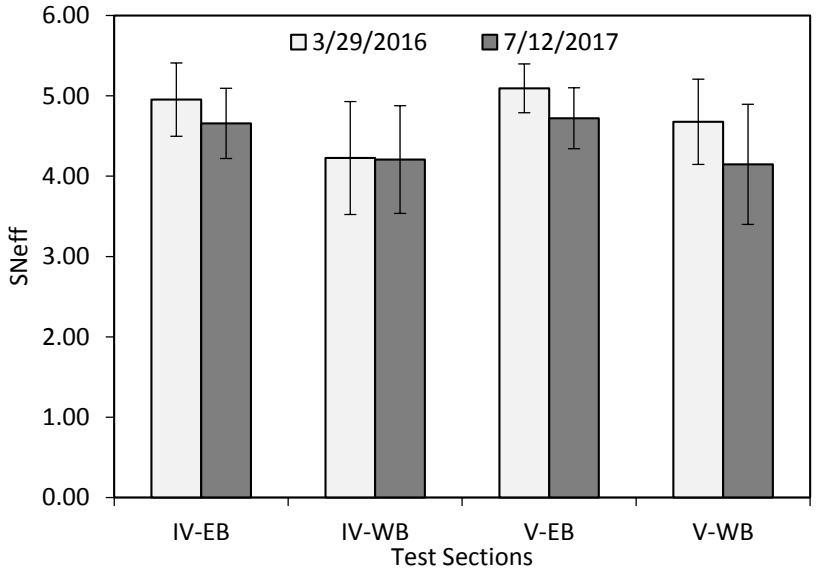
6.00
5.00
4.00
3.00
2.00
1.00
0.00
SNeff
3/29/2016
7/12/2017
IV-EB
IV-WB
V-EB
V-WB
Test Sections

(b)

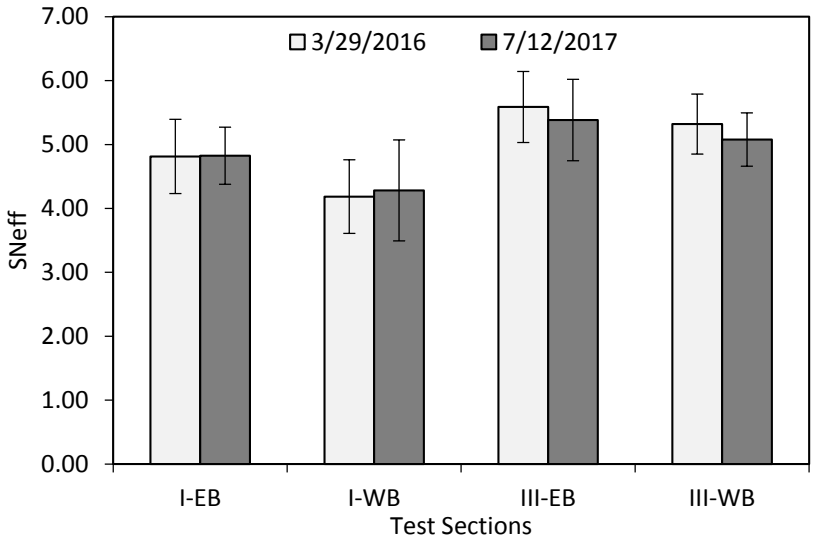

(c)

Figure 81

Effective structural numbers on LA 1003 (a) Section I vs. Section II (b) Section IV vs. Section V (c) Section I vs. Section III

Table 28

Effective structural numbers of the LA 1003 test sections

SNeff: LA 1003	Date	Days after Constr.	T-test				
			Control Sec.Ave	Standard Dev.	MC/DL Sec. Ave	Standard Dev.	p-value
SecI-II EB	3/29/2016	553	4.81	0.58	5.22	0.48	0.0752
	7/12/2017	1023	4.83	0.45	5.03	0.50	0.3703
SecI-II WB	3/29/2016	553	4.18	0.58	5.18	0.48	0.0009
	7/12/2017	1023	4.28	0.79	5.14	0.53	0.0154
SecIV-V EB	3/29/2016	553	4.95	0.45	5.09	0.30	0.4471
	7/12/2017	1023	4.66	0.44	4.72	0.38	0.7431
SecIV-V WB	3/29/2016	553	4.22	0.70	4.68	0.53	0.1401
	7/12/2017	1023	4.21	0.67	4.15	0.75	0.8602
SecI-III EB	3/29/2016	553	4.81	0.58	5.59	0.56	0.0069
	7/12/2017	1023	4.83	0.45	5.38	0.64	0.0378
SecI-III WB	3/29/2016	553	4.18	0.58	5.32	0.47	0.0003
	7/12/2017	1023	4.28	0.79	5.08	0.42	0.0194

* DL=Double Layer

LA 599

Four FWD/HWD tests were conducted on the westbound lane of all the LA 599 test sections. The service life of the test sections during the FWD/HWD tests ranged from 89 and 719 days after base construction. Only one HWD test was performed on the eastbound lane on August 15, 2017, which was 746 days after base layer constructions. Figure 82 shows the comparison of M_r of the micro-cracked sections and control sections. For the 12-in. CTD sections [Figure 82 (a)], the micro-cracked section (Section II) had lower M_r values in both lanes and the results of t-test indicate that the differences in both lanes are statistically significant (Table 29).

For the 8.5-in. CSD sections [Figure 82 (b)] in the westbound lane of LA 599, the subgrade resilient moduli decreased after the 2-year service. The M_r of the micro-cracked section (Section IV) was slightly higher than its control section (V) at 89-day after the base construction; however, the M_r of Section IV was significantly lower than that of Section V after two years, as indicated by the statistical results in Table 29.

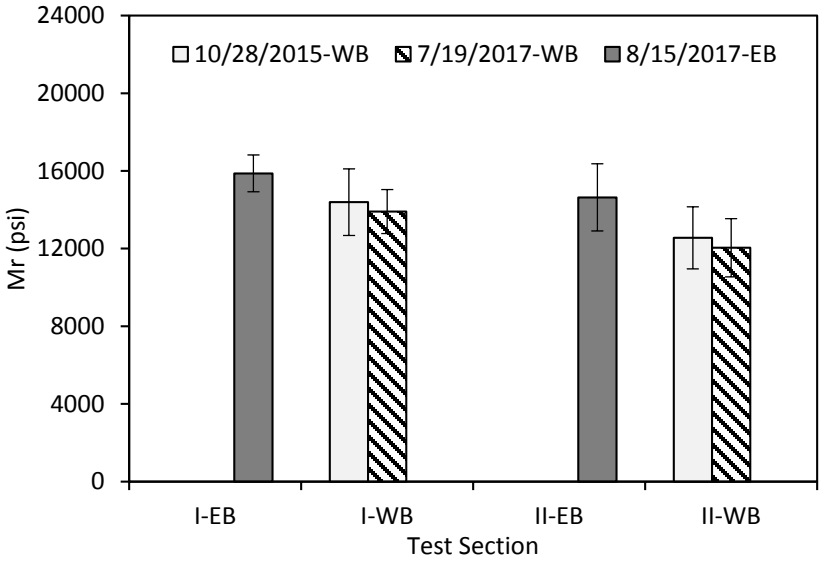

(a)

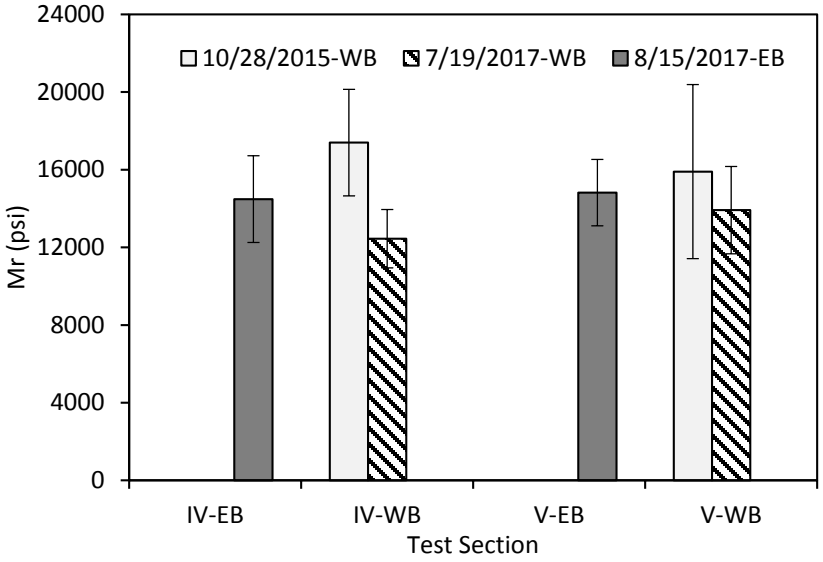

(b)

Figure 82

Subgrade resilient moduli of the LA 599 Test Sections (a) Section I vs. Section II (b) Section IV vs. Section V

Table 29

Subgrade resilient moduli LA 599

Mr LA 599	Date	Days after Constr.	T-test				
			Control Sec.Ave	Standard Dev.	MC Sec. Ave	Standard Dev.	p-value
SecI-II EB	8/15/2017	746	15870	948	14636	1732	0.0077
SecI-II WB	10/28/2015	89	14389	1714	12554	1597	0.0011
	7/19/2017	719	13911	1133	12041	1499	<0.0001
SecIV-V EB	8/15/2017	746	14821	1709	14485	2235	0.5938
SecIV-V WB	10/28/2015	89	15900	4483	17396	2745	0.1964
	7/19/2017	719	13918	2246	12447	1503	0.0018

Figure 83 shows the SN_{eff} of the four test sections on LA 599. As shown in Figure 83, SN_{eff} of the westbound lane of LA 599 did not decreased after the two-year service. This was mainly because of the cement hydration during this period. For both the 8.5-in CSD and 12-in. CTD sections, micro-cracked sections had higher effective structural numbers than their control sections; however, the difference became not significant after the two-year service according to the statistical analysis (Table 30).

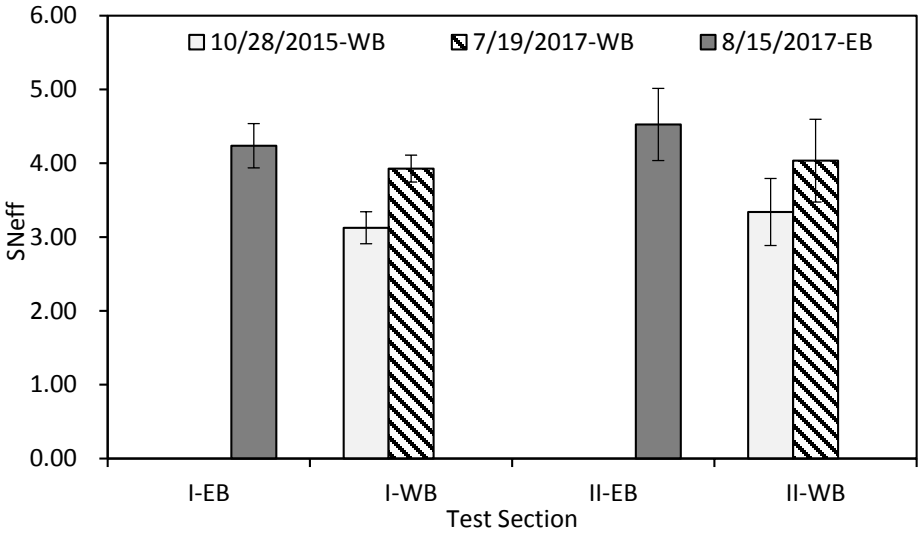

(a)

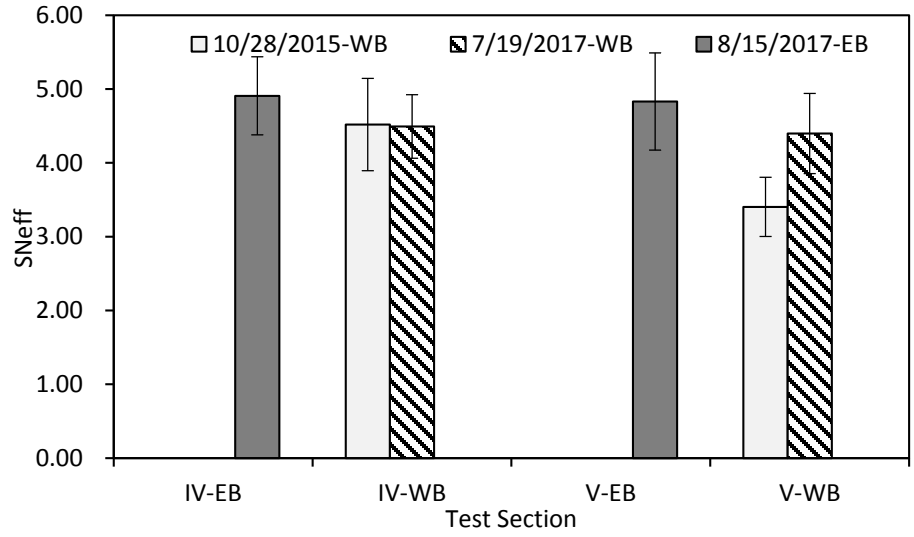

(b)

Figure 83

Effective structural numbers on LA 599 (a) Section I vs. Section II (b) Section IV vs. Section V

Table 30
Effective structural numbers LA 599

SNeff: LA 599	Date	Days after Constr.	T-test				
			Control Sec. Ave	Standard Dev.	MC Sec. Ave	Standard Dev.	p-value
SecI-II EB	8/15/2017	746	4.24	0.30	4.53	0.49	0.0284
SecI-II WB	10/28/2015	89	3.13	0.22	3.34	0.45	0.0617
	7/19/2017	719	3.93	0.18	4.04	0.56	0.4112
SecIV-V EB	8/15/2017	746	4.83	0.66	4.91	0.53	0.6790
SecIV-V WB	10/28/2015	89	3.40	0.40	4.52	0.63	<0.0001
	7/19/2017	719	4.40	0.54	4.49	0.43	0.5349

Discussion of the Cracking Performance of the Micro-Cracked Sections

Overall, the cracking performance of the micro-cracked test sections was comparable to that of the control sections on LA 1003. According to the analyses of the structural numbers and subgrade resilient moduli, it was found out that the structural numbers did slightly increase for most of the micro-cracked sections, but the increase was not significant statistically. The results indicate that the application of micro-cracking may be beneficial to the pavement structure. Double Layer section (Section III) might have a better structural condition than the control section (Section I). However, considering the decreasing significance, further investigation is necessary.

The structural number analysis of the LA 599 test sections also indicates that micro-cracking may be favorable to the pavement structure, even though the benefit was not significant statistically. However, the cracking performance of the micro-cracked test sections on LA 599 was worse than that of the control sections. The possible reasons resulting in the worse cracking performance of the micro-cracked sections are summarized below:

- The unsatisfactory cracking performance may be attributable to the weak subgrade of the micro-cracked test sections. Based on the back-calculation, the subgrade resilient moduli of the micro-cracked sections (Sections II and IV) were much lower than those of the control sections. According to the NCHRP soil properties of Louisiana, the distribution of the subgrade properties around the LA 599 test sections are shown in Figure 84 and the detailed subgrade properties of the test sections are summarized

in Table 31. As shown in the table, the subgrade resilient moduli of the micro-cracked test sections are approximately half of those of control sections. Due to the weak subgrade, the stresses in the asphalt layer and base layer of the micro-cracked sections induced by traffic loading were higher than those of the control sections. Therefore, the deterioration of the asphalt layer of the micro-cracked test sections was accelerated.

- Differential settlement of the subgrade embankment might be another reason. The differential settlement due to the weak subgrade may result in the generation of voids at layer interface and subsequently increase the cracking potential of the asphalt layer under traffic loading. In addition, the slope instability at the edge of the subgrade embankment under traffic loading may cause cracks on the pavement surface directly.

- Superelevation at the curve and substandard asphalt thickness were not favorable to the performance of the micro-cracking sections. Coring showed that the thickness of the asphalt layer was less than 3 in., while the designed thickness was 3.5 in. These factors might aggravate the unsatisfactory crack performance of the micro-cracked sections.

It should be noted that most of the cracks observed were not reflective cracking; therefore, it is difficult to conclude whether the micro-cracking technique is effective or not in mitigating reflective cracking. Therefore, further monitoring of the cracking performance of the test sections may be necessary.

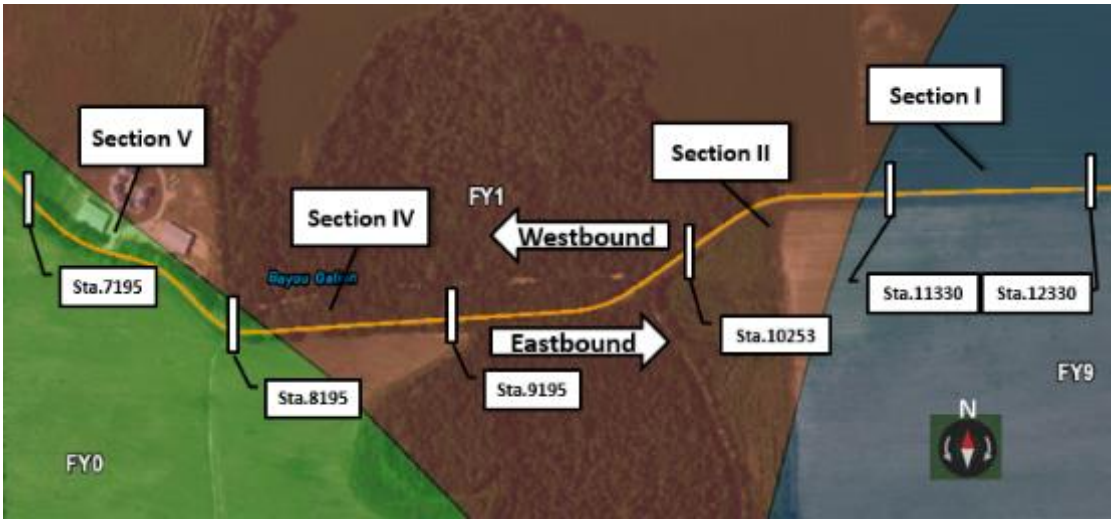

Figure 84
Subgrade soil distribution on LA 599 area

Table 31
Subgrade soil properties of LA 599 test sections

Section	Items	Top Layer	Layer 2	Layer 3
I (FY9)	AASHTO Classification	A-4	A-6	A-6
	Thickness (in)	9.8	27.2	35.0
	Resilient Modulus (psi)	19,124	8,207	11,535
	Liquid Limit (%)	21.0	38.0	31.0
	Plasticity Index (%)	3.5	16.5	10.5
II and IV (FY1)	AASHTO Classification	A-7-6	A-7-6	A-7-6
	Thickness (in)	5.9	24.0	29.9
	Resilient Modulus (psi)	5,191	4,549	5,403
	Liquid Limit (%)	60.0	70.0	62.5
	Plasticity Index (%)	33.5	41.5	36.0
V (FY0)	AASHTO Classification	A-4	A-6	A-4
	Thickness (in)	9.8	34.3	15.7
	Resilient Modulus (psi)	14,883	8,894	12,183
	Liquid Limit (%)	21.5	34.0	28.5
	Plasticity Index (%)	5.5	14.0	8.0

Possible Reasons for the Low Modulus Reduction during the Micro-Cracking Process

The TTI recommended a modulus reduction of 60% for the micro-cracking process, which could not be achieved in this study even a few more passes were applied. For most of the test sections in this study, the modulus reduction achieved was less than 40%. This may indicate the micro-cracking process highly depends on the soil type and soil properties. The possible reasons for the low modulus reduction achieved in this study may include:

- The bonding between the soil particles and the cement hydration products was weak at the early age (3-day) and easily broken after a few passes. The excessive passes may cause the hardening of the cement stabilized soil bases.

- After a few passes, further compaction became ineffective to the degraded soil cement bases due to the existing of weak subgrade underneath the bases.

CONCLUSIONS

In this study, a total of 15 micro-cracked and non-micro-cracked pavement test sections were constructed with different soil types, cement contents, and soil cement base designs. Various in-situ NDT tests were conducted during the micro-cracking process and the post-construction pavement monitoring. Based on the obtained in situ performance results, the following observations and conclusions were made:

- No severe shrinkage cracks were found on any of the PRF test sections after three and half years of construction. Substantial amounts of hairline-type shrinkage cracks were first observed on all test sections during the early curing periods, but the surface cracks were all disappeared in approximately six months thereafter. Saw-cut beams showed no full-depth wide cracks along the beam thickness, indicating no hidden severe shrinkage cracks have been developed.

- The possible reasons for severe shrinkage cracks developed on PRF sections may be due to (1) sufficient curing time and less moisture loss due to covered by visqueen; (2) short section length (each section is only approximately 70-ft. long); (3) possible effect of micro-cracking; and (4) no traffic loading on PRF sections.

- The base stiffness increased with time for all PRF sections. This result indicates that the micro-cracking did not damage the base layer, and the base strength could fully regain after curing with time.

- Based on the results of the crack performance, high-speed pavement profile survey, and FWD testing, it was found that the sections with an 8.5-in. micro-cracked soil cement base layer generally performed similar to the control sections with an 8.5-in. non-micro-cracked soil cement base layer on both the LA 1003 and LA 599 testing sites. However, only limited cracks were found on both the control and micro-cracked sections and the pavements were in service for less than three years. Therefore, whether or not the micro-cracking technique is suitable for implementing on the 8.5-in soil cement pavement in Louisiana cannot be concluded at this time.

- From the performance in LA 1003 and LA 599, it may be concluded that micro-cracking seems not to be an effective method in the mitigation of reflective cracking for a 12-in. cement treated soil base layer in Louisiana. The dissatisfactory pavement cracking performance of the 12-in. cement treated soil base micro-cracked test sections may be partially attributable to its less cement content, non-uniformity of

base after construction, and possibly differential settlement on a relatively weak subgrade.

- Based on the structural number analysis, it was found that the effective structural numbers of the micro-cracked sections were generally similar to or even slightly higher than the control sections, indicating the micro-cracking process might not weaken the pavement structures due to the extra compaction.

- The 8.5-in. CSD section with a double-layer AST on LA 1003 was compared to the 8.5-in. CSD control section. The double layer section did not show a better crack or rutting performance, even though its effective structural number was found greater than the control section.

RECOMMENDATIONS

Based on the observations from this study, the following recommendations are proposed:

- The micro-cracking technique is not recommended for implementing on the asphalt pavements containing a 12-in. cement treated soil base in Louisiana;

- Long-term pavement cracking performance of an 8.5-in. micro-cracked soil cement pavement could not be obtained from the current study. Whether or not the micro-cracking technique is suitable for implementing on the 8.5-in. soil cement pavement in Louisiana still cannot be concluded.

- Continuously field monitoring of the constructed micro-cracked test sections on both the LA 599 and LA 1003 are recommended (i.e., once per year for at least another five years) in order to determine if the micro-cracking has any long-term benefits in the control of reflective cracking on the asphalt pavement with an 8.5-in. soil cement in Louisiana.

ACRONYMS, ABBREVIATIONS, AND SYMBOLS

AASHTO	American Association of State Highway and Transportation Officials
AC	Asphalt concrete
ADT	Annual daily traffic
AST	Asphalt surface treatment
ASTM	American Society for Testing and Materials
ASTL	Asphalt surface treatment layer
Caltrans	California Department of Transportation
cm	centimeter(s)
CIST	Clegg impact soil tester
CSB	Cement stabilized base
CSD	Cement stabilized design
CTB	Cement treated base
CTD	Cement treated design
DOTD	Louisiana Department of Transportation and Development
DPU	Data processing unit
EB	Eastbound
FHWA	Federal Highway Administration
ft.	foot(feet)
FWD	Falling weight deflectometer
HWD	Heavy weight deflectometer
in.	inch(es)
IRI	International roughness index
ITM_r	Indirect tensile resilient modulus
ITS	Indirect tensile strength
LFWD	Light falling weight deflectometer
LL	Liquid limit
LTRC	Louisiana Transportation Research Center
lb.	pound(s)
m	meter(s)
MC	Micro-Cracked; Micro-Cracking
mm	millimeter(s)
NCHRP	National cooperative highway research program
NDT	Non-destructive tests

PFWD	Portable falling weight deflectometer
PI	Plasticity index
PRF	Pavement research facility
PSB	Profiler system boards
RAP	Recycled asphalt pavement
SIF	Stress intensity factor
SN	Structural number
SN_{eff}	Effective structural number
TTI	Texas Transportation Institute
UCS	Unconfined compressive strength
WB	Westbound

REFERENCES

1. George, K. P. “Mechanism of shrinkage cracking of soil-cement bases.” Highway Research Record, 442, 1973, 1-10.

2. Litzka, J., and Haslehner, W. “Cold in-place recycling on low-volume roads in Austria.” Transportation Research Board Conference Proceedings. No. 6. 1995

3. Thoegersen, F., Busch, C., and Henrichsen, A. “Mechanistic design of semi-rigid pavements-An incremental approach.” Mechanistic Design of Semi-Rigid Pavements 138 2004.

4. George, K. P. “Soil Stabilization Field Trial.” Final Report, University of Mississippi. 2006.

5. George, K. P., Bajracharya, M., and Gaddam, M. “Precracking mitigates shrinkage cracks in cemented materials.” Damage and Fracture Mechanics VII, 2003, 79-90.

6. Scullion, T. “Precracking of Soil-Cement Bases to Reduce Reflection Cracking: Field Investigation.” *Transportation Research Record: Journal of the Transportation Research Board,* 1787, 2002, 22-30.

7. Sebesta, S. “Effectiveness of Minimizing Reflective Cracking in Cement-Treated Bases by Microcracking.” Texas Transportation Institute, 2004.

8. Sebesta, S. “Continued Evaluation of Microcracking in Texas.” Texas Transportation Institute, Texas Transportation Institute, 2005.

9. Halsted, G. E. “Minimizing Reflective Cracking in Cement-Stabilized Pavement Bases.” The pavement maintenance and preservation session of the 2010 annual conference of the transportation association of Canada, Halifax, Nova Scotia. 2010.

10. Bofinger, H. E., Hassan, O.H., and Williams, R.I.T. “The Shrinkage of Fine-Grained Soil-Cement.” Australian Road Research Board Symposium. No. Supp. Report 398. 1978.

11. Sebesta, S., and Scullion, T. “Effectiveness of minimizing reflective cracking in cement-treated bases by microcracking.” No. FHWA/TX-05/0-4502-1, 2004.

12. Bofinger, H. E. and Sullivan, G.A. “An Investigation of Cracking in Soil Cement Bases for Roads,” Road Research Laboratory (RRL) Report LR 379, Road Research Laboratory, Crowthorne, Berkshire. 1971

13. George, K. P. “Shrinkage characteristics of soil-cement mixtures” Highway Research Record, 225, 1968, 42-58.

14. Gaspard, K. J. “In-place Cement Stabilized Base Reconstruction Techniques Interim Report: Construction and Two Year Evaluation”. No. FHWA/LA-02/361,. 2002.

15. Gaspard, K., Mohammad, L., Wu, Z. “Laboratory Mechanistic Evaluation of Soil Cement Mixtures with Fibrillated-polypropylene-fibers,” TRB 2003 Annual Meeting CD-ROM, Washington, DC. 2003.

16. Hope, C. A. *Evaluation of Portable Devices for Monitoring Microcracking of Cement-Treated Base Layers. Master Thesis*, Brigham Young University, 2011.

17. Miller, H. J., Guthrie, S. W., Rebecca, C. A., and Smith, B. “Evaluation of Cement-Stabilized Full-Depth-Recycled Base Materials for Frost and Early Traffic Conditions.” 2011.

18. Holt, C., Barnes, C., Sullivan, P., and O’Toole, L. “Full depth remediation of roads using Portland cement.” 2009 Annual Conference of the Transportation Association of Canada, Vancouver, Canada, 2009.

19. Sebesta, S. “Microcracking for Reduced Shrinkage in Cement-Treated Base.” Project Summary report 0-4502-S, Texas Transportation Institute, 2006.

20. Louw, S. and Jones, D., “Pavement Recycling: Literature Review on Shrinkage Crack Mitigation in Cement-Stabilized Pavement.” Technical Memorandum: UCPRC-TM-2015-02, Department of Transportation, California, 2015.

21. Walker, P. J. “Strength, durability and shrinkage characteristics of cement stabilized soil blocks.” *Cement & Concrete Composites*, 17(1995), 1995, 301-310.

22. George, K. P. “Shrinkage cracking of soil-cement base: theoretical and model studies.” Highway Research Record 351, 1971, 115-133.

23. Pais, J. C. and Pereira, P. A. A. “Prediction of existing reflective cracking potential of flexible pavements.” Fourth International RILEM Conference on Reflective Cracking in Pavements Research in Practice. 2000, 155-164.

24. Lytton, R. L., Tsai, F. L., Lee, S-I., Hu, S., Luo, R., and Zhou F. “Models for Predicting Reflection Cracking of Hot-Mix Asphalt Overlays.” NCHRP 01-41. Texas Transportation Institute, 2010.

25. Paris, P. C. and Erdogan, E. “A Critical Analysis of Crack Propagation Laws, Journal of Basic Engineering, Transaction of the American.” Society of Mechanical Engineering, Series D., Vol. 85, pp. 528-883, 1963.

26. Elbagalati, O., Elseifi, M.A., Gaspard, K. and Zhang, Z. “Prediction of In-Service Pavement Structural Capacity Based on Traffic-Speed Deflection Measurements.” *Journal of Transportation Engineering* 142.11 (2016): 04016058.

27. Elseifi, M. A., Gaspard, K., Wilke, P. W., Zhang, Z., and Hegab, A. Evaluation and validation of a model for predicting pavement structural number with rolling wheel deflectometer data. Transportation Research Record: *Journal of the Transportation Research Board,* 2015 (2525): 13-19.

28. AASHTO, AASHTO Guide for Design of Pavement Structures, The American Association of State Highway and Transportation Officials (AASHTO), Washington, D.C., U.S.A. 1993.

APPENDIX A

TxDOT Updated Guidelines for Microcracking *[8]*

How and When Should Micro-Cracking Be Performed?
After placement and satisfactory compaction of the CTB according to the applicable bid item, the base should be moist cured by sprinkling for 48 to 72 hours before micro-cracking. If performing micro-cracking during winter months when average daily temperatures are 60°F or below, moist cure the base for at least 96 hours before micro-cracking. Micro-cracking should be performed with the same (or equivalent tonnage) steel wheel vibratory roller used for compaction. A minimum 12-ton roller should be used. Typically, three full passes (one pass is down and back) with the roller operating at maximum amplitude and traveling approximately 2 to 3 mph will satisfactorily micro-crack the section. After satisfactory completion of micro-cracking, the base should be moist cured by sprinkling to a total cure time of at least 72 hours from the day of placement.

What to Look for during the Micro-Cracking Process
Inspect the micro-cracking operation and look for:

- Satisfactory completion of three full passes that achieve 100% coverage.
- Signs of cracking in the CTB. Although new cracks are rarely observed (oftentimes some transverse cracking will have already taken place during the moist-curing stage), hairline cracks imparted by the roller occasionally may be visible. If available, the FWD can be used to ensure adequate completion of micro-cracking by testing every station immediately before micro-cracking, then retesting at each station immediately after completion of the three micro-cracking passes. The average base modulus should be reduced at least 50% by micro-cracking with three passes of the roller.
- Signs of detrimental damage to the CTB. If properly designed and cured, micro-cracking should not damage the CTB. However, if the base appears to start to break up excessively at the surface, stop micro-cracking and use a static roller until a satisfactory surface finish is obtained.

Satisfactory completion of continued moist curing to an age of at least 72 hours from the day of placement.